MACHINABILITY OF MICRO-FEATURES ON TiN-Al_2O_3 CERAMIC-COMPOSITE BY HYBRID-EDM FOR MICRO-REACTORS

Ph.D. Thesis

RUPALI BAGHEL
ID No. 2014RME9009

DEPARTMENT OF MECHANICAL ENGINEERING
MALAVIYA NATIONAL INSTITUTE OF TECHNOLOGY
JAIPUR

July 2019

Machinability of Micro-Features on TiN-Al_2O_3 Ceramic-Composite by Hybrid-EDM for Micro-Reactors

Submitted in

fulfillment of the requirements for the degree of

Doctor of Philosophy

by

RUPALI BAGHEL

ID: **2014RME9009**

Under the supervision of

Dr. Harlal Singh Mali
&
Prof. Sampad Kumar Biswas

DEPARTMENT OF MECHANICAL ENGINEERING
MALAVIYA NATIONAL INSTITUTE OF TECHNOLOGY JAIPUR

July 2019

Malaviya National Institute of Technology, Jaipur

DECLARATION

I**, Rupali Baghel**, declare that this thesis titled, "**MACHINABILITY OF MICRO-FEATURES ON TiN-Al_2O_3 CERAMIC-COMPOSITE BY HYBRID-EDM FOR MICRO-REACTORS**" and the work presented in it are my own. I confirm that:

- This work was done wholly or mainly while in candidature for a research degree at this university.
- Where any part of this thesis has previously been submitted for a degree or any other qualification at this university or any other institution, this has been clearly stated.
- Where I have consulted the published work of other, this is always clearly attributed.
- Where I have quoted from the work of others, the source is always given with the exception of such quotations; this thesis is entirely my own work.
- I have acknowledged all main sources of help.
- Where the thesis is based on work done by myself, jointly with other, I have made clear exactly what was done by others and what I have contributed myself.

DATE **RUPALI BAGHEL**

(2014RME9009)

CERTIFICATE

This is to certify that the thesis entitled "**MACHINABILITY OF MICRO-FEATURES ON TiN-Al_2O_3 CERAMIC-COMPOSITE BY HYBRID-EDM FOR MICRO-REACTORS**" being submitted by **Rupali Baghel (2014rme9009)** is a bonafide research work carried out under my supervision and guidance in fulfillment of the requirement for the award of the degree of **Doctor of Philosophy** in the Department of **Mechanical Engineering,** Malaviya National Institute of Technology, Jaipur, India**.** The matter embodied in this thesis is original and has not been submitted to any other University or Institute for award of any other degree.

Signature of Supervisor

Dr. Harlal Singh Mali

Signature of Supervisor

Prof. Sampad Kumar Biswas

The Ph.D. viva voce examination of Ms. **Rupali Baghel** has been conducted by the Oral Defense Committee (ODC) constituted by the Dean (Academic Affairs), as per 9.4.3, vide letter No. F.4(P) PhD/Acad/MNIT/2018-19/2359 dated 7 June 2019 on Monday, **29th July, 2019**. The ODC declares that the student has successfully defended the thesis in the viva-voce examination.

Dr. Harlal Singh Mali
(Supervisor)
Associate professor,
Department of Mechanical Engineering
MNIT Jaipur

Prof. Sampad Kumar Biswas
(External joint supervisor)
Ex. Professor Department of Metallurgical and Materials Engineering
MNIT Jaipur

Prof. Promod Kumar Patowari
(External examiner)
Department of Mechanical Engineering
National Institute of technology
Silchar, Aasam

DEDICATION

I wish to dedicate this thesis to my mother,

Late. Smt. Neeru Baghel

Although she is not here to give me support but I always feel her presence that guide me throughout my life

ACKNOWLEDGMENTS

I would like to express my sincere gratitude to my supervisor **Dr. Harlal Singh Mali**, Associate Professor, Department of Mechanical Engineering for giving me this opportunity and providing precious guidance, valuable discussions, constant supervision and encouragement for working with integrity and efficiency during the course of time. His constant, constructive criticism leads to timely completion of experimental work. While working in Advanced Manufacturing and Mechatronics (AMM) Lab, I got the opportunity to access a wide range of machining facilities and enhance academic knowledge. I also want to thanks my external joint supervisor **Prof. Sampad Kumar Biswas** for his valuable discussions and support. I want to thank them wholeheartedly for providing moral support, facilities and a comfortable environment.

I thank Malaviya National Institute of Technology (MNIT) Jaipur for supporting my research by providing institute assistantship so that work is completed without any financial constraint. I am thankful to Professor **Dr. Dilip Sharma,** H.O.D. in Mechanical Engineering Department, Professor **Dr. Govind Sharan Dangayach,** Associate Professor **Dr. Amar Patnaik, and** Assistant professor **Dr. Anoj Meena** for providing me a positive and supportive environment during my research work. I would like to thanks all other faculty members and staff of MNIT Jaipur for their help and support.

I express my sincere gratitude to **Prof. Upender Pandel** (Metallurgical and Materials Engineering, MNIT Jaipur), my M.Tech supervisor who encouraged me for higher studies. I am thankful for his valuable guidance, unconditional support and for being a source of inspiration for me.

I am thankful to my seniors **Dr. Deepak R. Unune** (assistant prof. LMNIT Jaipur), **Dr. Jai Kishan** (assistant prof. Government Engineering College Ajmer) and **Dr. Bhargav Prajwal (**assistant prof. Effat University, Saudi Arabia) for helping me in my research work by sharing their knowledge and research experience time to time. I would like to express my sincere thanks to my Ph.D. colleagues **Pragati Priyanka,** and **Siddhartha Kumar** for providing a healthy environment. I always felt lucky to have wonderful colleges like **Nancy, Arjun, Divyanshu, Aniket, Shivendra, Vivek and Deepanshu.** I am thankful to these guys for creating unforgettable memories of lab work,

short-trips and friendship during my stay in MNIT Jaipur. I am thankful to AMM Lab technician **Mr. Sandeep Thakur** and **Mr. Deepak Kumar** for their support.

I express my wholehearted appreciation and respect for my beloved family for their unconditional love and patience especially to my elder brother **Dheeraj Singh Baghel** who always stands beside me in every up and down. I would like to thank my friend **Apoorv** for providing me mental support by understanding each and every day without getting tired and cheering up even in my tough days. I am also thankful to my friend **Nitika** for being there for much needed emotional support and for creating countless memorable moments. I would like to thanks **Priya, Jyoti** and **Monika** for being such good friends during my stay in MNIT Jaipur.

To sum up my experience of Ph.D., I have made many mistakes and have faced many failures but I learned to always get up and never stop trying which enabled me to evolve into a better version of myself.

RUPALI BAGHEL

(2014RME9009)

ABSTRACT

Micromachining of advanced-ceramics is an emerging research area that is significant for the development of miniaturized products. Miniaturization of devices necessitates micro features like micro holes, microchannels, high aspect ratio holes, and micro groves etc. to be fabricated on its parts. Unconventional machining processes play a dominant role in fabricating microfeatures on advanced ceramics. Electro Discharge Machine (EDM) is a very important process for generation of micro-features as it is able to cut complex shaped, precise features in onerous to machine advanced ceramics. EDM process can be revamped to hybrid EDM by applying assisting method.

Aluminium-oxide based ceramic-composites are making an appreciable contribution to the aerospace, automotive and electronics industry. Although such composites have been successfully introduced in few commercial applications, their potential of widespread applications is still impeded due to the challenges in machining of these ceramic-composites. This investigation is conducted on Titanium Nitride Aluminium Oxide ($TiN\text{-}Al_2O_{3)}$ ceramic-composite having TiN content 66 mol percentage and electrical resistivity 0.25 Ω.m. $TiN\text{-}Al_2O_3$ ceramic-composite is a newly developed advanced ceramics-composite. It possesses mechanical properties especially hardness and strength at elevated temperatures. It is being used in high-end areas i.e. medical implants, drug delivery systems, gas turbines, aerospace parts, and micro-pumps. $TiN\text{-}Al_2O_3$ ceramic-composite is chemically inert and it is having high resistance to thermal and abrasion wear. These properties suits for the applicability of this material as micro-chemical reactors, tool-insert and high-temperature heat exchanger. Due to its high hardness, it has an impediment in machining by traditional machining methods. The work accentuated in this thesis is on the surfacing of samples and fabricating microfeatures on $TiN\text{-}Al_2O_3$ ceramic-composite with hybrid micro EDM process. The effect of control factors i.e. gap voltage, capacitance, electrode rotational speed, feed rate, pulse on time, duty cycle current and discharge energy are examined for analyzing performance measures like Material Removal Rate (MRR), Electrode Wear Rate (EWR), Electrode Wear Ratio (EW Ratio), Taper Angle (TA) and Radial Overcut (ROC). Based on results, single and multi-optimization of performance measures are also carried out for response parameters. This has been performed using Minitab®-16 and Design Expert®18 software.

Face structured, Central Composite Design (CCD) of Response Surface Methodology (RSM) is used for analyzing and optimizing the performance measures. ANOVA (analysis of variance) is used to statistically analyze the performance. Finally, regression is performed to establish an empirical relation between performance measures and factors. The machined surfaces of TiN-Al_2O_3 ceramic-composite have also been analyzed by Field Emission Scanning Electron Micrographs (FESEM) coupled with Energy Dispersive X-ray Spectroscopy (EDS) to understand the mechanism of material removal.

Fabrication of microfeatures on one of the most challenging classes of materials and studies on the effect of process parameters on geometric characteristics of micro-features with regard to its application as a microchemical reactor has been done. The complete experimental work is divided into the following phases: (1) Preliminary Experiments on Electronica® ZNC (ENC-35) and Hybrid µ-EDM (DT110i), (2) Parametric studies on Diamond grinding assisted EDM of TiN-Al_2O_3 ceramic-composite and multi-objective optimization using response surface methodology (RSM), (3) Parametric studies on electrode discharge milling (ED-Milling) for fabricating micro-channels on TiN-Al_2O_3 ceramic-composite and multi-objective optimization using RSM, (4) Fabrication of high aspect ratio micro holes using Powder mixed micro-EDM and parametric studies using RSM technique

In the preliminary experiments, Taguchi's experimentation strategy was used. In, these experiments, various machining parameters i.e. Pulse On-Time, Duty Cycle, Peak Current, Maximum Feed, Wheel Rotation Speed, Flushing Direction were selected for experimentations on Electronic® ZNC (ENC-35). For Hybrid µ-EDM (DT110i), Input Voltage, Capacitance, Electrode Rotation Speed, and Tool Feed Rate, Powder Concentration, Vibration, Electrode material were selected for preliminary studies. Based on the results of these experiments, the ranges of input parameters which had an influential effect on machining were chosen for further parametric study.

In Parametric studies of Diamond-grinding assisted EDM of TiN-Al_2O_3 ceramic-composite, Response surface methodology (RSM) was employed and an empirical model for MRR is presented in chapter 4. The input parameters included were Pulse On-Time (t_{on}), Duty Factor (DF) and Wheel Rotation Speed (S). The mechanism of materials removal was explained with the help of Scanning electron microscopy (SEM) images. The material removal rate was found to improve significantly and smooth surfaces were obtained for micro-features fabrication. The results of multi optimization, using RSM were found to be very promising. In this study, the mechanism of material removal was

also explained for TiN-Al_2O_3 ceramic-composite, the presence of cracks and debris in the metal pool on machined surface confirm that material removal takes place by melting and vaporization. The material removal also takes place by thermal cracking and flakes removal i.e. thermal spalling. It was also observed that at higher speed, recast layer was removed due to the grinding effect. The surfacing of the TiN-Al_2O_3 ceramic composite was done and on an average 2.54 μm average surface roughness (Ra) value was achieved at high speed.

Fabrication of micro-channels and micro holes on TiN-Al_2O_3 ceramic-composite by ED Milling and parametric studies using response surface methodology for developing smooth surface is reported in chapter 5. In this work, microchannels were fabricated keeping in mind its application in microreactors. Material Removal Rate (MRR) and Electrode Wear Rate (EWR) are optimized and influencing factors on response parameters are also studied. In parametric studies on electrode discharge milling (ED-Milling) for fabricating micro-channels on TiN-Al_2O_3 ceramic-composite, center composite design matrix (CCD) with three input parameters i.e. Electrode Rotation Speed (S), Voltage (V) and Capacitance (C) are employed. Electrode Feed Rate (FR) is kept constant. Empirical models for Material Removal Rate (MRR) and Electrode Wear Rate (EWR) are developed using RSM. These models are found to adequately represent the performance measures.

In chapter six, fabrication of high aspect ratio micro-holes using powder mixed micro-EDM (PMμ-EDM) in TiN-Al_2O_3 ceramic-composite with the view of improving MRR and geometrical characteristics was performed on hybrid μ-EDM. The parametric study of the PMμ-EDM process was carried out taking powder concentration (Conc.), voltage (V) and electrode rotation speed (S) as control factors. The powder-concentration in the dielectric was found to be a significant factor for MRR as well as for EWR. An experimental investigation of SiC powder mixed μ-ED machining of TiN-Al_2O_3 ceramic-composite using response surface methodology is reported in a view of improving machining parameters. Material Removal Rate (MRR) and Electrode Wear Rate (EWR) are optimized. Comparison of geometric-characteristics is also being reported between EDM and PM-μEDM.

Based on the experimental investigation, the mechanism of material removal is discussed for each machining process. The study on surface morphology of machined surface and fabricated microfeatures were also conducted. The circularity and accuracy of microchannels and holes were also analyzed by SEM. SEM images of the inner surface of

holes give information about the formation of craters, and flakes on the machined surface. Energy-Dispersive X-Ray Spectroscopy (EDS) was used for analyzing the chemical composition of the machined surface and for creating the element composition map. Thus, this work has contributed to the knowledge of hybrid micro EDM of TiN-Al_2O_3 ceramic-composite by putting forward the complexities associated with the machining of the most challenging class of materials i.e. advanced ceramics. It was found that Diamond grinding assisted Electro-discharge machining (DGA-EDM) shows better material removal rate as compared to EDM and diamond grinding, for surfacing of the samples. The MRR improves threefold by hybridizing diamond grinding with EDM. The surfaces generated by DGA-EDM were found to be suitable for developing micro features by hybrid μ-EDM. For the fabrication of micro-channels, micro ED milling is selected and it was found that high discharge energy i.e. combination of high capacitance and high voltage leads to better MRR. A further process enhancement is done by PM μ-EDM by the inclusion of SiC powder in a dielectric fluid. It was found that not only MRR is improved in this process but geometrical characteristics i.e. taper angle and radial overcut are also found to improve. The mechanism of material removal was also different in TiN-Al_2O_3 ceramic-composite than that of metal. Thermal spalling was found to be the dominant mechanism of material removal than melting and vaporization. Experimental results show that DGA-EDM and hybrid μ-EDM are suitable methods for surfacing and machining respectively on TiN-Al_2O_3 ceramic-composite. Successful fabrication of micro features such as micro blind holes, micro holes, and micro-channels will pave the way for developing micro-chemical reactors out of TiN-Al_2O_3 ceramic-composite.

Key Words: Ceramic-composite, TiN-Al_2O_3, Diamond grinding assisted EDM, ED-milling, powder mixed micro-EDM, Scanning electron microscopy (SEM), Energy-Dispersive X-Ray Spectroscopy, Mechanism, Thermal-Spalling, geometric characteristics, MRR, EWR, EW ratio, Taper angle, Radial overcut.

TABLE OF CONTENTS

LIST OF FIGURES

LIST OF TABLES

LIST OF ABBREVIATIONS

EDM	Electric discharge machining
EDDG	Electro discharge diamond grinding
AJM	Abrasive jet machining
WJM	Water jet machining
USM	Ultrasonic machining
LASER	light amplification by stimulated emission of radiation
DGAEDM	Diamond grinding assisted electro-discharge machining
PMEDM	Powder mixed electro-discharge machining
MRR	Material removal rate
EWR	Electrode wear rate
ROC	Radial overcut
TA	Taper angle
SEM	Scanning electron microscope
EDS	Energy-Dispersive X-Ray Spectroscopy
SiC	Silicon carbide
ANOVA	Analysis of variance
DOF	Degree of freedom
Seq SS	Sequential sum of squares
LOF	Lack of fit
P	Probability
V_f	Vibration frequency
I	Current
t_{on}	Pulse on time
Fr	Feed rate
V	Input Voltage
C	Capacitance
S	Electrode rotation speed
Con.	SiC powder concentration

CMC	Ceramics Matrix Composite
AMC	Alumina matrix composite
MEMS	Micro-electronic and mechanical devices
HAZ	Heat affected zone
RC-type	Resistor-capacitance type
Al_2TiO_5	Tialite
EDDSG	Electro-Discharge Diamond Surface Grinding
MWCNT	Multiwalled Carbon Nanotubes
GNPs	Ceramics Containing Graphene- Nanoplatelets
WC–Co	Cobalt-Bonded Tungsten Carbide

1. INTRODUCTION

1.1 Importance of machining of advanced ceramics

Engineering advancement is based on the manufacturing and fabrication industry of advanced materials. Although tremendous progress has been attained in material engineering and production engineering in the last decades, there is still a need for exploring it to meet the technological challenges for the present applications. Inspired by the desire of reducing cost, size, weight, raw material, and energy consumption, one can witness miniaturization across almost all domains of industrial and consumer products. Few examples of these miniaturized products include micro-chemical reactors, micro-heat exchanger, micro-electronic, and mechanical devices (MEMS), etc. While manufacturing these miniaturized products which include various kinds of miniaturized components, production-engineers face many technological challenges in fabrication and handling of these components. Challenges are also faced due to technological limitations of conventional materials like metals and alloys, thus leading to the origin of advanced ceramics-composite based miniaturized products or micro-devices to enhance the system productivity and effectiveness. Advanced ceramics-composite are mainly prepared by high-temperature sintering. The excellent properties of advanced ceramic-composite are attained by the amalgamation of metal or semi-conductive particles like SiC, ZrO_2 with the conventional ceramics. Advanced ceramic-composite are oxides, nitrides, and carbides that can be operated at very high temperature. They are resistant to various kinds of wear, including abrasion, chemical and thermal. Advanced ceramic-composite are mostly employed to fulfill such demands that cannot be fulfilled by metals and their alloys because advanced ceramics are the materials with high mechanical and chemical resistance. The impact can be understood by the significant quantities of energy involved in the process by a reduction in weight (automobile, aircraft, trains, etc.), as well as to increase the operating temperature, it can also improve the fuel efficiency. Such need in materials can be easily fulfilled by advanced ceramics materials or ceramics matrix composite (CMC). Advanced ceramic-composite are unconquerable when applied in some commercial applications but their challenges in machining hindered their widespread potential for many applications. In addition, they are very hard and extremely

brittle; they also possess insulating property against the conduction of heat and electricity and also have the presence of very hard abrasive ceramics reinforcements. Such properties of ceramics lead it to be very difficult to form material. Therefore the machinability study of very hard to machine materials that have a high potential for application will encourage designers to go beyond the performance limit of metals but also help in overcoming the technological limitation imposed by conventional material.

1.2 **Challenges in the machining of advanced ceramics**

Materials doubtlessly play a significant role in developing miniaturized products. Advanced ceramics and CMC can significantly fulfill the present requirements of materials, devices, and components. The exposure of the manufacturing and production industries to use advanced ceramics is increasing in the last decades because of their outstanding mechanical, chemical and thermal properties. Mostly, oxides of aluminum and zirconium are widely used for industrial applications such as gas sensors, components of the pump and medical instruments [1], etc. Also, advanced engineering ceramics are used as machine tool, aerospace parts, automotive parts, and electronics parts such as automotive brakes, sensors, advanced computer memory products, etc. [2]**.** Advanced ceramics usage is also found in dental implants and prosthesis such as a crown, denture, orthopedics [3], etc. Advanced ceramics not only encourage going beyond the performance limit of metal but also overcoming the technological limitation imposed by conventional materials used in industries. Advanced ceramics possess high resistance to wear even at elevated temperature, stronger electromagnetic response and high refractoriness, etc. [4]. Though such properties are well suited for applications, the fabrication and machinability characteristics such as high machining force, high melting temperature, and poor surface integrity and shortened tool life, makes advanced-ceramics very difficult to cut materials and consequently results in partial acceptance in the field of industrial application [5] [6]**.** To overcome the problems associated with the machining of advanced ceramics, both conventional and advanced machining processes are explored and is found that there are numbers of challenges faced by manufacturing and fabrication industries in advanced ceramics as listed below-

- The stress-strain curves for ceramic are similar to concrete and cast iron rather than metals [7]. Owing to low toughness, the advanced ceramics are not able to

sustain high machining forces generated by conventional machining process thus leading to the poor machined surface.

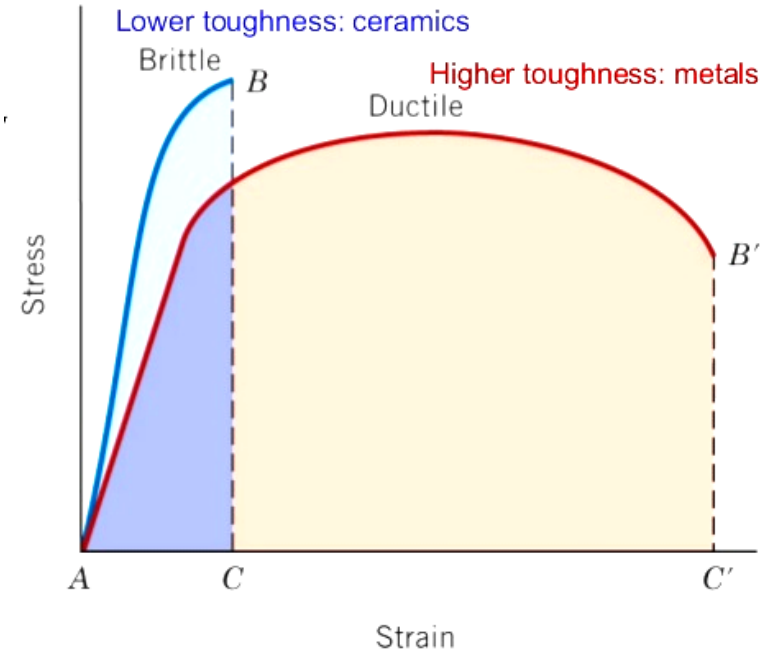

Figure 1.1 Stress-strain curves for ceramics and metal [8]

- Owing to high brittleness and no plasticity as compared to metals as shown in Fig. 1.1, the ceramic fracture occurs before the plastic limit under the application of load. It does not show any plastic deformation and sudden failure takes place without any indication.
- The brittle materials such as ceramics, concrete allow stress magnification in the presence of a flaw in the workpiece. According to Griffin's theory proposed in 1920, if any elliptical flaw exists in the workpiece, the stress tends to magnify itself by a large quantity. Thus if there are cracks present in the workpiece, the material gradually tends to fail in the presence of small pressure as shown in Fig. 1.2.
- The applied stress may be very low but the magnified stress is very high. The magnified stress is given by equation 1.1. Where $\boldsymbol{\sigma}$ = external stress, $\boldsymbol{\sigma}_{m=}$ magnified stress at the cracked tip, L= cracked length and ρ=radius at the cracked-tip.

$$\sigma_m = 2\sigma\sqrt{\frac{L}{\rho}} \quad \text{..... (1.1)}$$

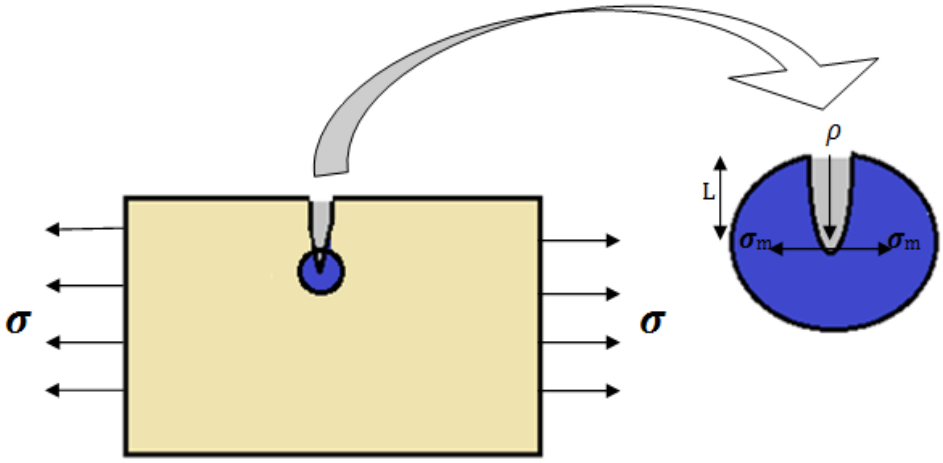

Figure 1.2 Stress magnifications in a brittle material

- The ceramics tend to have a Transgranular fracture as shown in Fig. 1.3. This type of fracture follows the edges of the lattice in granular materials by ignoring the grains in the individual lattice. Such fracture cannot be stopped, once initiated. So as a matter of principle during machining of ceramics, chatter and vibrations should be avoided.

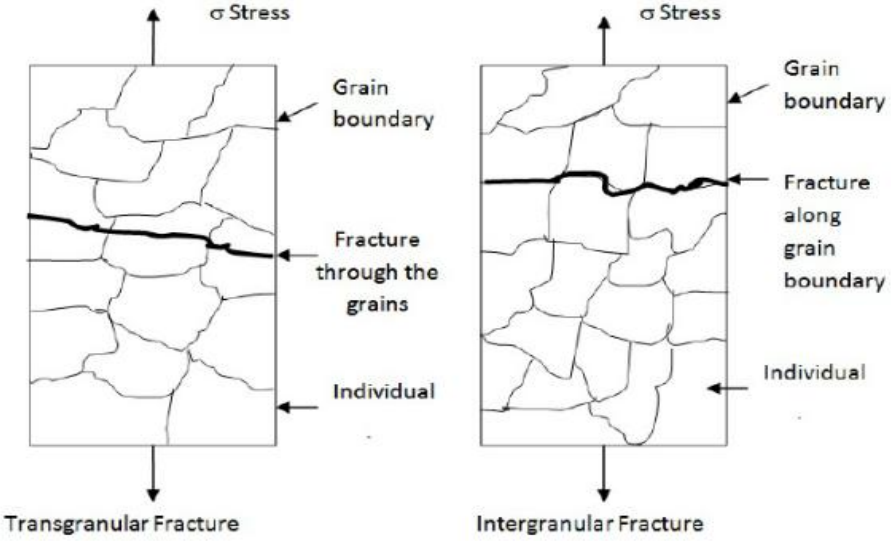

Figure 1.3 Transgranular and Intergranular fracture [9]

- Owing to excellent hot hardness (Fig. 1.4) ceramics are applicable at an elevated temperature where most metals tend to fail but on the other hand, they are very difficult to machine by a heating process like laser machining, Electro-discharge machining.

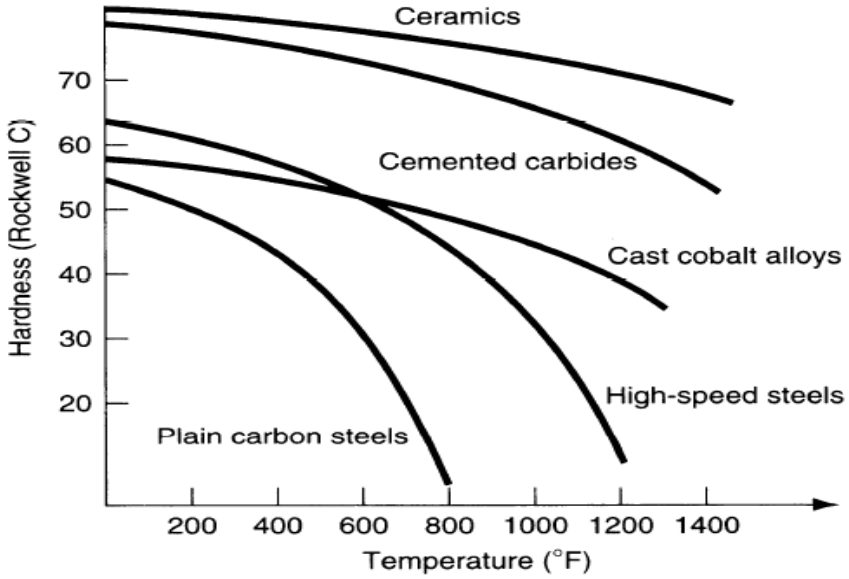

Figure 1.4 Hardness v/s temperature curve for various materials [10]

The difficulty in the machining of advanced-ceramics arises not only due to their hardness and brittleness but also due to its strong tendency for forming a built-up edge owing to low thermal conductivity during conventional machining such as turning, milling, drilling, etc. To overcome the challenges faced while machining of advanced ceramics; machining processes are needed to be explored in terms of improving process parameters. The requirements of advanced-ceramics machining are to have a good surface finish, high accuracy in geometrical characteristics of microfeatures and high material removal rate but these requirements are very difficult to achieve by the conventional machining process. High cutting forces induced during conventional machining process cause strength abasement due to the origin of cracks on machine surface as shown in Fig. 1.5. Advanced- machining process could be used to overcome the machinability limitation of advanced ceramics as their material removal mechanisms are different than that of the conventional machining process. In the advanced machining process, mechanical (abrasive jet machining, ultrasonic machining, water jet machining, abrasive

waterjet machining), electro-thermal (electro-discharge machining, laser machining, electron-beam machining), chemical (chemical etching, electrochemical machining, photochemical milling), etc. energies are utilized to machine the material. Among various non-conventional machining processes, electro-discharge machining (EDM) is explored for machining of intricate shaped, hardened parts in recent year in a flexible and accurate manner [11].

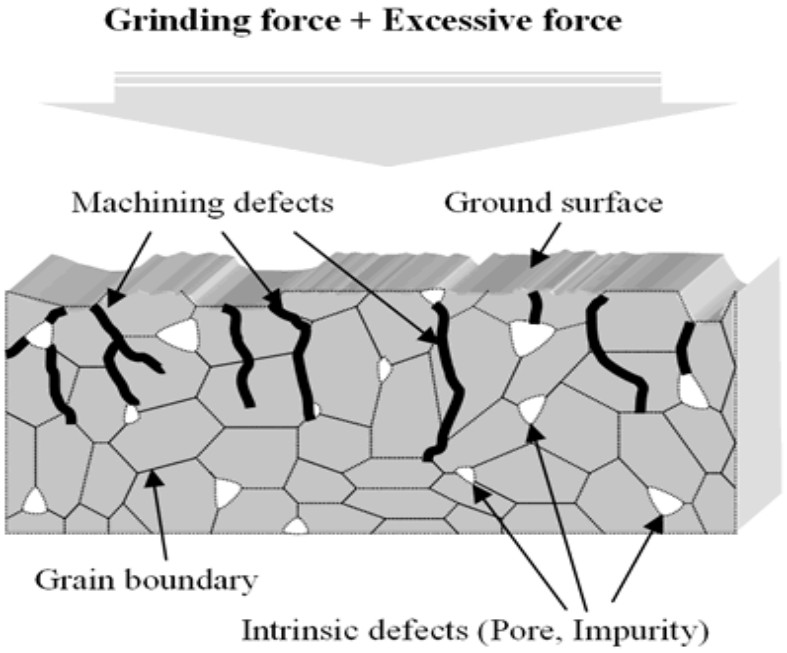

Figure 1.5 Machining defects in ceramics [12]

The ceramic applications are versatile but still a lot of research in machinability of ceramics materials from conventional as well as non-convention methods is needed to meet the required product precision and accuracy. Although many researchers have worked in the area of machining of advanced ceramics by EDM process, Improvements in the EDM process with respect to process parameter and quality of the end-product are still required.

1.3 The significance of advanced ceramics machinability in the microdomain

Advanced ceramics such as alumina-composites, Zirconia, Sialon are being put to outspread industrial applications as they possess superior physical properties than conventionally used materials. These advanced ceramics offer engineers liberty in designing high performance, the precision part /device as these materials have improved

technological properties such as hot hardness, low weight to volume ratio and resistance to various kind of wear. Newly developed ceramics/ composite have properties that make them difficult or nearly impossible to the machine by the traditional machining process as discussed in section 1.2. The machinability problem with such advanced ceramic/ composite is more severe while working in microdomain as accuracy and precision requirements are high during micromachining. Thus micro-machining of advanced ceramic/composite needs to be explored in terms of machining processes that are technically and economically viable as miniaturization is required in every aspect of designing. Consequently, most widely accepted advanced machining processes such as EDM and its hybrid machining processes are employed for successful machining of the advanced ceramics. This work is related to the micro-machining of advanced ceramic or CMC. It will contribute to the knowledge of hybrid μ-EDM machining and will encourage processing engineers for developing miniaturized devices of advanced ceramics such as micro-chemical reactors, micro heat exchanger, etc.

1.4 **Organization of the Thesis**

The research work has been organized as follows:

Chapter 1 describes the importance of machining of advanced ceramics/composite. It also discusses the various challenges that are faced during the conventional-machining of advanced ceramics due to their superior properties. This chapter also includes the significance and scope of this research work.

In chapter 2, a brief background of advanced ceramics in general, and ceramic-composite, in particular, is given and an introduction of machining of advanced ceramics by EDM along with EDM process & characteristics are also presented. The literature review includes applications of advanced-ceramics with fundamental and advantage of micro-chemical reactors and applicability of advanced-ceramics as micro-chemical reactors. It also covers classification, properties, applications and machining characteristics of advanced-ceramics. The chapter concludes with the research gap, obtained from the literature review and formulation of objectives of the current study.

In chapter 3, the introduction of materials i.e. Titanium Nitride Aluminium Oxide (TiN-Al_2O_3) ceramic-composite and its applications, properties with the scope of TiN-Al_2O_3 ceramic-composite machining by hybrid EDM are explained. This chapter also includes

various machinery setups that are used in experimental studies. This chapter ends with the detailing of process parameters of each experimentation and equipment used for the characterization of the machined samples.

In Chapter 4, a systematic experimental investigation of Diamond Grinding Assisted Electro-Discharge Machining (DGA-EDM) of TiN-Al_2O_3 ceramic-composite using response surface methodology is reported. Development of empirical models of material removal rate and mechanism of material removal is also been reported. A comparison of the machining performance of EDM and DGA-EDM is also included.

In Chapter 5, a systematic experimental investigation of micro ED-milling of TiN-Al_2O_3 ceramic-composite using response surface methodology is reported. Material Removal Rate (MRR) and Electrode Wear Rate (EWR) are optimized and influencing input parameters on response parameters are also studied. Mechanism of material removal with effects of ED-milling on the machined surface is also reported.

In Chapter 6, a systematic experimental investigation of SiC powder mixed micro ED machining (PMμ-EDM) of TiN-Al_2O_3 ceramic-composite using response surface methodology is reported. Material removal rate and electrode wear rate are optimized. Comparison of geometric characteristics of micro-features fabricated by EDM and PM-μEDM is also reported.

In chapter 7, summaries of important conclusions from each experimental investigation with suggestions for future work in micro-machining of TiN-Al_2O_3 ceramic-composite is presented.

Three appendixes are also presented with this work. These are the outcome obtained during the study. Appendix "A" is based on the effect of low-frequency vibration on EDM of TiN-Al_2O_3 ceramic-composite. Appendix "B" is about the effects of discharge energy on geometrical characteristics of high aspect ratio micro-holes and appendix "C" is about the on-machine fabrication of micro-electrodes.

2. LITERATURE REVIEW

This chapter presents background and an overview of the machining of advanced ceramics by electro-discharge machining (EDM) and its variants highlighting the process characteristics and research possibilities in the area of advanced ceramics machining by EDM and its hybrid variants. A comprehensive review of EDM of advanced ceramics is also presented. Details of powder mixed-EDM are also included with major research work in this area. Research possibility in advanced ceramics machining by EDM and possible outcomes, classification of advanced ceramics and applications are also discussed. The future direction and research gap are presented in the last section.

2.1 **Background**

Scientific research and engineering advancement have placed unusual demands on the materials and manufacturing industry. Requirements for advanced materials are also felt due to technological limitations of conventional materials like metals and alloys, thus leading to the origin of advanced material based products or devices to enhance the system productivity and effectiveness. Metal-matrix composite, advances ceramics and ceramic-matrix composite with high strength to weight ratio and low density could be used for such specific demands. Advanced ceramic-composite is an emerging class of material. They are superior to metals as they possess (as discussed in chapter 1 section 1.2) high strength, toughness, hot hardness and excellent wear resistance. They also have a high potential for a broad variety of industrial applications because of their outstanding mechanical, chemical and thermal properties. In advanced ceramic-composite, one of the constituents is metal or alloy which forms a continuous phase and termed as matrix and the other constituent, that is embedded, serves as reinforcement. The reinforcement is usually a non-metallic material, generally ceramic such as Aluminium oxide (Al_2O_3), Silicon carbide (SiC), etc. Advanced ceramic-composite have advantages as compared to unreinforced materials such as reduced density, hot hardness, improved stiffness, etc. Alumina matrix composite (AMC) is one of the high-performance ceramic-composite. AMCs have excellent physical and mechanical properties and are widely applied in aircraft technology, electronics engineering, and automobile industry. Advanced ceramics

are widely used in dental implants, orthopedics, proximity sensors, disc-break, sealing, computer memory products, and tool insert, etc. [13] [14].

Although few commercial applications of advanced ceramic-composite have been successfully introduced their full potential for widespread applications is still impeded due to the challenges in their machining, as they are difficult to form/cut due to the presence of hard and abrasive reinforcements. Issues like rapid tool wear, surface, and sub-surface damage, along with the high cost of machining are associated. Therefore, these materials have attracted researchers worldwide since last decade. As a result of this lot of work has been carried in conventional machining of these materials. In addition, nonconventional machining process like electrical discharge machining has also been employed to machine these materials.

2.2 **Electro-Discharge Machining (EDM)**

Advanced-ceramics encourage engineers for going beyond the performance limit of metal. To overcome the issue machining of advanced ceramics, both traditional and advanced machining processes are need to explore. The applications of advanced-ceramics require a good surface finish, low dimensional tolerance, and good machinability but such responses are very difficult to achieve by conventional machining process due to their inability to be machined. Advanced machining processes that are mostly non-contact type can be used. In these processes, material removal mechanisms are different than that of conventional machining process as they used mechanical (AJM, USM, WJM, AWJM), electro-thermal (EDM, laser, EBM), chemical (CHM, ECM), etc. energies to machine the material. Among various unconventional machining processes, EDM and its variants are explored for the machining of complex-shaped, hardened parts in recent year in a flexible and accurate manner [15]. Advanced ceramics-composite are prepared by high-temperature sintering. The excellent properties of advanced ceramic-composite are attained by the amalgamation of metal or semi-conductive particles like SiC, ZrO_2 with the conventional ceramics. Advanced ceramic-composite are oxides, nitrides, and carbides that can be operated at very high temperature. They are resistant to various kinds of wear including abrasion, chemical and thermal.

EDM is a promising technique for the production of ceramic parts. EDM came into being due to the works of two Russian scientists, B. R. Lazarenko, and N. I.

Lazarenko, who, in 1943, were tasked to investigate ways of preventing the erosion of tungsten electrical contacts due to sparking. They failed in this task but found that the erosion was more precisely controlled if the electrodes were immersed in a dielectric fluid. This led them to invent the electro-discharge machine used for difficult-to-machine materials such as tungsten [16]. The Lazarenko's' machine is known as a resistor-capacitor (R-C) type machine. This process is based on removing material from a part by means of a series of repeated electrical discharges between the tool called the electrode and the workpiece in the presence of a dielectric fluid. The electrode is moved toward the workpiece until the gap is small enough so that the input voltage is great enough to ionize the dielectric [17] [18]. The material is removed due to melting and erosive effect of the electrical discharges from tool and workpiece. In EDM there is no direct contact between the electrode and the workpiece and thus it can eliminate mechanical stresses, chatter and vibration problems during machining as shown in Fig. 2.1. Materials of any hardness can be cut as long as the material can conduct electricity [19]. EDM can machine irrespective of the hardness of the sample thus there is a variety of parts that can be machined efficiently by EDM process [20].

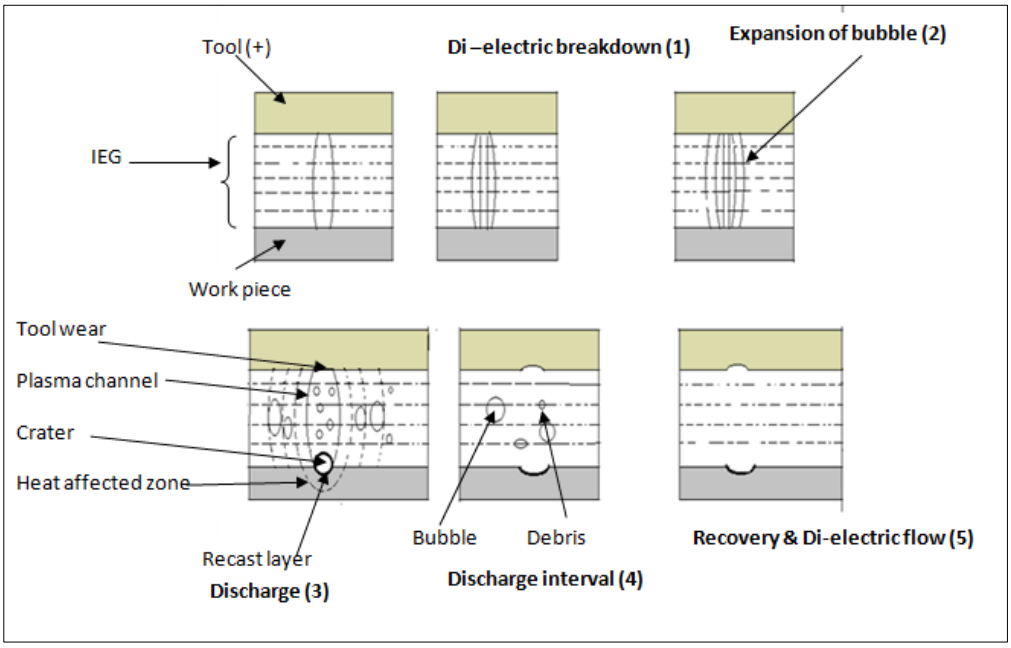

Figure 2.1 Mechanism of sparking in EDM

The capability of EDM to machine without any physical contact eliminates mechanical chatter and vibration that could damage advanced-ceramics. Thus, EDM holds the

capability of machining and fabricating low cost, tool, and parts from conducting-ceramic blanks in a precise manner. It is also claimed that even insulated ceramics could be machined by assisted electrode method in EDM. Once the process is established, the process parameters are required to be optimized for their use in industry as non-conductive ceramic machining by EDM is currently limited to lab experiments only. Thus, among the barriers to the widespread application of advanced ceramics, machining is one of the most important challenges. To address this, many research activities have been undertaken during the last decade as discussed in section 2.3. Some characteristics of the EDM process highlighting areas for improvement are listed in the successive text.

2.3 **Characteristics of the EDM process**

2.3.1 **Ultra miniaturized machine parts**

EDM has the ability to machine miniaturized machined parts of metal, metallic alloy, graphite, and ceramics irrespective of the hardness and brittleness [21]**.** Liu et al. [22] have developed ultra-miniaturized gas turbine impeller (diameter 20 mm) of Si_3N_4-TiN ceramics for the micro-fuel based power unit that is nearly impossible to fabricate by the conventional machining process.

2.3.2 **High-precision machining**

EDM can successfully machine intricate shapes accurately and effectively irrespective of the dimensions and material properties. Gupta et al. [23] have manufactured miniature spur gears by wire electro-discharge machining (WEDM) that are of better geometrical quality than miniature gear fabricated by the conventional machining process.

2.3.3 **Number of hybrid-variants**

EDM provides the advantage of providing a number of varieties in the process which make it agreeable to be applying for various kinds of materials, with quick changes in tooling and setup. EDM variants provide the opportunity of machining different shapes on various materials [1]. ED drilling, Wire EDM, ED diamond grinding and ED-milling are some of the variants of EDM. Kumar et al. [24] have modified electrodes by creating inclined micro slots on it for eliminating the accumulation of debris during machining which resulted in better geometrical characteristics i.e. higher aspect ratio, low taper angle, the low corner radius of the drilled hole. Koshy et al. [25] have fabricated regular

and non-regular polygon shapes features with sharp corner using kinematics of the Reuleaux triangle in tooling.

2.3.4 **Inability to machine electrically non-conducting material**

The applications of EDM are limited to metal, alloys, and composite which possess electrical resistivity of below 100 Ω.cm [2] [26]. Though some researchers claim to have successfully worked on non-conductive ceramics by EDM with assisting electrode method but such processes are limited to the surfacing of workpiece only as material removal is very low in those cases. Sabur et al. [27] have machined ZrO_2 by copper (Cu) as an assisting electrode and succeeded in removing a small amount of material. Schubert et al. [13] have used a starting conductive layer as an assisting electrode for micro-machining of non-conductive ceramics.

2.3.5 **Low energy efficiency**

Only a small percentage i.e. 18-50 % of the total input energy is used for material removal through electrodes in EDM. The maximum amount of input energy is lost in dielectric due to the small discharge area and temperature gradient in the dielectric fluid [28] [29]. Many researchers are working on the enhancing EDM energy utilization in material removal as only a small part of the process energy is used for material removal and is transmitted through electrodes in EDM. Most part of the energy is lost in dielectric due to its comparatively larger mass and low temperature of the dielectric. Approximately 18–50% of the total energy is utilized in the EDM. Obwald et al. [30] observed that only 40 % of total energy is distributed to electrodes.

2.3.6 **Non-economical process**

EDM is a costly process as compared to the conventional machining process not only in terms of low material removal rate but also tool fabrication is an exorbitant process [19]**.** High tool wear in EDM process also added the extra cost of the machining and inaccuracies in machining components. Being a costly process, it should be used where conventional machining processes are failed to work. Researchers are trying to compensate for the cost of machining by improving productivity, optimizing the tool wear and surface integrity.

2.4 **Advanced-ceramics applications**

Advanced ceramic or ceramic-composite is an emerging class of materials well known for its superior properties as compared to metals [31]**.** Although ceramics possess phenomenal physical properties, their full-scale application is still not achieved due to difficulties in processing and high manufacturing cost [32]**.** Advanced ceramics are likely to have extensive application in industries because of their outstanding mechanical, chemical and thermal properties. The advanced ceramics have extensive applications in the fields of aerospace, automobile, tool industry, human implants, etc. Advanced ceramics applications in various areas with typically used ceramics are shown in Fig. 2.2 and Fig. 2.3.

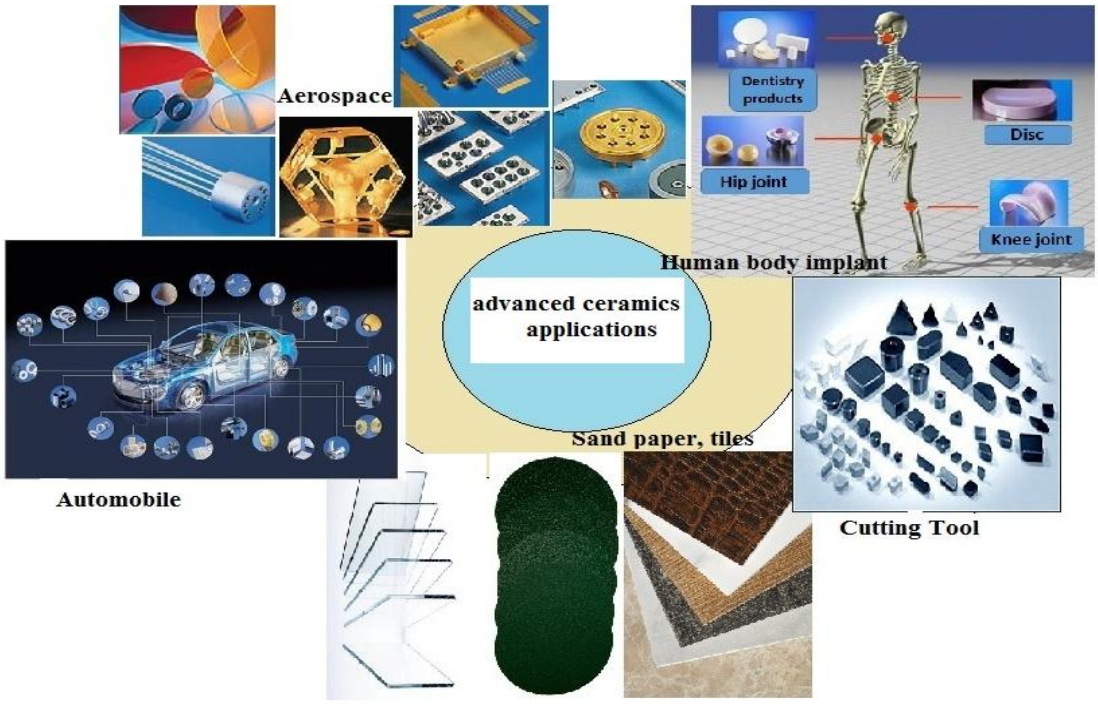

Figure 2.2 Advanced ceramics applications [32, 33]

2.4.1 **Aircraft industry**

The technical requirements for the material to be used in the aircraft industry are low weight to volume ratio, sustainability at very high temperature and safety. The components of ceramic-composites and alloys are desirable for such critical operating conditions. The advanced ceramic-composites are a potential solution in this industry as

they possess low density as compared to metals, very high mechanical strength, and phase stability at the critical working condition in terms of pressure and temperature range. For such applications, a wide range of suitable high-grade ceramic materials are available for selection: Al_2O_3, ZrO_2, AlN, SiC, Si_3N_4, ferrites, piezo-ceramics, and fiber composites. Some of these applications involve (1) Inertial references i.e. gyroscopes made of zero expansion glass ceramics used for precise position measurement in any aircraft. (2) Proximity sensors help to increase the safety of an aircraft e.g. by controlling whether any outside door is closed properly or not. Since proximity sensors often have to be placed in a difficult environment, their performance must be ensured by protecting them adequately which is done by the ceramic casing. (3) Technical-glass and filters are used to enhance the contrast, night vision. Glass ceramics and glasses with conductive-coating are used as technical glasses; they enable precise vision under challenging circumstances/ environments.

2.4.2 **Automobile industry**

In the automobile industry, advanced-ceramics are being used at a place where metal or plastic failed to fulfill the purpose such as spark plug made of Al_2O_3 ceramics. Automobile components made of advance-ceramics or its composite could be highly reliable and cost-efficient in long-term operation. The properties mainly required for the automobile industry are the high coefficient of friction and abrasive behavior even in critical conditions, high wear resistance for dimensional stability with temperature, phase stability, and chemically inertness, etc. Mostly, monolithic ceramic materials, composites, piezoceramics, and magneto-ceramics are used for these applications to achieve effectiveness for the specific application. In automobile industry ceramics are mostly used in two forms (1) Structured ceramics e.g. pump components (sealing), brake discs, catalyst support, particulate filter etc. and (2) Functional ceramics e.g. spark and glow plugs, oxygen sensors, knocking-sensors, parking distance control sensor, fuel injection system [33].

2.4.3 **Medical industry**

In the medical industry, many products made of advanced-ceramics or ceramic-composite are used in machine components of diagnostic-systems, radiotherapy and in implantology. The mainly used advanced-ceramics for such applications are Al_2O_3 and ZrO_2. The

properties required for medical applications are high electrical insulation, corrosion resistance and reliability over long periods. The human body implant (Fig. 2.2) should possess properties such as bio-inertness, approved in compliance with medical product laws and high resistance to abrasion, etc. Implants are the products made of monolithic ceramic materials. For dental applications, aesthetic aspects must is also taken into consideration as it is the visible part of the teeth.

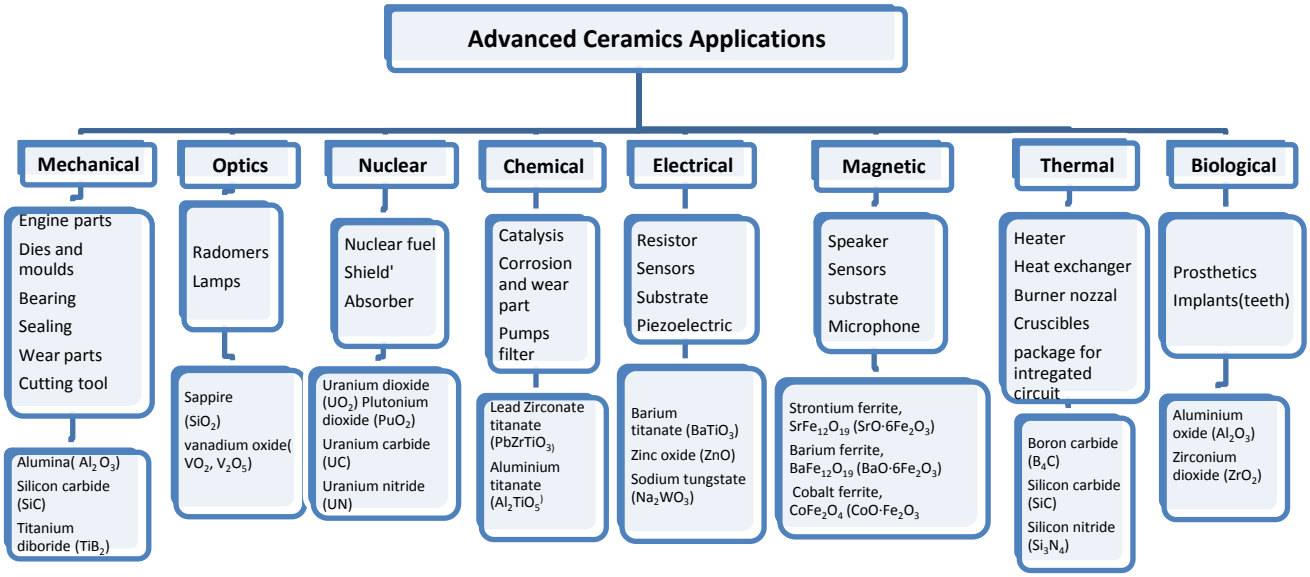

Figure 2.3 Advanced ceramics classification based on their properties and applications

2.5 Electro-Discharge Machining of advanced ceramics

Conventional machining process such as diamond grinding is the most commonly used for machining of advanced-ceramics, but this method is costly and inefficient. The high cutting force is also generated due to the high hardness of ceramics that results in quick wear of diamond cutting edges. The machined surfaces also found to have surface and subsurface cracks that lead to strength degradation in ceramics sample. [1]. Advanced ceramics are facing difficulty in machining as mostly process are slow and expensive. Electro-discharge machining (EDM) is an appropriate process to machine ceramics because of it's near the forceless non-contact type of machining that is independent of hardness and brittleness of material [13].

EDM allows machining complex shaped harden conductive parts in a flexible and accurate way. In order to enhance the response parameters in the EDM, many augments are provided with the primary configuration. These changes result in developing EDM based hybrid method for further process enrichment.

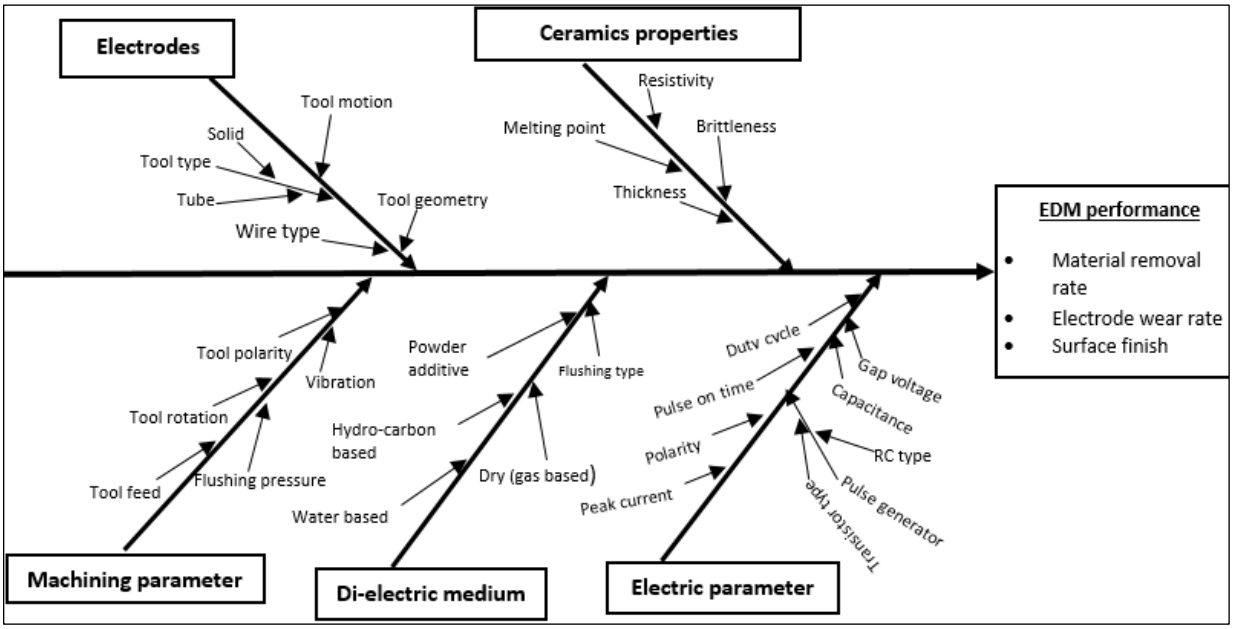

Figure 2.4 Fishbone-diagram of parameters influencing on EDM of advanced-ceramics

The capability of EDM to machine without any physical contact eliminates mechanical chatter and vibration that could damage ceramics during conventional machining. Thus, EDM holds the capability of machining and fabrication of low cost, tool, and parts from conducting ceramic blanks in a precise manner. The EDM performance of ceramics is affected by various parameters as shown in Fig. 2.4. Materials of any hardness can be cut as long as the material can conduct electricity [11]. Lauwers et al. [34] have successfully machined ZrO_2 ceramic-composites by wire EDM and explained there flakes removal in ceramics leads to speed up the material removal process. As shown previously, it is also claimed that even insulated ceramics could be machined by assisted electrode method in EDM. Advanced ceramics of high hardness and strength could be machined by EDM if their electrical conductivity exceeds a particular threshold value of the order of 0.01 S/cm (or resistivity less than 100 Ω.cm) [6]. While machining advanced ceramics by EDM, the

thermal spalling mechanism is more predominant material removal mechanism [1]**.** EDM is coming out to be a reliable potential technology for the machining of advanced-ceramics. There is also a number of EDM variants possible as shown in Fig. 2.5, showing the feasibility of machining various different type of shape and properties of the material.

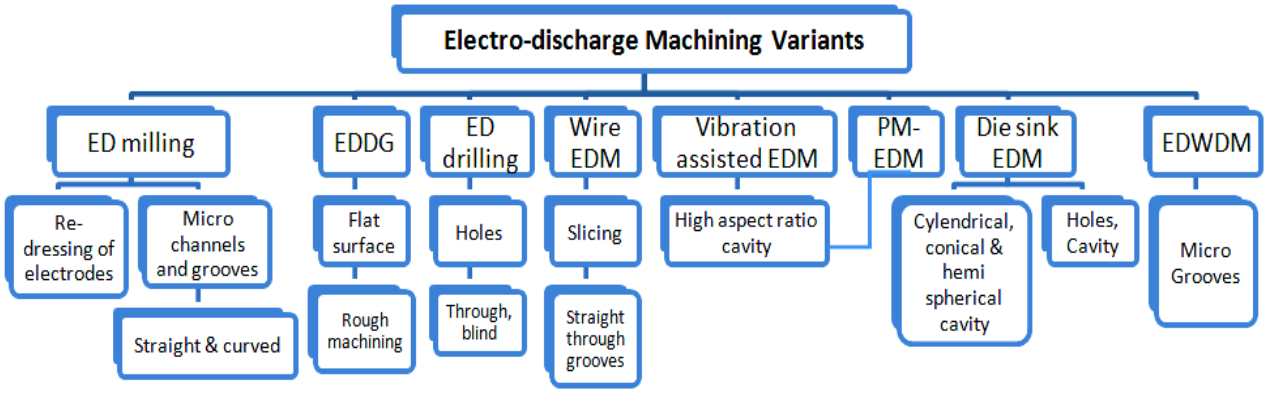

Figure 2.5 Electro-discharge machining variants

In the case of ceramics that are nonconductive in nature, an electrically conductive component like alumina, silicon nitride or Zirconia matrix, needs to be added to the material while maintaining or improving the mechanical properties [35]**.** The major research outcomes of machining of advanced ceramic with EDM and its hybrids are enlisted in Table 2.1. The conductive ceramics show better technological properties as they are easily machinable as compared to metal. Melk et al. [36] have successfully machined Zirconia reinforced MWCNT nano-composites with electro-discharge machining and concluded ceramics are not only machined by melting and vaporization but also in the form of flakes.

Table 2.1 Research conducted in the various field in ceramics machining by EDM since last decade

2017	Insulated zirconia SiC [37] , modeling of thermal stress, hybridization of process [38] [39] [40] , composite ceramics [41] [39] [37], technology table development [24] [30], surface layer control [42], micro machining, application [43]
2016	Composite ceramics [3], hybridization of process, surface improvement [44], parameter optimization, Micro machining [3], process study, insulated ceramics [44]

2015	Ceramics machining [45] , hybridization of process [45] [46] [47] [48], mechanism of material removal [48], Process parameter effect study [49] [50] [51] [52]
2014	Hybridization of process [53], ceramics-composite machining [54] [55], effects of control parameter [56] [57]
2013	Insulated ceramics [58] [27], Assisted layer control [27] [13] [59], micro machining, mechanism of material removal [59] [60], hybridization of process [61]
2012	Hybridization of process
2011	Machined surface improvement [62], ceramic-composite [63] [64] [62], hybridization of process
2010	Material removal rate study [65] [66], parameter optimization study [67]
2009	Machining characteristics [4] [68], Hybridization of process, machined surface study [69] [70], insulated ceramics [18]
2008	Hybridization of the process, a machined surface study [71], new technology development [72], ceramic-composite [34]
2007	Machined surface, characterization, modeling [73] [74], micromachining

Although, EDM has the remarkable advantage of machining complex micro-features in MMCs and CMC [75] [76] it also has the limitations of high energy consumption, low Material removal, high tool wear, and poor surface integrity. In the case of high aspect ratio micro-features, there is always the problem of poor flushing debris [77] [78]. To overcome these limitations, many researchers have come with the idea of hybrid EDM in both macro and microdomain. In hybrid μ-EDM, one more process simultaneously works with μ-EDM to improve the response parameters and overcome the limitation of μ-EDM i.e. low MRR. Baghel et al. [26] [79] have experimentally concluded MRR improved by 1.98 times under the influence of low-frequency vibration while machining of advanced-ceramics. They also machined Titanium Nitride Aluminium Oxide with diamond grinding assisted EDM and observed a significant improvement in MRR. Chen et al. [80] have studied the effects of hybridization of EDM with ultrasonic vibration and TiC particle and experimentally

concluded that although MRR, the surface roughness is improved with hybridization, heat affected zone (HAZ) was also observed near the machined surface. Zhao et al. [81] have experimentally concluded that powder mixed EDM helps for easier discharge because of large discharge gap.

Table 2.2 Major conclusions and finding in EDM of conductive ceramics

Sn.	Machining process	Work material	Major conclusions / findings / benchmarks
1	Electrical discharge machining (EDM)	Ti_3SiC_2 ceramic [71], zirconia reinforced MWCNT nano-composites [36], Titanium Nitride-Aluminium-Oxide Composite [64], conductive SiC [20], cobalt-bonded tungsten carbide (WC–Co), boron carbide (B_4C) and RB-SiC (SiSiC), SiC±TiB2 and sialon ±TiN [82],silicon carbide (SiC) ceramics containing graphene-nanoplatelets (GNPs) [37], aluminum oxide-based ceramic, multiwalled carbon nanotubes (MWCNT) [36]	Melting and decomposing [37], machining rate increases with the increase in the value of supply current and voltage, thermal shock cracks and loose grains in subsurface [71]. Melting/evaporation and spalling [64] are the mechanisms of material removal. In ceramics, the material is also removed by a thermal shock-induced fracture in which material is released as large flakes [82] [36]. The periphery of the drilled holes was free from bulging [64]. The presence of cracks, flakes, and re-solidified metal lead to rough machining of ceramics [20].
2	Ultrasonic cavitation-assisted micro-EDM	Reaction-bonded SiC	Ultrasonic vibration becomes more significant in the presence of carbon nanoparticles in a dielectric fluid, leads to better MRR [55].

Sn.	Machining process	Work material	Major conclusions / findings / benchmarks
3	Powder mixed electric discharge machining (PMEDM)	Aluminum/alumina metal matrix composite [50], reaction bonded silicon carbide [83], SiCp/Al composite [61], Ti-6Al-4V-ELI composite [84]	An increased in MRR and low surface roughness is observed as compared to conventional EDM [50] [83]. The corrosion resistance is increased as the roughness of the machined surface is decreased by 31.5 % and wear resistance is also observed to increase by 100 % [61]. Low pulse current and high concentration of particles in a dielectric, enhance the material transfer mechanism [84].
4	Wire electrical discharge machining (WEDM)	TiN/Si_3N_4 nano-composite ceramics [56], WC-based and ZrO2-based composites [62], ZrO2 ceramic composites [34], 65% SiC/A356.2 composite [42], ZTA–TiC ceramics [31], Al203+ TiC and Sialon [1]	Craters, droplets, micropores, and microcracks were observed on the machined surface. The mechanisms of material removal are melting, evaporation and thermal spalling [56]. The machined surface was more finished and having lower flexural strength compared to grinding [62]. Spalling increases cutting speed due to the low strength that facilitates crack formation and propagation [34]. The recast layer thickness is more in the denser reinforced matrix, this is due to the high rate of thermal spalling [42]. The thermal spalling erosion is the main mechanism of material removal leading to a damaging effect on the surface [1].

Powder mixed-EDM for improving process parameters is also explored in recent year. In PM-EDM, foreign particles are mixed in the dielectric in a view of improving its dielectric strength as machinability in EDM is highly depended on dielectric properties and presence of micro powder accelerates the frequency of discharge. Many researchers have been working in PM-EDM to increase surface quality and polishing process performance i.e. discharges process modification. Various powders that include Aluminium, chromium, copper, etc. that are used by researchers to improve the EDM performance [78]. Shabgard et al. [85] have used carbon Nanotube (CNT) mixed EDM on Ti-6Al-4V alloy and concluded that by adding CNTs in the dielectric, the length and size of microcracks are reduced. In powder mixed μ-EDM (PM-μEDM), foreign particles are mixed into dielectric in view of decreasing the spark gap and increasing the spark frequency so that machinability of the part can be improved [81] [86]. Marashi et al. [87] have reviewed powder mixed EDM and concluded that powder mixed EDM facilitates producing micro parts with high surface quality. Balbir et al. [86] have experimentally observed that while machining AA6061/10%SiC Composite with tungsten electrode by PM-EDM, The MRR is improved by 48.43 % and recast layer is reduced by 42.85 %. Deepak et al. [88] have machined Inconel-718 with abrasive mixed electro-discharge diamond grinding and concluded that process parameters are significantly improved with the inclusion of powder in the dielectric. Long et al. [89] have machined SKD61, SKD11, and SKT4 die steels using titanium powder mixed EDM and concluded that MRR is improved by 42.1 % as compared EDM. Kung et al. [19] have machined cobalt bonded tungsten carbide with aluminum PM-EDM and observed a significant improvement in both MRR and EWR. The ability of powder mixed-μEDM to the machine in advanced-ceramics in microdomain is needed to explore in order to expand the applications of potential ceramics such as TiN-Al_2O_3 ceramic-composite. Table 2.3 is showing various researchers worked on PM-EDM.

Table 2.3 Research and outcome in powder mixed electro-discharge machining

SN	Sample	Powder Mixed	EDM Process Parameters	Outcome of PM-EDM
1	Copper [78]	MoS_2 Powder Concentration (g/l)=2, Powder size (mm)=0, 2, 5	Type - RC generator Capacitance(pF)- 3300 Voltage (V)- 110 Electrode- Brass Dielectric fluid- kerosene	-Increasing the material removal rate and improving surface quality
2	Reaction-Bonded Silicon Carbide (RB-SiC) [59]	CNF Concentration(g/l)=06-0.28 diameter = 0.15µm, length = 6–8 µm	Type - RC generator Capacitance(pF) - 10,110,220 ,330 Voltage(V)- 60-110	-Materials migration mechanism (MMM) is observed during machining. -Carbon nano-fiber addition can significantly reduce the deposition of tool material on the workpiece surface.
3	SiCp/Al composite Electrode [61]	Al powder Concentration (g/l)=35 Particle sizes <2 µm	Current-0.5 A Pulse time- 12 s Pulse interval- 40 s Gap voltage-50 V	-Surface properties improved -Roughness decreases by 31.5% in PMEDM as compare to EDM. -The corrosion resistance is also better and the wear resistance increases by almost 100%
4	Hardened mould steel AISI H13 [90]	silicon powder particles concentration(g/l) = 1,2,3,4,5,10,20	Electrode - Copper Dielectric - kerosene- Castrol SE Fluid 180)	-Recast layer thickness is significantly reduced. -The increase of the silicon content for higher values only slightly reduces the crater dimensions.

SN	Sample	Powder Mixed	EDM Process Parameters	Outcome of PM-EDM
5	OHNS die steel D2 die steel H13 die steel [70]	Tungsten powder Concentration (g/l)=15 Particle size=30-40 µm)	Sparking voltage - 135 ± 5% V Peak current - 2, 4, 6 A Pulse on-time- 5, 10, 20µs Pulse off-time -38, 57, 85 µs	-Suspended powder particles can react with carbon (from the breakdown of the hydrocarbon dielectric) at high temperatures of the plasma channel to form carbides. -Micro-hardness of the machined surface is increased by more than 100%.
6	AISI D2 steel [47]	Ti Nano-powder Concentration (g/l)=2 Particle size=40-60 nm	Voltage (V)- 120 Duty factor (%)-60 Dielectric fluid-Hydrocarbon oil	-Material removal rate (MRR) and surface roughness significantly improved. -The addition of Ti Nano-powder dielectric enhanced the morphology of machined surface as a result of shallower craters and the formation of low-height ridges.
7	CK45 steel [91]	Al_2O_3 Fine abrasives, density =2.9 g/cm^3, thermal conductivity= 1–2 W/cmK, electrical resistivity= 103 µΩcm	Electrode- Copper Dielectric- Kerosene Peak current (A)- 5–11 Pulse-on time (µs)- 50 to 150 Voltage (V)- 50–70 Duty factor-0.5	-Suspending Al_2O_3 fine abrasive powders into the dielectric oil of EDM machine produces more widened gap compared to the pure case. - Smooth surfaces are obtainable at low currents and pulse-on times

SN	Sample	Powder Mixed	EDM Process Parameters	Outcome of PM-EDM
8	OHNS die steel (hardened and tempered) [92]	manganese powder concentration (g/l)=15	electrode - Copper Discharge current (A)- 2, 4, 6 Pulse on-time (μs)- 5, 10, 20 Pulse off-time (μs)- 38, 57, 85	-Microhardness of the machined surface has improved with powder mixed EDM.

2.6 Micro chemical-reactors

The micro-chemical reactor is a device in which chemical reactions take place in a confined volume with a typical lateral dimension less than 1 mm as shown in Fig. 2.6. The most common form of such confinement is microchannels. The miniaturization of chemical processes using microchannel based micro-reactor exhibits a significant advantage over existing conventionally used reactors such as improvement in energy efficiency, reaction speed, yield, safety, reliability, scalability, a finer degree of process control and short diffusion distance [93] [94].

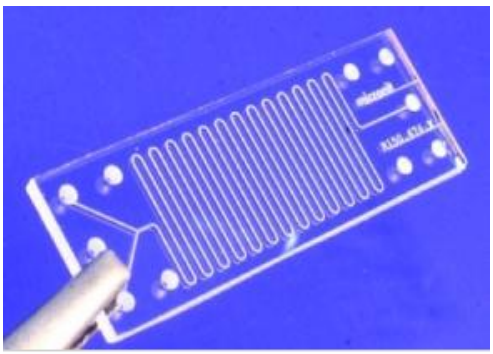

Figure 2.6 Micro-chemical reactors [131]

At the beginning of chemical experimentation i.e. in the age of alchemy, a chemical substance like sulphuric acid or ammonia were much more valuable than gold and very small reaction-vessels were used to economize the precious materials. These days, chemical engineers try to use less material for chemical reactions in order to avoid

consuming large portions of the product for analysis; this job is fulfilled by microreactors. A microreactor is a casing for performing reactions in which fluid follows the pulsating flow and the channel's dimensions in it are in the range of few millimeters [95].

2.6.1 **Fundamentals of microreactors**

Microreactor is a concept aimed at notable intensification in the chemical processing plant. The process intensification takes place to design the reactor in which a huge reduction in the physical size of the plant is taking place while aiming the same objective. Therefore process intensification encompasses both novel apparatus and techniques that are aimed to have improvements in production and processing [95]. The use of microreactors is required for sustainable developments of the plant; the following are the key benefits of using micro-chemical reactors.

- System size reduces
- Energy consumption reduces
- Chemical waste reduction

  As a result, hazard-free, compact, sustainable and energy-efficient technologies are obtained.

The chemical-reactors miniaturization leads to two different types of phenomenon that are observed: surface effects and volume effects. The surface effects dominate in microreactors as compared to volume effects. The downscaling of the chemical reactor leads to changes in the following properties:

- Diffusion distance of mixing or heat transfer decreases
- The concentration and temperature gradient increases
- The specific surface area increases.
- The specific interfaces increases

2.6.2 **The advantages of microreactors in chemical processing**

Micro-reactors are used to synthesize material more effectively; the primary benefit is to enable enhanced mass transfer, thermodynamics, and high surface to volume ratio as well as engineering advantage in handling unstable intermediates. These days the chemical used for chemical-synthesis are of analytical grade and used without further purification,

thus they are very reactive in nature. Micro-chemical reactors provide the following benefits in chemical processing:

2.6.2.1 Micro total analysis system (μ-TAS)

Miniaturization of chemical reactors provides the concept of the chip-based micro-channel system by integrating various functional modules for complete analysis [96]. Such systems provide an opportunity to create a complete analytical microsystem by integrating various function modules like sample preparation, reaction, and detection in a single chip. Guijt et al. [97] have studied systems that go one step further and are capable of periodically executing the analytical protocol to translate the chemical information into electronic data as shown in Fig. 2.7.

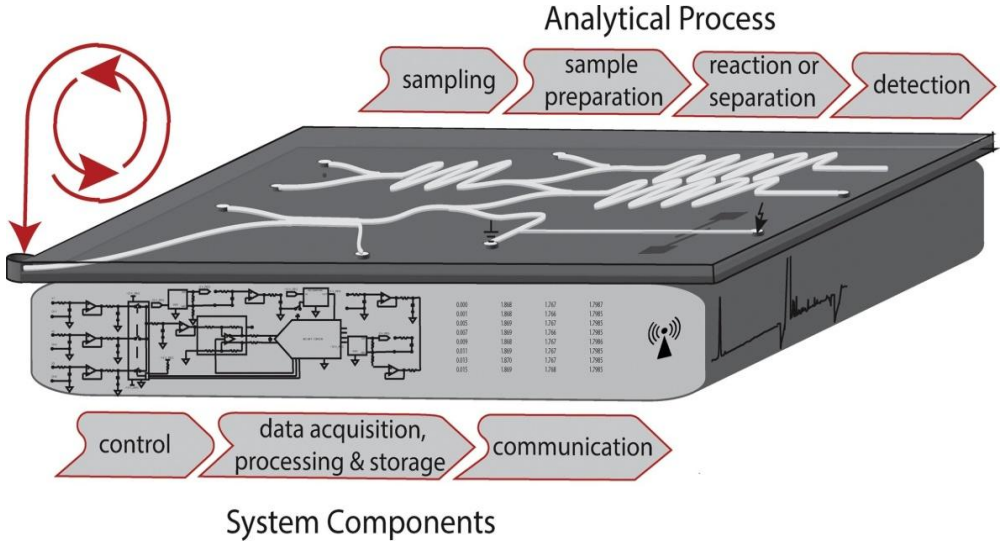

Figure 2.7 An example of micro-TAS analytical processing [79]

2.6.2.2 Green chemistry and sustainable development

Green chemistry refers to the optimum use of material, energy with sustainable use of environmental resources. In this area, microreactors fulfill the criteria of sustainability as they possess high selectivity, high efficient heat management and use high reactant concentration thus reducing solvent volume. The planned use of available chemical resources leads to sustainable development.

2.6.2.3 Micro-fluidic tectonics (µ- FT)

In microfluidics, the behavior of fluid is precisely controlled in a miniaturized system that typically ranges in sub-millimeter scale at which capillary penetration governs mass transport. Micro-fluidics becomes significant for the following reasons:

- Working with a small volume
- Increase in the speed of reaction
- Lower power consumption
- Reduction in the cost of reagent
- Higher surface to volume ratio
- Low Reynolds number
- Minimizes the size of the chip

Micro-channel flow facilitates the generation of mono-droplets. At the micro-level, surface tension and inertia force dominates thus encourage the flow in the form of droplet cluster as shown in Fig. 2.8.

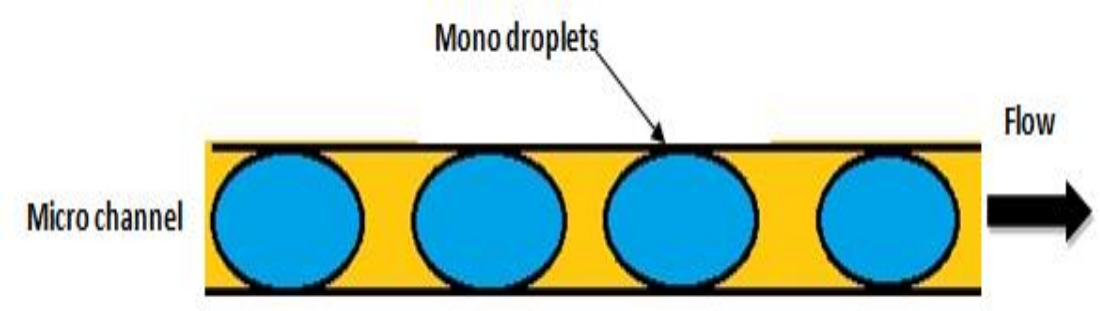

Figure 2.8 Liquid flows in the microchannel in the form of mono droplets

Emulsion and double emulsions can be used for nanoparticle synthesis, drug micro-encapsulation, and active substance encapsulation. Microdroplets can be used as single microreactors in the bio-detection system. Tectonics is the science of assembling or shaping of material during construction. Microfluidic tectonics (µFT) is seen as a new strategy to generate an organic and biomimetic design for microfluidic systems.

2.6.2.4 Mixing and heat transfer

The confined channel flow mainly depends on the diffusion mixing mechanism. The micro-channel mixing leads to a decrease in diffusion distance and consequently increase

in mixing rate. Apart from the enhancement of mixing speed, a very uniform spatial distribution of mixing achieved with micromixers. There is also a significant increase in heat transfer rate by microchannel processing [95]. Table 2.4 shows the numerical example of an increase in surface area on the miniaturization of industrial reactors.

Table 2.4 Numerical example showing an increase in the normalized specific surface by miniaturization [77]

Scale of reactor	**Volume/ internal dimension**	**Normalized specific surface**
Production	30 m^3	1
Laboratory	11-10^{-3} m^3	30
Micro	30 μm	3000

Zhongyuan et al. [93] have successfully fabricated microchannel based microreactors by a novel kind of the capillary-based photo-catalytic microreactor with TiO_2 nano-particle coated ZnO nano-rod arrays grown in the inner wall of the capillary and come out with the highly efficient microreactor.

2.7 **The scope of machining of ceramic-composite by hybrid EDM**

As we know, advanced ceramics are the emerging class of material known for its high strength, chemical inertness, high toughness, and excellent wear resistance. They have a high potential for a wide variety of industrial applications such as wear parts, micro-sensors, micro fuel pump, bearings and medical implants [51]. Although ceramics possess phenomenal physical properties, ceramic's full-scale applications are still not achieved due to difficulties in processing and high manufacturing cost [32]. A classification of advanced ceramics based on their applications in various fields is shown in Fig. 2.3. The main problem with ceramics is that they are very difficult to machine material [5]. Diamond grinding is used commonly for machining of ceramics, but this method is expensive and inefficient. Higher grinding forces are induced in this process leading to quick decay of tool edges. While machining by diamond grinding, the strength degradation of ceramics is also there due to the surface and subsurface cracks [1]. Advanced ceramics are facing difficulty in conventional machining as most processes are

slow and not able to produce the desired surface. The capacity of EDM to machine without any physical contact eliminates mechanical chatter and vibration that could damage ceramics during conventional machining. Thus, EDM holds the capability of machining and fabrication of low-cost tool, and parts from conducting ceramic blanks in a precise manner. As shown previously, it is also claimed that even insulated ceramics could be machined by assisted electrode method in EDM.

2.8 **Applicability of TiN-Al_2O_3 ceramic-composite as micro-chemical reactor**

Metals are more tends to get corrode in critical working conditions in terms of temperature, pressure and hazard chemicals. Corrosion is the deterioration or destruction process of metals and alloys in the presence of an environment by chemical or electrochemical means. In simple terminology, corrosion processes involve the reaction of metals with environmental species; on the other hand, ceramics are generally chemically inert. The advanced ceramics are suitable for microreactors fabrication as they are chemically inert in nature and also have hot hardness so they could work in critical working conditions more accurately. Micro-reactors of advanced ceramics like TiN-Al_2O_3 ceramic composite has the potential to be used in plasma-assisted chemical reactors as it could sustain very high temperature as compared to metal. A thermal plasma can provide an ultra-high-temperature environment (i.e. 10^3-10^4 K), which is not reachable in conventionally used metal reactors. Plasma-assisted chemical processes and ceramics-reactors have drawn more and more attention not only in academic research but also in industrial applications [98]. Fusion reactors which provide enormous thermal energy at a higher temperature and advanced ceramics are good while working on higher temperature [99]. TiN-Al_2O_3 ceramic-composite could be used as the material of the chemical reactor in plasma-assisted chemical processes. Fabrication of micro features such as blind holes, high aspect ratio holes and microchannels will pave the way for developing micro-reactors out of TiN-Al_2O_3 ceramic-composite.

2.9 **Research Gaps**

Advanced engineering ceramics have potential applications in industries because of their superior mechanical properties such as high hardness, high compressive strength, chemical inertness, and high abrasion resistance. EDM process and its hybrid variants

enable us to machine advanced ceramics and ceramic-matrix composite (conductive ceramics). To fabricate miniaturized parts on hard to cut material and composite with high material removal rate and accuracy, the EDM process is extremely beneficial. From the literature review presented, it is evident that insulated ceramics could be machined by assisted electrode method in EDM. Although various researchers have claimed to have machined non-conductive ceramics by EDM, the repeatability of the experiments are not ensured. The ED machining of non-conductive ceramics by various assisting electrode needs to be explored further in terms of the exact mechanism. Once the process is established the process parameters are required to be optimized for its use in industry as non-conductive ceramic machining by EDM is currently limited to lab experiments only. Assisted-electrode method of machining has great potential for machining ceramic-composite and non-conductive ceramics with high accuracy, precision and surface quality that are very difficult and costly to the machine by any other conventional machining process. Insulated ceramics machining area needs to be explored more precisely so that ample opportunities for its industrial use can be opened.

Moreover, conductive ceramics, ceramic-composite, ceramic-metal matrix (CMC) machining by EDM and its variants need to be investigated in terms of developing a novel hybrid machining process that leads to better-machined surface and to optimize material removal rate in a cost-effective manner. The process physics of machining advanced ceramics (conductive and non-conductive) in terms of simulations models, metrology techniques and industrial implementation should be taken into consideration. The conductive ceramics and ceramic-composites have huge potential to be used in the various applications where metals tend to fail. The ceramic-composite machining process needs to be explored extensively as they provide technological properties that are suitable for a large number of applications but there are few studies regarding its machinability thus failing to meet the demands.

Table 2.6 Research possibilities in various areas in EDM of advanced ceramics and possible outcome

Research Area	Research Needed	Possible Outcomes
Machinability of Ceramics, ceramic-composites	In hybridizing the process to machine non-conductive ceramics as well as ceramic-composite by assisting electrode method. Hard and difficult to machine material.	Products of better performance than metal.
Material removal rate	Improve the dielectric properties. Optimized the process parameter. Hybridizing the process.	Better MRR and Lower machining cost.
Electrode wear rate	Use of coated tool, the composite tool. Tool geometry change. Optimized the input parameter.	lower the EWR and also a reduction in machining cost.
Surface integrity	Improve the dielectric property of the fluid by minimizing the heat-affected zone (HAZ). Optimized input parameter to minimized microcracks, recast layer.	More finished surface with low HAZ.
Geometrical characteristics	Tool shape modification. Hybridizing the process.	Reduction in taper angle. Reduction in radial overcut. Reduction in corner radius.
Aspect ratio	Dielectric circulation improvement Tool shape improvement Hybridization of the process (V-EDM, PM-EDM)	Deep holes and shapes can be fabricated. Micro features can be fabricated.

Dielectric	Environment-friendly dielectric-fluid. Sustainable fluid (waste vegetable oil, reusable oil).	Lower machining cost. Reduction of hazardous effect on the environment

Although EDM is one of the most significant machining processes for hard to machine materials, Rare studies have reported on a fundamental understanding of electro-discharge machining and its variants for ceramic-composite. In order to improve the response parameters of the EDM process, many augmentations have been provided with the basic configuration of EDM as shown in Table 2.3. These augmentations result in the development of EDM based hybrid methods for further process enrichment. Based on the literature review following research gaps are found:

1. Studies are required for the development of the technological-tables for ceramics composites that are capable of controlling major EDM process parameters to meet the required material removal rate and quality of the surface. Rare studies are reported on developing technological tables for TiN-Al_2O_3 ceramic-composite.
2. Studies are needed on developing a numerical and analytical model that considers material removal mechanism or physics in less conductive ceramics, as the presence of a second insulating phase makes material removal unanticipated. In the author's knowledge, no study is reported in this regard.
3. Use of hybrid micro-machining technologies to overcome the machining limitations for advanced ceramics and their composites are sparsely reported i.e. Diamond grinding assisted EDM, Vibration-assisted EDM and powder mixed EDM for TiN-Al_2O_3 ceramic-composite has not been explored.
4. Development of newer technology for multi-purpose micromachining of advanced ceramicscs and their composite with regard to improvement in surface finish, accuracy, and precision of the machined micro-features needs exploration.
5. On-machine tool fabrication for the reduction in tooling cost; on-machine measurement to meet the accuracy, precision requirements and improve repeatability also needs to be investigated for these materials.

6. Studies are required on the topography of machined surfaces in the view of low machinability as material properties and surface characteristics change after machining.

7. Miniaturized part development by micro-EDM and its variants with energy optimization for these materials needs to be explored.

8. Cost-effectiveness of micro-EDM and hybrid micro EDM also needs to be considered for these materials.

2.10 **Objectives**

Based on the research gaps, the primary aim of this work is to investigate the machinability of TiN-Al_2O_3 ceramic-composite due to its widespread applications in many fields. To identify the scope of studies, it was decided to undertake the investigations on machinability of TiN-Al_2O_3 ceramic-composite by hybrid EDM process aimed at improving and enhancing the performance of μ-EDM keeping their micro-reactor application in mind, while fabricating micro-features like blind micro holes, through holes, high aspect ratio holes, micro-channels, etc. have been studied. In this regards the following objectives have been set to accomplish:

1. To study the EDM process characteristics and EDM variants with regard machining of conductive as well as non-conductive ceramics for their potential application in micro-chemical reactors.
2. Experimental investigation and parametric optimization on the feasibility of achieving high material removal rate and better quality surfaces with Diamond Grinding Assisted EDM of TiN-Al_2O_3 ceramic composite and also study the mechanism of material removal.
3. Experimental investigation on the feasibility of machining by ED milling and enhancement of performance parameters for fabricating micro-features on the TiN-Al_2O_3 ceramic composite.
4. An experimental investigation, parametric optimization, and feasibility of machining of powder mixed micro-electro-discharge machining to improve the response parameters in the machining of TiN-Al_2O_3 ceramic-composite.

3. MATERIALS AND METHODS

In this chapter, material procurement, properties of the material used, experimental setup and experimental procedure adopted for fabricating micro-features on Titanium Nitride Aluminum Oxide Ceramic-Composite with hybrid EDM process are explained. A brief introduction to the machinery, tool-electrodes, equipment and the dielectric used in this study is also given.

3.1 Titanium Nitride-Aluminum Oxide ceramic-composite material

Titanium Nitride-Aluminum Oxide (TiN-Al_2O_3) is a newly developed advanced ceramic-composite that could work at an elevated temperature as it possesses high resistance to thermal degradation. Moreover, as TiN and Al_2O_3 are high wear and abrasion-resistant materials, this ceramic-composite has a good potential to be used as cutting tool material [4]. Titanium Nitride-Aluminum Oxide (TiN-Al_2O_3) is prepared by hot pressing, the starting powders (TiO_2 and AlN) at 1450 °C for 30 minutes with graphite die and punch (70 mm in diameter) at Central Glass and Ceramic Research Institute (CGCRI) Kolkata. The inside wall of the die and outside wall of the punch was coated with Boron Nitride for lubrication and protection of the powders from reaction with graphite. The average roughness value (Ra) of these sintered samples was measured with a contact type surface-roughness measuring instrument (Taylor Hobson Surtronic 100). The Ra value of these samples ranges from 7.43 μm to 11.26 μm. The samples (Fig. 3.1) were then characterized by X-Ray Diffraction for phase analysis, Ultrasonic test for elastic modulus, Universal Testing apparatus for 4 points flexural strength, Hardness Tester for micro-hardness and Laser Flash test for measuring thermal diffusivity.

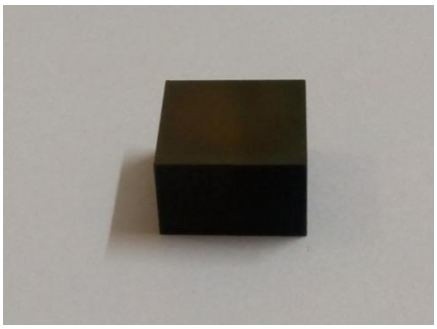

Figure 3.1 Titanium-Nitride Aluminium Oxide ceramic-composite sample

Table 3.1 Physical properties of TiN-Al_2O_3 [14]

TiN-Al_2O_3 ceramic-composite (workpiece)	
TiN content	66 mol%
Density	4342 kg/m^3
Vickers's hardness	20 GPa
Young's modulus	270 GPa
Strength (flexural)	446 MPa
Thermal conductivity	21$\pm$ 1 $Wm^{-1}K^{-1}$
DC electrical resistivity	0.25 Ω.m

Bulk densities were measured by Archimedes method and Electrical conductivity was measured by a semiconductor device analyzer with 4 point contact probe station. The physical properties of the composite are presented in Table 3.1 [14]. High chemical stability, corrosion-resistant, low friction coefficient, and hot hardness, etc. are the key properties responsible for its application in a component of complex shapes and structure specifically as a cutting tool, micro-chemical reactors, and high-temperature heat exchanger.

3.2 **Machine tools**

3.2.1 **Diamond grinding assisted EDM**

Diamond grinding assisted EDM (DGA-EDM), a hybrid of diamond-grinding and electro-discharge machining is used for machining of TiN-Al_2O_3 ceramic-composite for smooth surface generation. These experiments are carried out on modified Electronica® ZNC ENC-35 electro-discharge machine with diamond abrasive grinding wheel setup. The grinding wheel is attached to the EDM machine with the help of direct current motor and V-belt. The specifications of the grinding wheel are given in Table 3.3. The specifications of ENC-35 are given in Table 3.2. This setup consists of grinding spindle wheel assembly in which the axis of the wheel is kept parallel to the machine axis. The V-belt drive is also mounted in the set up between DC motor and wheel axel for the grinding wheel rotation. The diamond-bronze grinding wheel is used as tool electrode while the servo motor is used to maintain the inter-electrode gap (IEG). A fixture is used to hold the workpiece in the dielectric tank filled with de-aromatized-hydrocarbon oil as shown in Fig. 3.2 & Fig. 3.3.

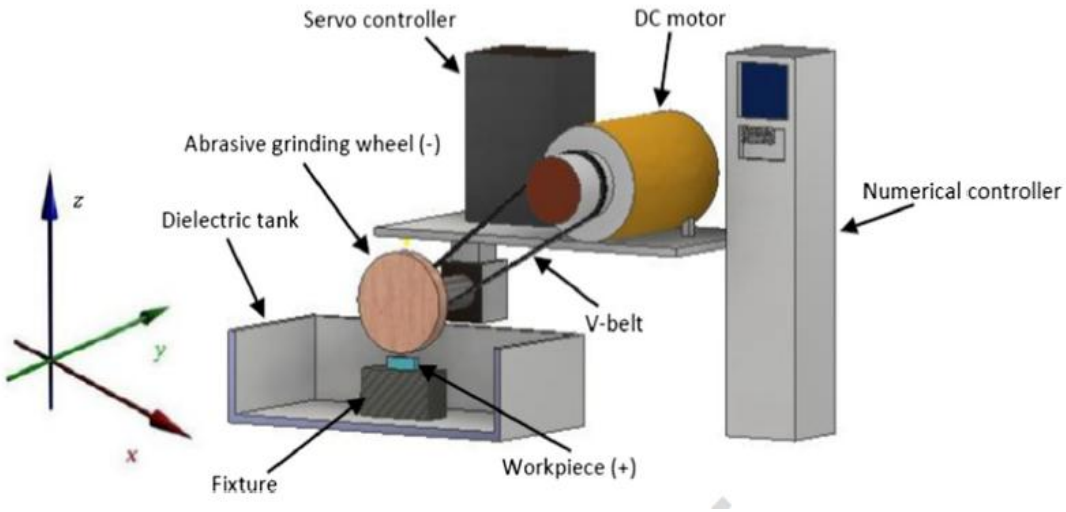

Figure 3.2 ENC-35 setup with an abrasive grinding wheel

Table 3.2 Machining specifications ENC-35 setup

Specification of ENC-35 grinding wheel	
Description	Specifications
Axis movement	Z-direction numerically controlled
Design	Fixed column, moving table
Power input	415 V, 3 phase supply
Current capacity	1-35 A
Open circuit voltage	200 V Direct current
Dielectric capacity	400 liter
Machine travel capacity	X-300 mm, Y-200 mm, Z-250 mm

Table 3.3 Diamond grinding wheel specifications

Diamond grinding wheel specifications	
Diamond wheel diameter	100 mm
Thickness	10 mm
Bore diameter	32 mm
Abrasive used	Diamond
Bonding material	Bronze
Abrasive concentration	75 %
Depth of abrasive	3 mm

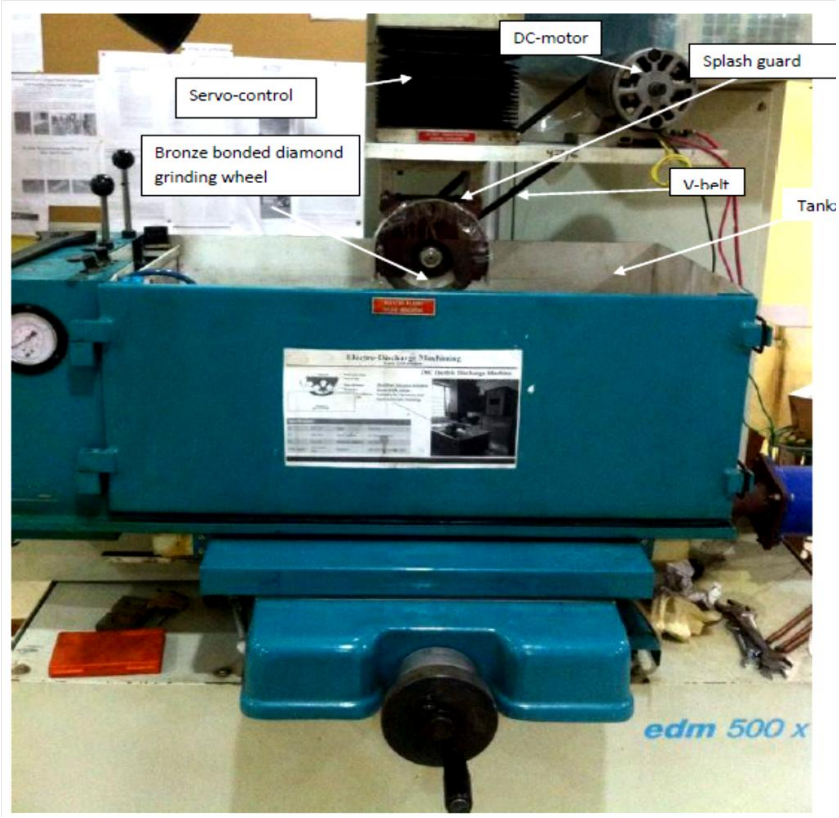

Figure 3.3 ENC-35 setup with grinding wheel

3.2.2 **Hybrid micro EDM**

All the experiments for the fabrication of microfeatures are conducted on Hybrid µ-Machine (Mikrotools DT-110i) shown in Fig. 3.4. The hybrid micro-EDM machine has the ability not only to perform multiple micro-machining processes but it also allows on-machine tool fabrication. The machine specifications are shown in Table 3.4.

Table 3.4 Specifications of DT 110i hybrid micromachine

Specifications	**Values**
Spindle speed	Low (0-2000 rpm), high (2000-5000)
Power requirement	230 V, 50 Hz
Machine travel capacity	X -200 mm, Y -100 mm, Z -100mm
AC servo motor (spindle head)	100 W
Voltage range	80- 130 V
Capacitance range	0.0001-0.4 µF

Figure 3.4 DT-110i Hybrid micro-EDM

It is accessorized with a PC based CNC motion controller with 0.1 micrometers (100 nanometres) programming resolution. It is a high precision machine tool based on RC pulse generation. It is equipped with a resolution of 0.1μm, the accuracy of +/- 1 μm and repeatability of 1 μm. It also includes an integrated CCD based camera for measuring the smaller dimensions.

3.2.3 Electrode material

Microelectrodes of pure tungsten in solid cylindrical rod form of size 0.2, 0.3 and 0.5 mm in diameter are used for fabrication of micro-features.

Table 3.5 Properties of tool material

Properties	Value
Melting point	3410 °C
Young's modulus	440 GPa
Coefficient of thermal expansion	4.36×10^{-6} m/m °C
Density	19300 Kg/m^3
Vickers Hardness	3430 MPa

99 % pure Tungsten is used as the material of the tool. Tungsten is well known for its hardness and high melting temperature. Major properties for Tungsten electrodes are enlisted in the following Table 3.5.

3.2.4 **Dielectric fluid**

The dielectric fluid serves as a medium to the spark in electro-discharge machining. Dielectric fluid not only helps in spark creation but also flushes away the debris and cools the workpiece and tool. It should have a higher resistivity and superior flushing ability. Commercially available dielectric "Total diel 7500 IN" is used as a dielectric medium in Diamond grinding assisted EDM. It has superior electrical resistivity. "Total diel 7500 IN" dielectric fluid is a mixture of hydrocarbon and additives, the properties of dielectric are shown in Table 3.6.

Table 3.6 Properties of dielectric fluid used in ENC-35

"Total diel 7500 IN" dielectric fluid used in ENC-35®		
Characteristics	**Reference method**	**Value**
Appearance	Visual	Clear colorless liquid
Density at 29.5 ° C	ASTM 1298	0.796
Flashpoint	ASTM D 92	110 °C
Viscosity at 40 °C	ASTM D 445	2.0 mm^3/s
Aromatics ,% by weight	Internal	0.1

Table 3.7 Properties of dielectric fluid used in DT110i hybrid micro-machine

"SUN EDM OIL" dielectric for DT110i Hybrid µ-Machine®		
Characteristics	**Reference method**	**Value**
Appearance	Visual	Bright and clear
Density @ 25 °C	D-1298	0.78 Kg/m^3
Flashpoint	D-92	103 °C
Pour point	D-97	-21 °C
Viscosity at 40 °C	D-445	3.0 mm^3/s
Aromatics %	SMS 2728	% m
Di-electric strength	IS-6792	45 MV/m

"SUN EDM OIL" is used in DT110i Hybrid μ-Machine. It is made of de-aromatized Hydrocarbons and additives. SUN EDM oil is a high quality, odorless, low viscosity dielectric which is a superior alternative to smoky, smelly viscose EDM oil. Its properties are given below in Table 3.7.

3.3 Experimental procedure

3.3.1 Machining of TiN-Al_2O_3 ceramic-composite by DGA-EDM

Diamond Grinding Assisted Electro-Discharge Machining for creating smooth surfaces on Titanium Nitride Aluminium Oxide is carried out on ENC-35 which is complemented with in-house fabricated "Diamond grinding attachment (DGA)". This diamond grinding setup consists of the diamond-bronze grinding wheel as tool electrode. The servo controller in it is used to maintain an inter-electrode gap (IEG) as shown in Fig. 3.3. The diamond grinding setup is connected with the help of V-belt and direct current motor for transferring power from a direct current motor to grinding wheel. The specifications of the wheel motor setup are given in Table 3.8.

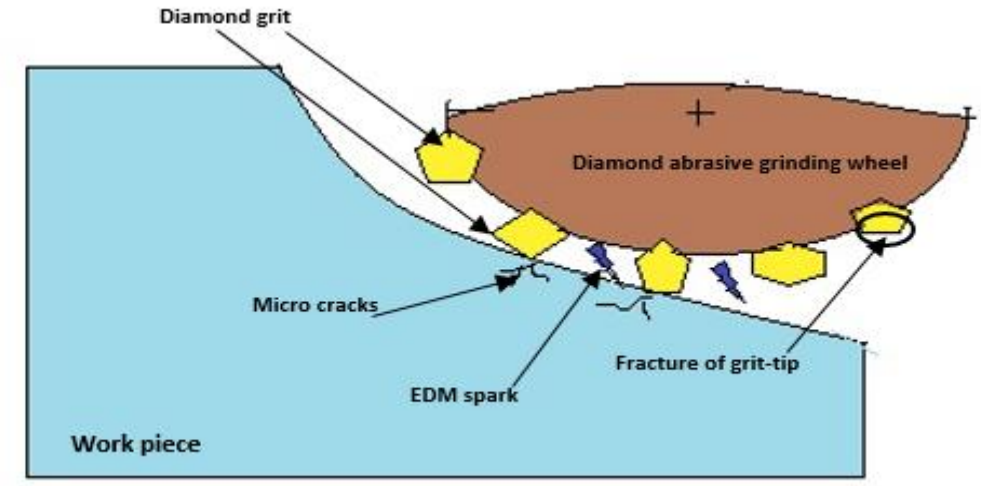

Figure 3.5 Schematic representation of DGA-ED Machining

In the machining zone, EDM spark takes place when there is an inter-electrode gap (IEG). In DGA-EDM, diamond grinding and EDM simultaneously works to improve the response parameters as shown in Fig. 3.5. For this study, the machinability of TiN-Al_2O_3 ceramic-composite is studied. MRR is experimentally obtained by measuring the total weight

loss and machining time for each experiment using a WENSOR electronic balance for precision weight measurement (before and after machining) and a stopwatch for measuring the machining time. The independent process parameters, their coded values, and level of parameters with their units are given in Table 3.9. Experimental design table is shown above (Table 3.10) with three input parameters and seven center points.

Table 3.8 Wheel motor setup specification

Wheel motor setup	**Value**
Direct current motor	HP:2, RPM:4600max
Horizontal shaft	Diameter 32 mm
V-Pulley diameter	32 mm

Table 3.9 Details of input parameters for ENC-35

Sn	**Input parameter**	**Description**	**Range (Low –High)**	**Unit**
1	Wheel rotation speed (S)	It is the rotational speed of grinding wheel	400-1200	rpm
2	Peak current (I)	It is the peak value of the current flowing through the electrode for giving pulse duration	3-9	A
3	Pulse on time (t_{on})	It is the time interval between continuous sparks	50-150	µS
4	Duty factor (DF)	It is the percentage of one period in which a signal or system is active	0.60-.070	%

Table 3.10 Experimental design matrix for DGA-EDM

Std. Order	**Run Order**	**Pt. Type**	**Blocks**	**S (rpm)**	**I (A)**	**T_{on} (µs)**	**DF (%)**
4	1	1	1	1200	9	50	0.60
25	2	0	1	800	6	100	0.65
17	3	-1	1	400	6	100	0.65

27	4	0	1	800	6	100	0.65
15	5	1	1	400	9	150	0.70
10	6	1	1	1200	3	50	0.70
18	7	-1	1	1200	6	100	0.65
5	8	1	1	400	3	150	0.60
22	9	-1	1	800	6	150	0.65
9	10	1	1	400	3	50	0.70
28	11	0	1	800	6	100	0.65
31	12	0	1	800	6	100	0.65
21	13	-1	1	800	6	50	0.65
12	14	1	1	1200	9	50	0.70
26	15	0	1	800	6	100	0.65
8	16	1	1	1200	9	150	0.60
16	17	1	1	1200	9	150	0.70
7	18	1	1	400	9	150	0.60
2	19	1	1	1200	3	50	0.60
24	20	-1	1	800	6	100	0.70
19	21	-1	1	800	3	100	0.65
13	22	1	1	400	3	150	0.70
14	23	1	1	1200	3	150	0.70
23	24	-1	1	800	6	100	0.60
30	25	0	1	800	6	100	0.65
3	26	1	1	400	9	50	0.60
6	27	1	1	1200	3	150	0.60
20	28	-1	1	800	9	100	0.65
1	29	1	1	400	3	50	0.60
11	30	1	1	400	9	50	0.70
29	31	0	1	800	6	100	0.65

3.3.2 Fabrication of microchannels on TiN-Al_2O_3 ceramic-composite by micro ED-milling process

Devices containing microchannels in ceramics are gaining importance for the miniaturization and reducing the weight to volume ratio. Microchannels have applications in Micro-Electro-Mechanical System (MEMS), Micro Chemical Reactor (MCR) and Biomedical Systems. These micro-channels could also be used in heat exchangers to provide rapid heat transfer [100]. Microdevices have the capability to enhance the power efficiency as they help in rapid heat transfer [22]. Kun et al. [22] have manufactured micro fuel-based power unit and concluded that although micro gas turbines can offer the highest power density, fabrication of miniaturized components or device that convert fuel-based energy into electricity is a challenging task in microdomain. Xia et al. [100] have studied the improvement in the effectiveness of heat exchangers using microchannels. They have concluded that a smaller inlet area in microchannel enhances the heat transfer rate. Khan et al. [101] have designed a micro heat exchanger and studied fluid flow behavior and temperature distribution. They concluded that the effectiveness is found to vary with the inlet geometry, pressure difference, and temperature. Materials of these heat exchangers play very important roles and recently ceramics are used to build heat exchangers and reactors where high temperature and corrosion resistance are the prime criteria apart from high strength and low weight to volume ratio [102] [103].

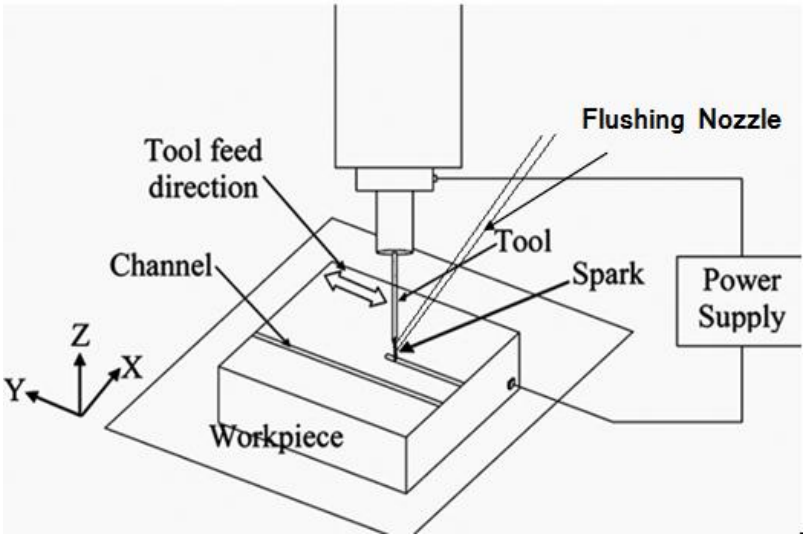

Figure 3.6 Schematic representation of the fabrication of channels by micro-ED milling

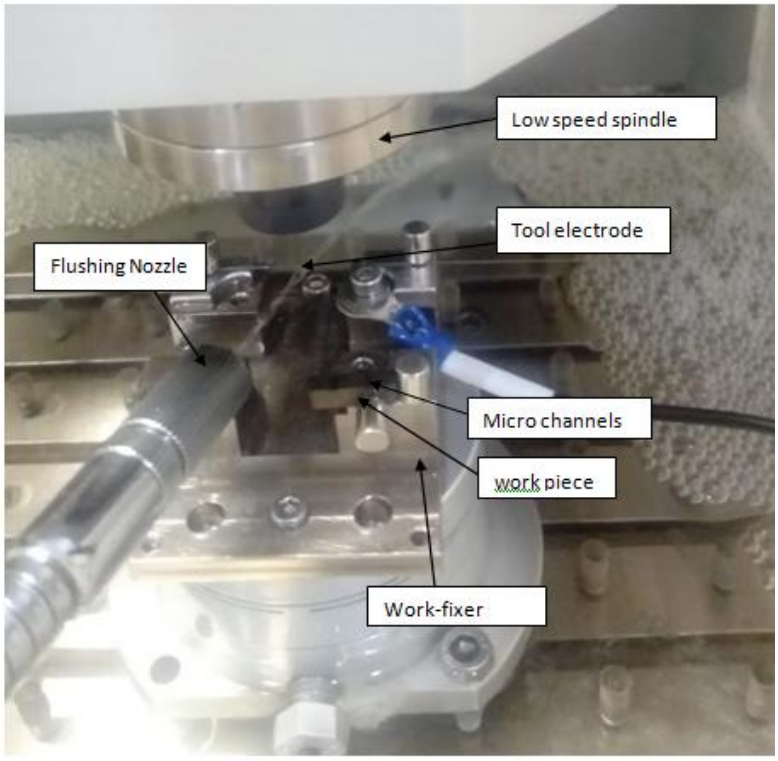

Figure 3.7 Micro -ED Milling setup

An attempt has been made to create microchannels of 500 µm depth and 5 mm length in the ceramic composite with the help of tungsten rod electrodes (diameter 500 µm) by micro electro-discharge milling (µ-ED Milling) as shown in Fig. 3.6 and Fig. 3.7. MRR and EWR are taken as a response parameter. MRR is calculated by geometrically calculating the volume of the cavity and dividing it by machining time. EWR is calculated as the volume of the tool lost in each machining cycle. The experimental design matrix is shown below (Table 3.11) with input parameters and their coded values.

Table 3.11 Experimental design matrix for micro-ED milling

Std Order	Run Order	Pt Type	Blocks	Spindle Speed (rpm)	Voltage (volt)	Capacitance (notation)
18	1	0	1	800	100	5
6	2	1	1	1100	80	6
8	3	1	1	1100	120	6

3	4	1	1	500	120	4
2	5	1	1	1100	80	4
16	6	0	1	800	100	5
5	7	1	1	500	80	6
1	8	1	1	500	80	4
13	9	-1	1	800	100	4
15	10	0	1	800	100	5
10	11	-1	1	1100	100	5
20	12	0	1	800	100	5
7	13	1	1	500	120	6
9	14	-1	1	500	100	5
17	15	0	1	800	100	5
14	16	-1	1	800	100	6
4	17	1	1	1100	120	4
19	18	0	1	800	100	5
12	19	-1	1	800	120	5
11	20	-1	1	800	80	5

3.3.3 **Fabrication of high aspect ratio micro holes on TiN-Al_2O_3 ceramic-composite by powder mixed µ-EDM Process**

EDM is able to machine material, regardless of its hardness, but there is some drawback in this process like very less material removal rate (MRR) and high machining cost. Researchers have come up with the idea of hybrid machining process (HMP) for enrichment & enhancement of this machining process. In HMPs two or more processes simultaneously work to improve the responses and to overcome the drawback of each process.

Sanjeev et al. [104] have used electro-discharge diamond grinding (EDDG), a hybrid of EDM and diamond grinding. They successfully machined very hard material and claimed output of the process had improved with HMPs. Mali et al. [79] have also used a hybrid of EDM and diamond grinding to successfully machine very hard materials like ceramic-

composites. Through experiments, they claimed that grinding wheel rotation speed and peak current are influencing parameters in improving MRR. The present study is, therefore, devoted to the PM-µEDM of advanced electro-conductive Titanium Nitride-Aluminium Oxide (TiN-Al_2O_3) ceramic-composite. Materials removal rate (MRR in mm^3/min) and electrode wear rate (EWR in mm/min) are taken as response parameters. In this work, the volume of microhole is calculated by an inverted frustum of a cone, as there is a difference between the upper and lower diameter of the hole. Electrode wear rate (EWR) is calculated by the loss of volume of the tool in each machining time. The ability of powder mixed-µEDM in the machining of ceramics need to be explored in order to expand the applications of TiN-Al_2O_3 ceramics. The PMµ-EDM process can be explained in three stages as shown in Fig. 3.8. The first stage is called the preparing stage, in this stage powder is mixed into the dielectric and a potential difference is applied. As the potential difference is applied to the system, it polarizes the particles which then arrange themselves in the bridge between electrodes. The second stage is called Electro-discharge stage, in this stage, a plasma bubble is formed and grows until equilibrium reached and generating extreme heat and pressure. The growing of discharge channel is due to the presence of powder particles. The particles present in dielectric-fluid facilitate the early breakdown of the dielectric-fluid [105]. The last stage is called the interval stage, in this stage plasma-channel deionization takes place and gas bubbles are released from overheated molten material and a crater is formed on the workpiece.

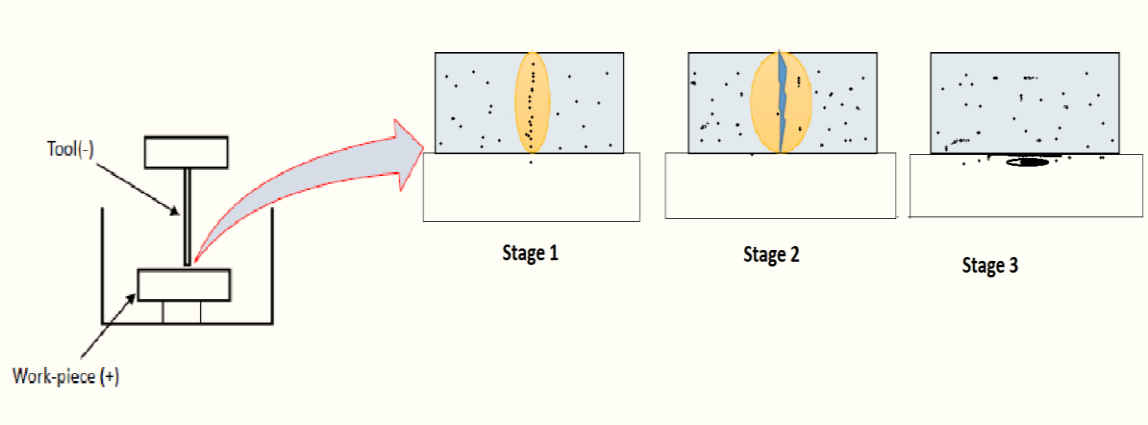

Figure 3.8 Powder mixed micro-EDM process

In this work, powder mixed μ-EDM is studied for understanding the effects of powder inclusion on geometric characteristics of microfeatures in TiN-Al_2O_3 ceramic-composite. The input parameters are spindle speed (S), voltage (V) and powder concentration (C). the response parameters are MRR, EWR, ROC, and a taper angle (α). MRR and EWR are calculated as volume reduced in the machining time. Radial overcut, Taper angles (Fig. 3.9) are measured by equation 3.1, 3.2.

$$\text{Radial overcut (ROC)} = \frac{(\text{top diameter of the drilled hole} - \text{tool electrode diameter})}{2} \quad \text{..... (3.1)}$$

$$\text{Taper angle } (\alpha) = \tan^{-1}\left\{\frac{(\text{top diameter} - \text{bottom diameter})}{(2 \times \text{depth of drilled hole})}\right\} \quad \text{..... (3.2)}$$

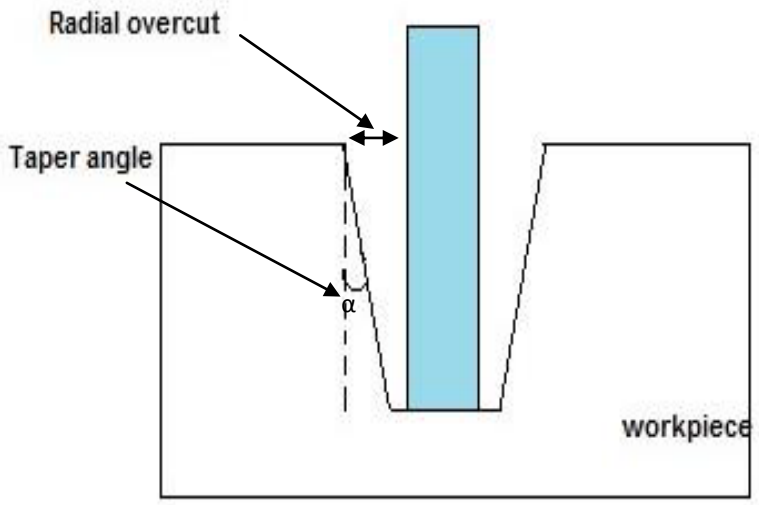

Figure 3.9 Taper angle and radial overcut in PM μ-EDM

Table 3.12 Process parameters range for powder mixed micro-EDM

Process Parameter Range		**Constant Process Parameter**	
Spindle speed (S)	900, 1200, 1500 RPM	Tool Electrode	Tungsten (ø = 500μm)
Voltage (V)	90, 110, 130 Volt	Machine Feed	1.5 mm/min

Concentration (C)	2, 4,6 gm./litre	Capacitance (C)	0.1 µF

Table 3.13 Experimental design table for powder mixed micro-EDM

Std	**Run**	**Factor 1**	**Factor 2**	**Factor 3**
		Speed	**Voltage**	**SiC Concentration**
		rpm	Volt	g/l
10	1	1736	115	4
8	2	1600	130	6
9	3	1064	115	4
3	4	1200	130	2
2	5	1600	100	2
17	6	1400	115	4
1	7	1200	100	2
20	8	1400	115	4
16	9	1400	115	4
15	10	1400	115	4
14	11	1400	115	8
11	12	1400	90	4
4	13	1600	130	2
5	14	1200	100	6
12	15	1400	140	4
13	16	1400	115	2
18	17	1400	115	4
19	18	1400	115	4
7	19	1200	130	6
6	20	1600	100	6

3.4 Equipment used for measurement and analysis

3.4.1 Scanning electrode microscope and Energy-dispersive X-ray spectroscopy

A scanning electron microscope (SEM) provides the enlarged view of machined surfaces from 50 to 1,00,000 × magnifications by forming a three-dimensional image on a cathode ray tube. In it, an electron beam is focused on the sample and this bombarding of electrons produces an image. The electrons emitted from the sample are then scanned to form a magnified image.

It provides the topography of the surfaces. The chemical composition of the constituent on the machined surface could also interpret by its data. For this study "Nova nano-SEM450" is used for taking the images of the machined surface as shown in Fig. 3.10.

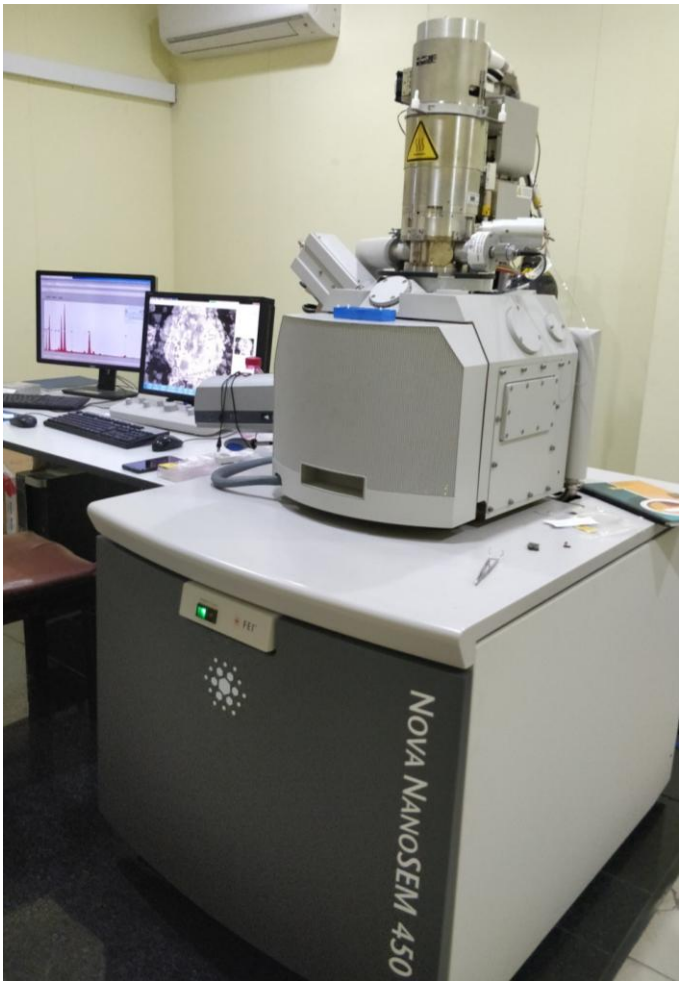

Figure 3.10 Scanning electron microscopy

The magnify images allow the examination of the structure and morphology of materials. High depth of focus SEM is frequently used for studying fracture surfaces. EDS system is integrated into the SEM instrument. In the EDS system, the interaction of an electron beam with the sample target produces a variety of emission, including x-rays. An energy-dispersive (EDS) is used to separate the characteristic X-ray of different elements and thus phase formation on the machined surface could understand.

3.4.2 **Profilometer**

Contact type surface roughness measuring instrument (Fig. 3.11) of Taylor Hobson (Surtronic 100) is used for measuring the surface roughness of the machined surface.

Figure 3.11 Taylor Hobson profilometer

3.4.3 **Optical microscope**

An optical microscope "multimode Scanning Probe Microscope (Bruker)." is used for optical analysis at high resolution as shown in Fig. 3.12. The dimensions of microfeatures are measured by this. The micro-holes dimensions, taper angles, radial overcut and circularity of the holes could measure using this optical microscope. The change in tool shape could also be studied with it.

Figure 3.12 "multimode Scanning Probe Microscope (Bruker)" Optical microscope

3.4.4 **Semi-automatic polishing machine**

Sample polishing or finishing is for characterization of samples is done on High-Speed Twin grinder/polishers MetaServ® 250 (Buehler) as shown in Fig. 3.13.

Figure 3.13 Semi-automatic polishing machines

In this machine, sandpaper is put on grinding plate of 8-inch diameter and it rotates with 50-500 rpm speed. Based on our requirements of the finished surface, one can alter the speed of the grinding plate and sandpaper quality. A built-in drainage system continuously washes away particles to and minimizes the build-up of grinding/polishing debris. The pressure of the nozzle could also alter for having a cooling effect if needed.

3.4.5 **Electronic balance**

"Wensar" electronic balance (Fig. 3.14) is used to measure the weight of the samples and tool-electrode. The weight of samples and tool is measured before and after machining to calculate weight loss during machining.

Figure 3.14 Electronic balance

4. EXPERIMENTAL INVESTIGATION ON DIAMOND GRINDING ASSISTED ELECTRO-DISCHARGE MACHINING OF TiN-Al_2O_3 CERAMIC-COMPOSITE

Preparation of machining surfaces for microfabrication on TiN-Al_2O_3 ceramic-composite is achieved by diamond grinding assisted electro-discharge machining (DGA-EDM). The machinability study of advanced-ceramics is a potential research area because of its increase in the demand for various advanced-ceramics and their characteristic problem related to machining. Ceramics are inorganic, non-metallic materials having ionic and covalent bonds. Unique properties of advanced ceramic-like high hardness, chemical inertness are because of such bonds and structure. Advanced ceramics are developed to meet the industrial requirements of ceramics by controlling microstructure to improve machinability. Machinability studies, parametric optimization, and study of the mechanism of material removal of ceramics are the potential research areas because of an increase in the demand in the various fields and characteristic problem related to their machining. Expensive equipment, tooling and high processing time make conventional machining process economically unviable for machining of these advanced ceramics [64]. Titanium Nitride-Aluminium Oxide (TiN–Al_2O_3) has a very low frictional coefficient, high hardness, high resistance to thermal as well as mechanical wear and chemical stability [106]. These properties lead this ceramic-composite to be a good material for applications in the field of cutting tools and components of complex shape [4]. Although ceramic composites find their usage in various applications, full-scale utilization of these ceramics-composite materials is limited due to some peculiar properties like anisotropy, less thermal conductivity, and availability of the reinforcing phase. For their machining, these properties are responsible for preferring non-conventional methods over conventional ones because non-conventional methods of machining are based on chemical, electrochemical, thermo-electrical methods of material removal as discussed in chapter 2. For such advanced materials, Electro-discharge machining (EDM) can be used as a machining process. In EDM, the removal of material depends on a series of electric flashes between the tool and the workpiece caused by the pulsed voltage in the presence of dielectric fluid. EDM provides some remarkable advantages, i.e. no contact between two electrodes which justify its use in the machining of

very hard or fragile materials because the only force is an impulse by the flashover [3]. In this non-conventional thermo-electrical machining process the material is eroded out due to continuous spark, in the presence of dielectric fluid between the tool and the work-piece. The discharge energy generated during this process causes the material to be melted and vaporized [107]. The main challenge in applying EDM in ceramic processing is the high resistivity of ceramics while EDM application needs an electrical resistivity less than 100 Ωcm. Therefore, the process is limited to only electrically conducting ceramics. D. Bhaduri et al. [4] [64] have experimentally shown that EDM has a high potential for machining of advanced ceramic composites. Material removal has been found to be affected by the gap voltage, peak current, duty cycle and pulse on time. Duty cycle used to show the least influence among these factors. Material removal rate (MRR) increases with the increase in the value of peak current and gap voltage.

Hybrid machining processes is a new technique often used to improve response parameters so that, two or more methods of machining could be simultaneously used in a way that shortcomings of each process could be overcome. Baghel et al. [26] have machined Titanium Nitride Aluminum Oxide by vibration-assisted ED-milling process and experimentally investigated that materials removal rate is improved by 1.98 times in the influence of low-frequency vibration. Ununu et al. [108] [109] have applied electro-discharge diamond surface grinding technique for machining Inconel-718 alloy and experimentally told that electro-discharge diamond surface grinding (EDDSG) could efficiently remove the material and the wheel rotation speed found to be the most influencing among the parameters like pulse on time, current, duty factor. They also studied machinability of Nimonic-80A alloy with abrasive mixed electro-discharge diamond grinding (EDDG) and claimed that MRR increases with the inclusion of abrasive particle as more number of wheel particles abrade more volume of the workpiece. Yadav et al. [110] have machined high-speed steel (HSS) with electro-discharge diamond grinding (EDDG) and concluded that peak current, wheel speed, and pulse on time have a positive influence on material removal rate. Koshy et al. [111] [112] have experimentally investigated that the mechanism of material removal for machining cemented carbide with EDDG. They experimentally explained that the grinding forces and specific energy of material removal decrease as EDM provides thermal softening of the work material. Yan et al. [113] have also applied a hybrid of EDM and grinding to

machines a single crystal SiC ceramic and Suggested that EDM spark soften the surface of the workpiece after that grinding removed the material. This work is focused on machining of Titanium Nitride Aluminum Oxide ($TiN–Al_2O_3$) ceramic-composite with Diamond grinding assisted electro-discharge (DGA-ED) machining: a hybrid of EDM and diamond grinding. TiN- Al_2O_3 ceramic-composite has been selected for experiments considering its applications in various industrial, engineering components and also to information on the material optimizing process parameters by EDM.

4.1 **Process parameters and their range**

TiN-Al_2O_3 ceramic-composite has been prepared by reactive hot pressing so that TiN particles could be dispersed homogeneously within the material [106]. The various properties of the $TiN–Al_2O_3$ ceramic, composite are given in Table 3.1. DGA-EDM experiments were performed on Electronica® ZNC ENC-35 electro-discharge machine with the customized diamond abrasive grinding wheel setup shown in Fig. 3.1. The ENC-35 set-up having diamond-bronze grinding wheel as tool electrode, the servo motor is used to maintain an inter-electrode gap (IEG), a fixture to hold the workpiece in the dielectric tank, alternating current reversible synchronous motor. The grinding wheel attached to the EDM machine with the help of attachments like direct current motor and v-belt. The specifications of the grinding wheel are given in Table 3.3. Fig. 3.3 shows the machining zone of hybrid machining processes i.e. DGA-ED machining. In this zone, the EDM spark takes place when there is an inter-electrode gap (IEG). These sparks remove the materials by melting and vaporization and also soften the adjacent material due to discharge heat. Diamond grinding wheel removes these soft layers of materials by grinding effect.

A series of pilot experiments are performed before selecting the range of the process parameters during preliminary experimentations. Peak current (I), pulse on time (P), wheel speed (S) and duty factor (DF) are selected as control-factors. The main purpose of this study is to explore the machinability of $TiN–Al_2O_3$ ceramic by DGA-ED Machining process and also find the effective parameters and effective interactions of these parameters for maximizing the material removal rate (MRR). The various process parameters such as Peak current (maximum current), pulse on time (t_{on}), wheel speed (S) and duty factor (DF) on the

MRR has also been investigated. The independent process parameters, their coded values, and level of parameters with their units are given in Table: 4.1.

Table 4.1 Independent parameters (factors) and their levels

SN	Input parameter/ factors (Symbol)	Unit	Level of parameters		
			-1	0	+1
1	Wheel speed (S)	RPM	400	800	1200
2	Current (I)	A	3	6	9
3	Pulse on time (P)	µs	50	100	150
4	Duty factor (DF)	%	0.60	0.65	0.70

4.2 **Design of experiments**

For surfacing of samples Response surface methodology (RSM) is selected with three control factors. In this study, central composite design (CCD) of RSM is chosen with seven center points. The combined effects of control parameters are analyzed by 3D surface plots. The mathematical relation between the input parameters and output parameters (responses); based on experimental results is also obtained. These experiments with the help of regression analysis modeled the desired response to several input parameters [114]. The local shape of response surface has also been created in Response Surface Methodology [114]. In RSM, a relationship is developed between the desired response (effect: Y) parameter and control factors (cause: x) that can be represented by equation 4.1.

$Y_i = f(x_1, x_2, x_3 \ldots X_k) \pm €$ ……(4.1)

In equation 4.1, Yi is response parameter and x_1, x_2, x_3…. x_k are the independent input parameters. The error can be expressed by €. The error obtained during regression analysis is called the residual or experimental error. The quadratic model for material removal rate Y and factors K is shown in equation 4.2.

$$Y_i = ho + \sum h_i x_i + \sum h_{ii} x_i^2 + \sum\sum h_{ij} x_i x_j \pm €$$ ……..…..…. (4.2)

In equation 4.2, the various term can be expressed as h_o=constant, h_i=coefficient of the linear term, h_{ii}=coefficient of quadratic term, h_{ij}=coefficient of the cross-product term [114]. In this

study, 31 experiments are required. Input parameter matrix and responses are shown in Table 4.2.

Table 4.2 Experimental details of Response surface methodology

Run Order	S	I	t_{on}	DF	MRR	MRR predicted	Error	Ra value
	rpm	A	µS		mg/min	mg/min	mg/min	µm
1	1200	9	50	0.60	0.33580	0.31618	0.05843	3.07
2	800	6	100	0.65	0.20110	0.20095	0.0007	5.98
3	400	6	100	0.65	0.11100	0.12196	-0.09874	7.65
4	800	6	100	0.65	0.12840	0.20195	-0.57282	6.11
5	400	9	150	0.70	0.17161	0.12366	0.27941	6.65
6	1200	3	50	0.70	0.31410	0.34294	-0.09182	3.15
7	1200	6	100	0.65	0.34590	0.36352	-0.05094	2.69
8	400	3	150	0.60	0.08880	0.07417	0.16475	5.99
9	800	6	150	0.65	0.03726	0.1257	-2.37359	7.11
10	400	3	50	0.70	0.06015	0.07285	-0.21114	6.12
11	800	6	100	0.65	0.27270	0.20195	0.25944	6.76
12	800	6	100	0.65	0.22920	0.20195	0.11889	6.27
13	800	6	50	0.65	0.16580	0.10594	0.36104	6.08
14	1200	9	50	0.70	0.31055	0.30341	0.02299	2.58
15	800	6	100	0.65	0.22857	0.20195	0.11646	5.43
16	1200	9	150	0.60	0.34797	0.31349	0.09909	2.52
17	1200	9	150	0.70	0.30450	0.34594	-0.13609	2.89
18	400	9	150	0.60	0.11470	0.10047	0.12406	7.11
19	1200	3	50	0.60	0.31185	0.33803	-0.08395	2.50
20	800	6	100	0.70	0.29160	0.13559	0.53501	5.03
21	800	3	100	0.65	0.21130	0.2036	0.03644	5.39
22	400	3	150	0.70	0.08080	0.11505	-0.42389	6.41
23	1200	3	150	0.70	0.48648	0.42799	0.12023	2.07

Run Order	S	I	t_{on}	DF	MRR	MRR predicted	Error	Ra value
	rpm	A	µS		mg/min	mg/min	mg/min	µm
24	800	6	100	0.60	0.22370	0.26491	-0.18422	3.93
25	800	6	100	0.65	0.18710	0.20195	-0.07937	4.67
26	400	9	50	0.60	0.10930	0.14349	-0.31281	4.28
27	1200	3	150	0.60	0.37220	0.37785	-0.01518	2.19
28	800	9	100	0.65	0.16071	0.19699	-0.22575	6.98
29	400	3	50	0.60	0.10400	0.07719	0.25779	6.49
30	400	9	50	0.70	0.11500	0.12367	-0.07539	6.91
31	800	6	100	0.65	0.25230	0.20195	0.19956	5.63

4.3 **An empirical model for performance measures**

The experiments are performed based on the data presented in Table 4.2 and the material removal rate is analyzed using Minitab®16 design of experimental software and surface roughness is measured by a profilometer. Model summary spastics have been performed using collected data. Lack of fit (LOF) test has been performed to check model adequacy and determination coefficient values collected to understand the goodness of fit of the model [115].

4.3.1 **ANOVA results for the material removal rate**

In table 4.3, ANOVA results for MRR are shown, the R^2 is 87.54. This value of R^2 shows that less than 13% of the total variances are not explained by the model. The value of adj R^2 is 76.64 that indicates close agreement with the determination coefficient and the significance of the given model. The Value of Prob >F Value less than 0.0500 indicates the significant model terms. The regression model for Linear and quadratic both are significant for this study. The wheel speed is observed to be significant term than pulse, on-time and duty factor. Wheel speed significantly affects the MRR as the high rotation speed of the wheel enables more no. of abrasive to come in contact with the work-piece in a minute.

Table 4.3 ANOVA results for the material removal rate

SOURCE	Degree of freedom	Seq SS	Adj SS	Adj MS	F	P value probability > F
Regression	14	0.310621	0.310621	0.022187	8.03	0.000
Linear	4	0.265410	0.265410	0.066352	24.0	0.000
Speed (S)	1	0.262568	0.262568	0.262568	95.0	0.000
current (I)	1	0.000197	0.000197	0.000197	0.07	0.793
Pulse on time (t_{on})	1	0.001756	0.001756	0.001756	0.64	0.437
Duty factor (DF)	1	0.000889	0.000889	0.000889	0.32	0.578
Square	4	0.030904	0.030904	0.007726	2.80	0.062
S × S	1	0.005799	0.004318	0.004318	1.56	0.229
$t_{on} \times t_{on}$	1	0.012141	0.019251	0.019251	6.97	0.018
I × I	1	0.000250	0.000007	0.000007	0.00	0.960
DF × DF	1	0.012713	0.012713	0.012713	4.60	0.048
Interaction	6	0.014307	0.014307	0.002385	0.86	0.542
S × I	1	0.008221	0.008221	0.008221	2.98	0.104
S × t_{on}	1	0.001836	0.001836	0.001836	0.66	0.427
S × DF	1	0.000086	0.000086	0.000086	0.03	0.862
I × P	1	0.001807	0.001807	0.001807	0.65	0.430
I × DF	1	0.000313	0.000313	0.000313	0.11	0.741
t_{on} × DF	1	0.002045	0.002045	0.002045	0.74	0.402
Residual Error	16	0.044200	0.044200	0.002762		
Lack of Fit	10	0.030627	0.030627	0.003063	1.35	0.369
Pure Error	6	0.013573	0.013573	0.002262		
Total	30	0.354821				
Standard deviation = 0.0525594			R-Sq = 87.54%			
PRESS = 0.197947			R-Sq (pred) = 44.21%			

	R-Sq (adj) = 76.64%

4.4 **Validation of the model**

The ANOVA results show lack of fit (LOF) value of F as 1.35. This value is not significant relative to pure-error. A non-significant value of lack of fit is good because it implies that for this experimental data, the model is fit and significant. A non-significant LOF value shows the lesser systematic variation that can be neglected for this particular model. The normal probability plot is a graphical technique to identify substantive departures from normal. The normal probability plot of MRR (Fig. 4.1) shows that not only the residuals fall within six-sigma limits, but also forms approximately a straight line.

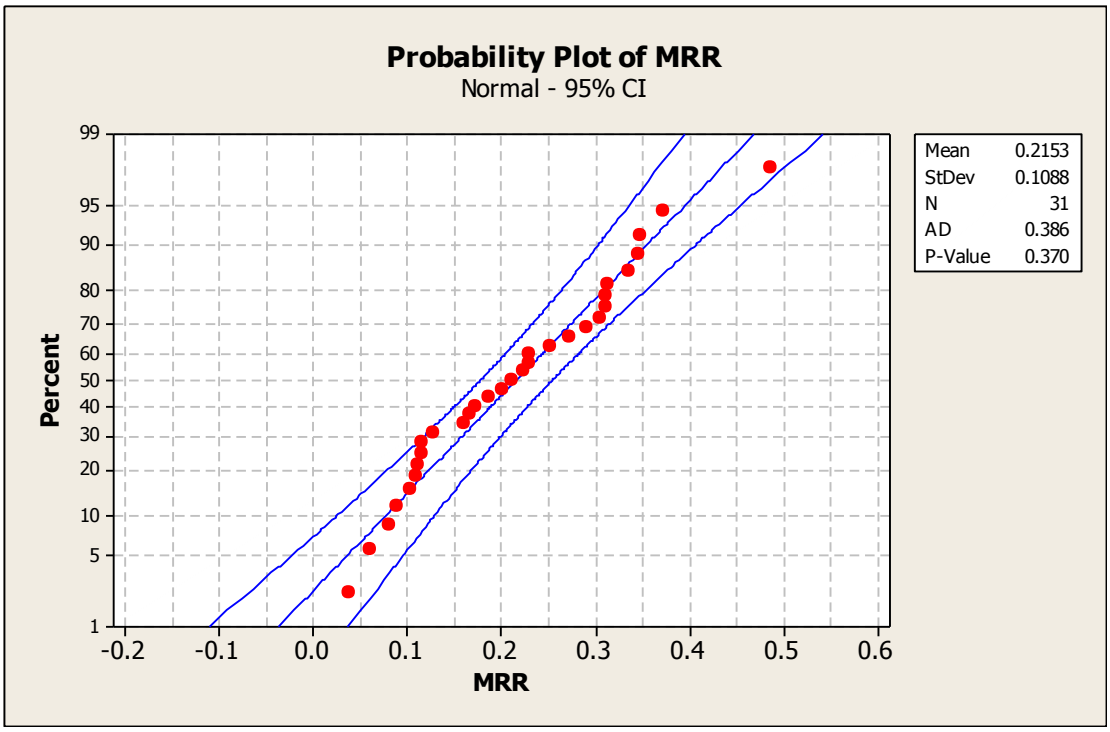

Figure 4.1 Normal probability plot of residuals for MRR

$$\begin{aligned}\text{MRR} = {} & 0.201947 + (0.120777 \times \text{S}) - (0.003308 \times \text{I}) + (0.009876 \times t_{on}) + (0.007026 \\ & \times \text{DF}) + (0.040792 \times S^2) - (0.001653 \times I^2) - (0.086128 \times {t_{on}}^2) \\ & + (0.069992 \times DF^2 - (0.022667 \times \text{S} \times \text{I}) + (0.010712 \times \text{S} \times t_{on}) \\ & + (0.002316 \times \text{S} \times \text{DF}) - (0.010628 \times \text{I} \times t_{on}) - (0.004424 \times \text{I} \times \text{DF}) \\ & + (0.011304 \times t_{on} \times \text{DF}) \ldots\ldots\ldots\ldots\ldots\ldots\ldots\ldots\ldots\ldots\ldots\ldots\ldots\ldots (4.3)\end{aligned}$$

The normal probability plot also shows that error is normally distributed. All the above statements point towards good adequacy of the regression model. The expression of the relationship between response and input parameters is expressed in equation 4.3.

4.5 Results and discussion

4.5.1 Influence of control factors on the material removal rate

In the machining of TiN-Al_2O_3 ceramic- composites, material removal rate is an important performance parameter because TiN-Al_2O_3 is very difficult and costly to machine. Fig. 4.2 shows the comparison data graph of five verification experiments of MRR of TiN-Al_2O_3 ceramics machined with EDM, DGAED Machining and diamond grinding at similar input parameters. It is observed from this plot that there is almost a two-fold increase in the MRR with DGAED machining as compared to EDM.

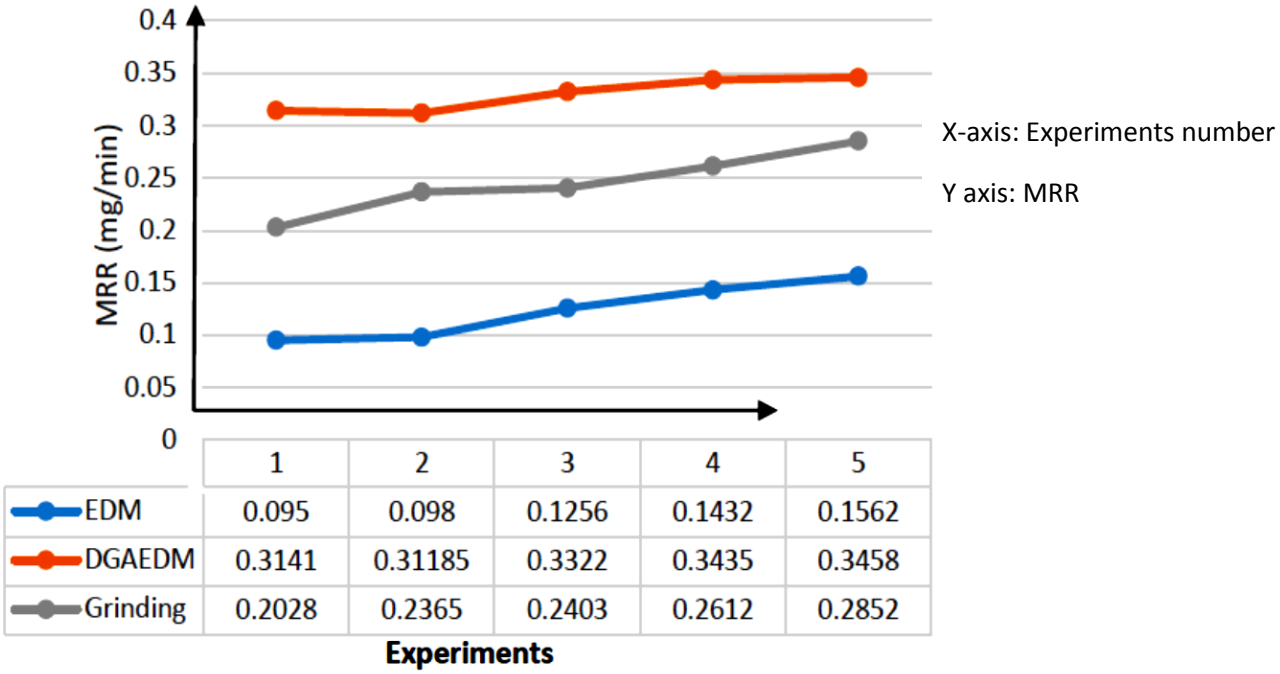

	1	2	3	4	5
EDM	0.095	0.098	0.1256	0.1432	0.1562
DGAEDM	0.3141	0.31185	0.3322	0.3435	0.3458
Grinding	0.2028	0.2365	0.2403	0.2612	0.2852

Figure 4.2 Plot for MRR in EDM, DGA-ED Machining and Diamond Grinding

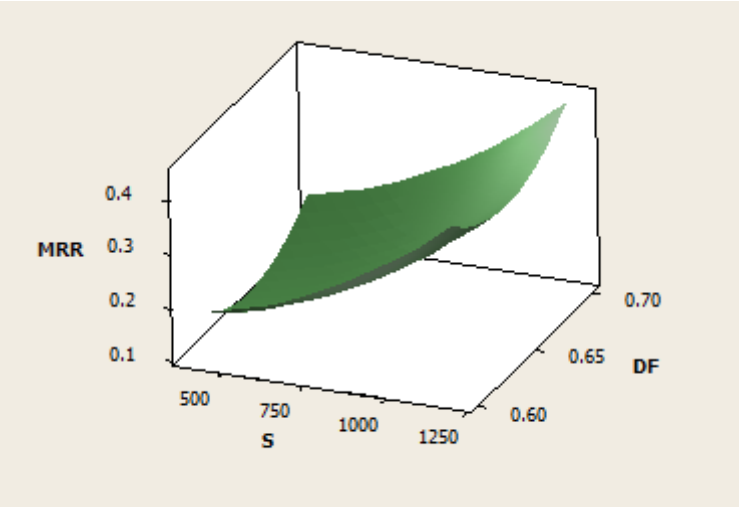

Figure 4.3 Surface plot of MRR with wheel-speed (S) and duty factor (DF)

Surface plots, for MRR with wheel speed (S) in RPM, duty factor (DF), and Pulse on time (t_{on}) in micro-second are shown in Fig. 4.3, Fig. 4.4 and Fig. 4.5. Surface plot for MRR with wheel speed and Duty factor shows, that MRR improves with an increase in the value of wheel speed as indicated in Fig. 4.3. The grinding capacity of the process improves with speed, thus a combination of higher wheel speed and duty cycle leads to maximum MRR. Fig. 4.4 shows that MRR first increases with an increase in pulse on time (t_{on}), reaches its peak and then starts decreasing. This is because, with an increased value of t_{on}, spark capacity increases, leading to higher MRR.

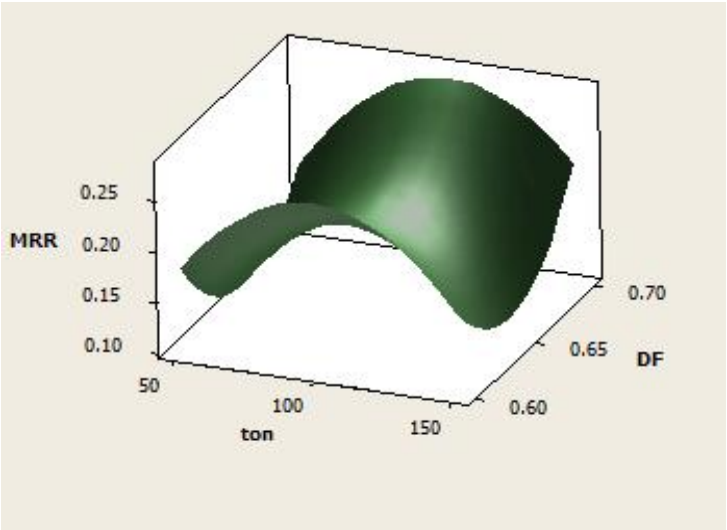

Figure 4.4 Surface plot of MRR with Pulse on time (ton) and duty factor (DF)

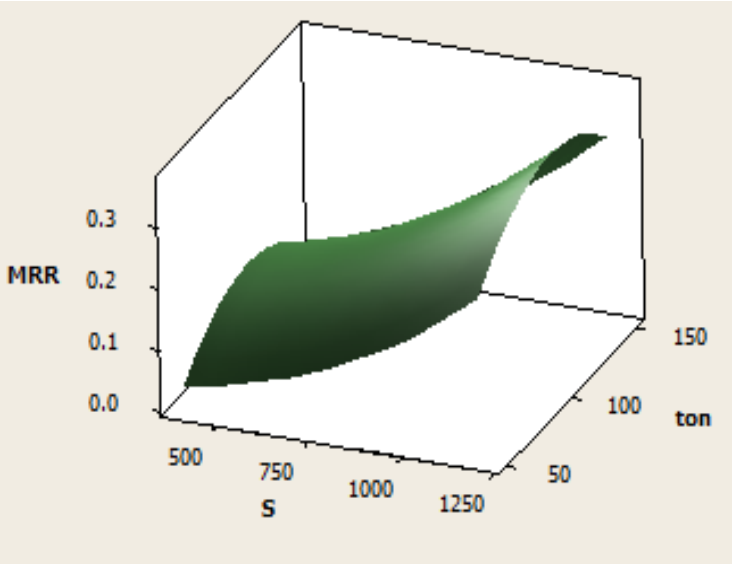

Figure 4.5 Surface plot of MRR with wheel-speed (S) and pulse on time (t_{on})

Fig. 4.5 shows the variation in MRR with wheel speed and pulse on time. An increase in the wheel speed enhances grinding capacity while a longer Pulse on time (t_{on}) increases the capacity of EDM. The combination of both results in an increase in the hybrid process capacity.

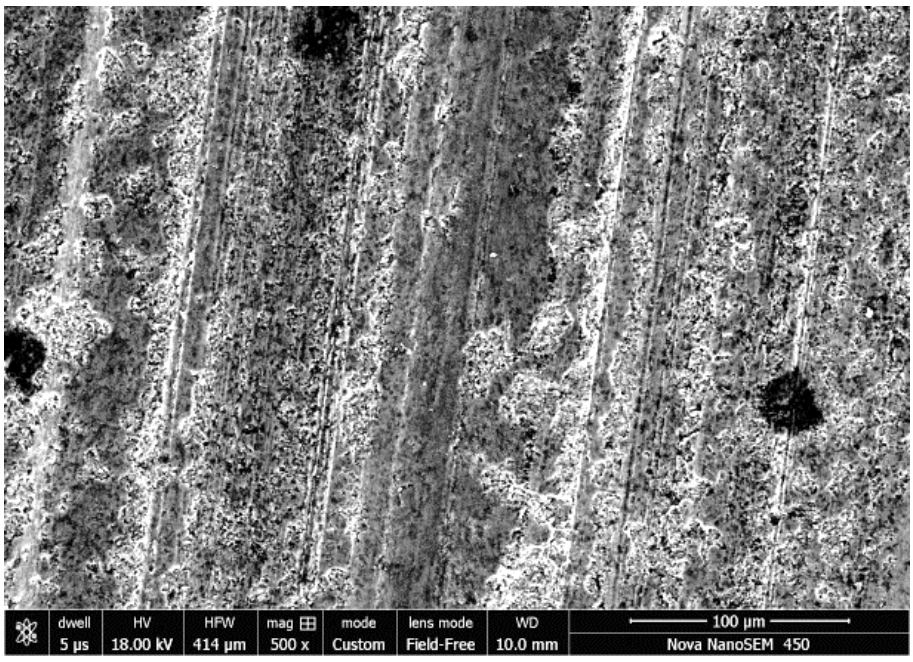

(a) 400 rpm (Ra = 6.12 µm)

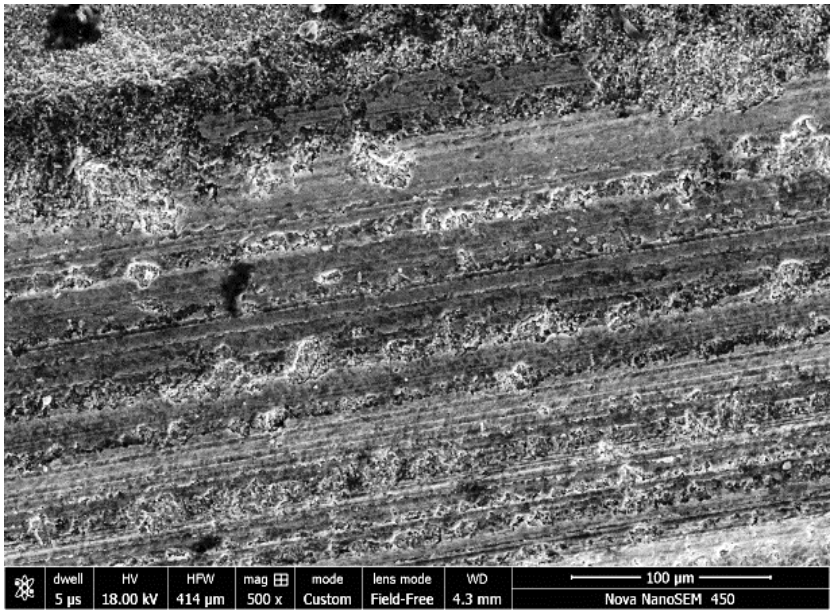

(b) 800 rpm (Ra = 5.43 µm)

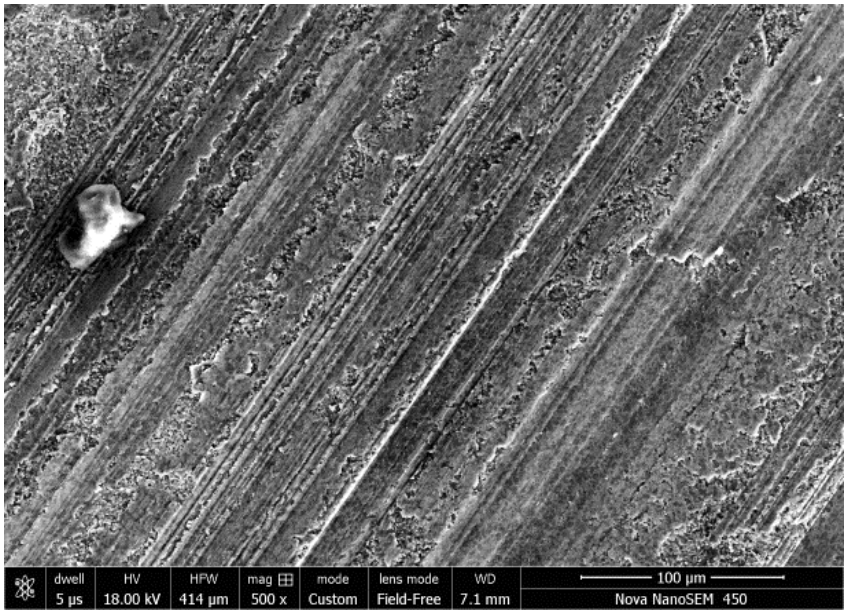

(c) 1200 rpm (Ra = 2.89 µm)

Figure 4.6 SEM images of the machined surface at different wheel speed

The plot shows that at higher speed, MRR is higher but with an increase in the value of pulse on time, MRR first increases and after reaching its peak value, it starts decreasing. This shows that at a high-wheel rotation speed, diamond grinding dominates in a hybrid process.

Scanning electron microscope (SEM) images of the machined surface at various wheel rotation speeds are shown in Fig. 4.6. In these images, it can be observed that there are clear marks of the recast layer at lower wheel rotation speed. Average surface roughness value is lesser in case of high RPM value as compared to low rpm. At 1200 rpm the average roughness value is 2.54 μm. At higher speeds, cast and pitted surfaces are removed due to ground effect. There is a gradual removal of the recast layer with the increase of wheel rotation speed. As recast layer can be removed using DGAED machining process, DGAED machining can be preferred over EDM.

4.6 **Mechanism of material removal**

The SEM images of machined surfaces (Fig. 4.7 and Fig. 4.8) are showing various patterns observed on the machined surface. From Fig. 4.7 (a), it can be observed that there are pools (with debris in it) of melting metals. The contraction due to the re-solidification of molten metal leads to the formation of micro-cracks. The cracks and debris in it confirm that melting and vaporization are the main mechanisms of material removal. The material removal also takes place by thermal cracking and flakes removal i.e. thermal spalling as shown in Fig. 4.7 (b).

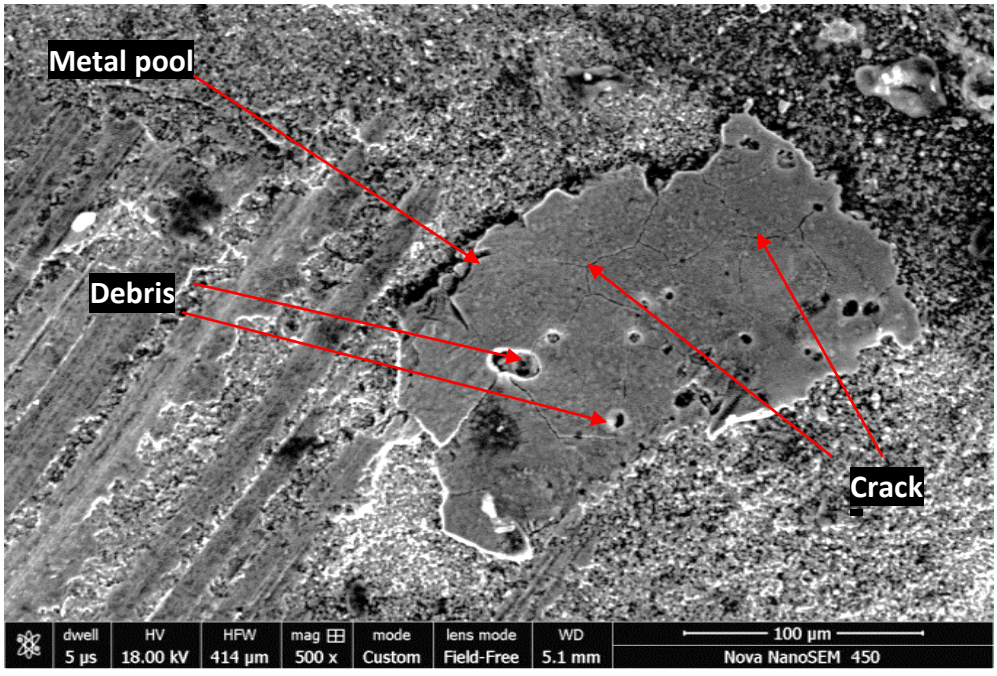

(a) Contracted metal pool after solidification

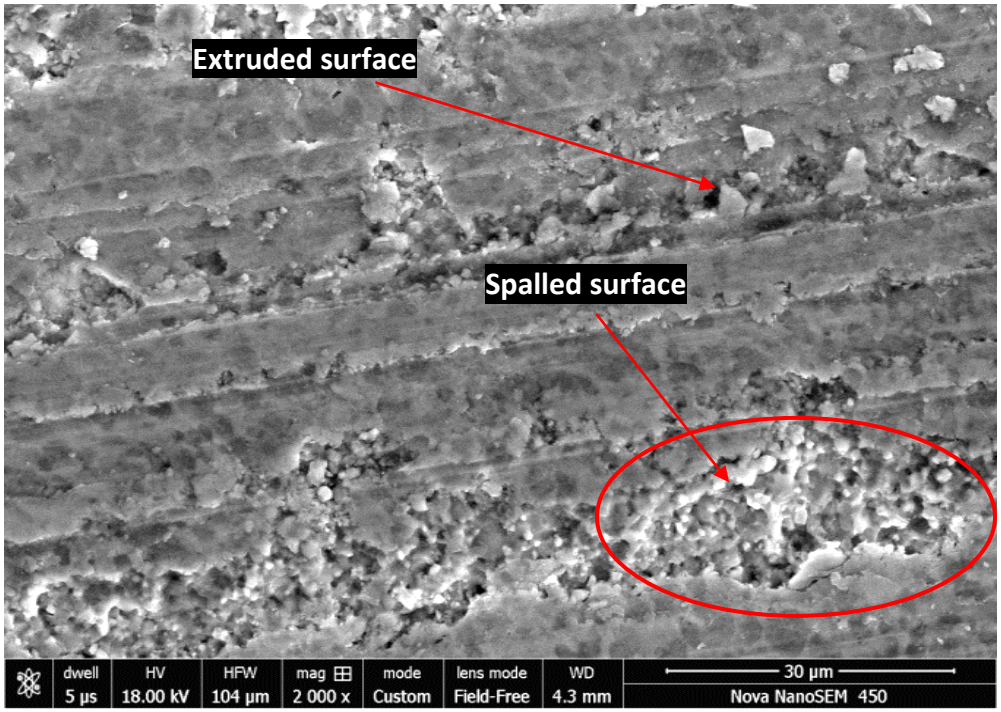

(b) The spalled area on parent material by removal of a flake

Figure 4.7 SEM images of machined surfaces

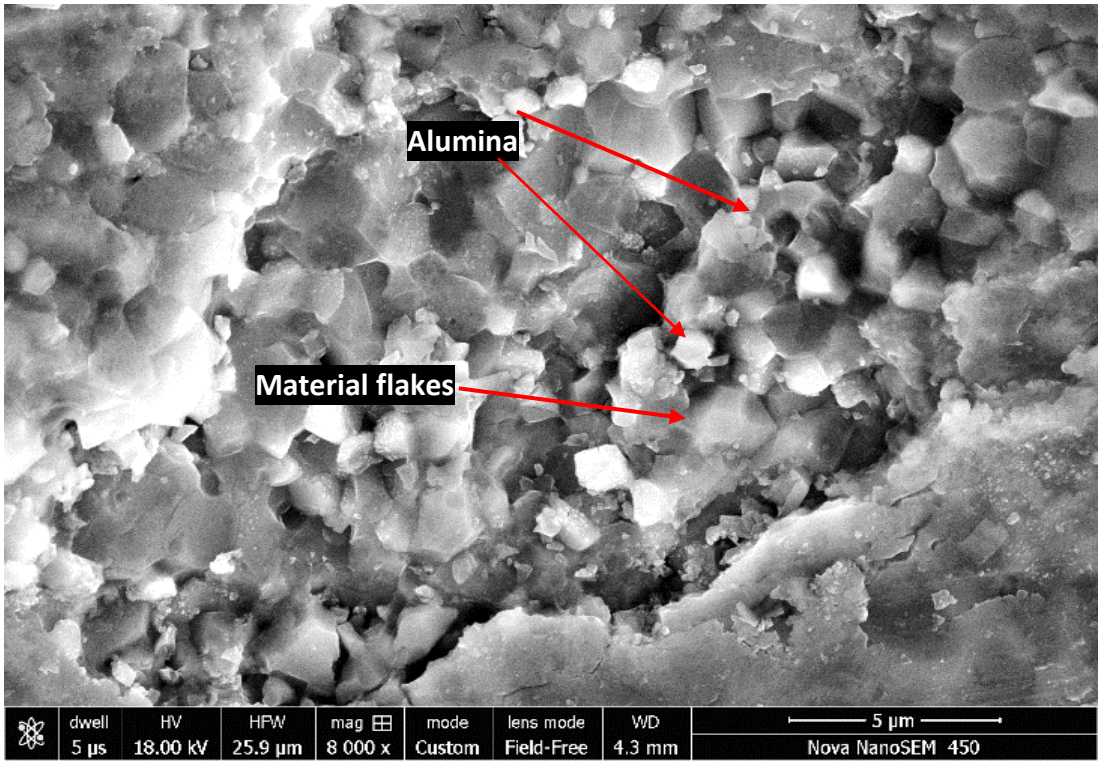

Figure 4.8 SEM images of the spalled surface

The chipped or spalled machined surfaces due to repeated heating could be clearly observed in the machined zones in enlarged SEM image Fig. 4.8.

The feasibility of machining TiN-Al_2O_3 ceramic by DGA-ED Machining is investigated. It is found that MRR increases almost two-fold as compared to the EDM process. This improvement in material removal rate is due to the hybrid effect of the process. It is feasible to machine TiN-Al_2O_3 ceramic composite by DGA-ED Machining. The material removal rate of the TiN-Al_2O_3 ceramic composite is increased by hybridizing the EDM process with diamond grinding. It is due to, the electro-thermal effect of EDM, by which the material gets locally softened and leads to more effective grinding in the successive cycle.

4.7 **Desirability based multi-response optimization**

Response optimization is done in response surface methodology by using Minitab-16, in which maximization of MRR is taken as the objective function. The composite design desirability obtained is 97.85 %.

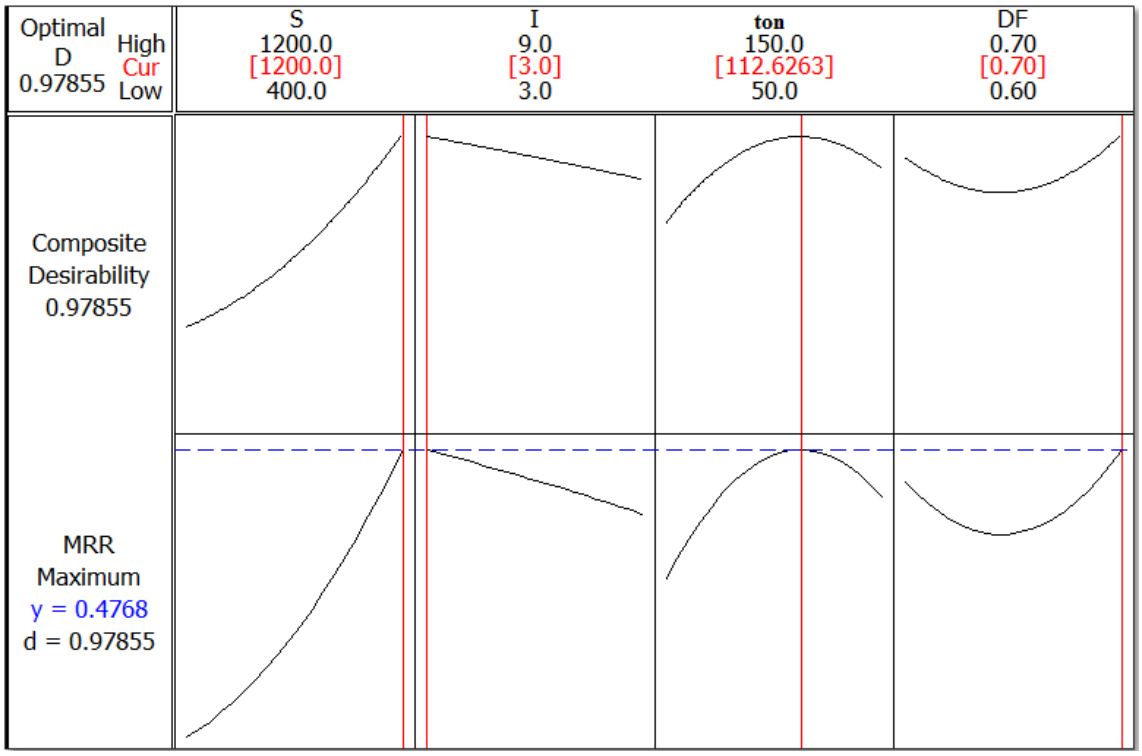

Figure 4.9 Optimization plot for MRR

The global solution for predicting responses for MRR is generated. The optimization plot (Fig. 4.9) shows the behavior of MRR with different values of process parameters.

It shows that higher the rotating speed of the grinding wheel, higher the MRR. In the case of the pulse of time (t_{on}), as it increases the material removal rate increases and after reaching the optimum point it starts decreasing. In the case of duty factor (DF), material removal rate first decreases with an increase in the value of duty factor from 0.60, but after reaching a value of 0.65 MRR starts increasing and reaches a maximum at 0.70.

Table 4.4 Global solutions by response optimization

SL	Solution Parameters	Values
1	Wheel rotation speed	1200 rpm
2	Current	3 A
3	Pulse on time	112.626 microsecond
4	Duty factor	0.7
5	Predicted responses (MRR)	0.476843 mg/min
6	Composite Desirability	0.978547

The global solution shown in Table 4.4 predicts MRR to be 0.476843 mg/min at wheel rotation speed 1200 RPM, current 3 Ampere, duty factor 0.7, and Pulse on time (t_{on}) 112.626 microsecond.

4.8 **Summary**

In this chapter, an in-house fabricated DGA-EDM setup is used on a commercial electro-discharge machine for experimentation. It is a hybrid machining process of EDM and diamond grinding. It is used for experimentations in a view of obtaining smooth surfaces for micro-features fabrication and to get better material removal rate (MRR). TiN-Al_2O_3 ceramic-composite is taken as a workpiece, which is otherwise very difficult to machine by a conventional machining process. The surfacing of the TiN-Al_2O_3 ceramic composite is done and process parameters are optimized. The grinding-wheel rotation speed, pulse on-time, and duty factors are coming out to be significant parameters. The surfacing of the TiN-Al_2O_3 ceramic composite is done and on an average 2.54 μm average surface

roughness (Ra) value is achieved. The main mechanism of material removal is thermal spalling that is totally different from the mechanism of material removal in metals. The material removal rate is found to improve significantly during DGA-EDM as compared to EDM. The results of multi optimization, using RSM are found to be very promising. In this study, the mechanism of material removal is also explained for TiN-Al_2O_3 ceramic-composite, the cracks and debris in it confirm that melting and vaporization are mechanisms of material removal. The material removal also takes place by thermal cracking and flakes removal i.e. thermal spalling. It is also observed that at higher speed, the recast layer is removed due to the grinding effect.

5. EXPERIMENTAL INVESTIGATION ON MICRO-ELECTRO-DISCHARGE MILLING OF TiN-Al_2O_3 CERAMIC-COMPOSITE FOR MICROCHANNELS FABRICATION

Motivated by the desire of reducing cost, size, weight, raw material, and energy consumption, one can witness miniaturization across almost all domains of industrial and consumer products. Few examples of these miniaturized products include micro-chemical reactors, heat-sink, micro-heat exchanger, micro-electronic and mechanical devices (MEMS), etc. Devices containing microchannels in ceramics are gaining importance for their miniaturization and reducing the weight to volume ratio. Microchannels have applications in Micro-Electro-Mechanical system (MEMS), Micro Chemical Reactor (MCR) and Biomedical Systems. Microdevices have the capability to enhance the power efficiency as they help in rapid heat transfer [116]. Kun et al. [117] have manufactured micro fuel-based power unit and concluded that although micro gas turbines can offer the highest power density, fabrication of miniaturized components or device that convert fuel-based energy into electricity is a challenging task. Xia et al. [116] have studied the improvement in the effectiveness of heat exchangers using microchannels. They have concluded that a smaller inlet area in microchannel enhances the heat transfer rate. Khan et al. [118] have designed a micro heat-exchanger and studied fluid flow behavior and temperature distribution. They concluded that the effectiveness is found to vary with the inlet geometry, pressure difference, and temperature. Materials of micro heat exchangers play very important roles and recently ceramics are used in heat exchangers and reactors where high temperature and corrosion resistance are the prime criteria apart from high strength and low weight to volume ratio [119]. However, conventional machining of ceramics is extremely difficult due to very high hardness and low fracture toughness. Generation of high tool wear and surface damage due to high cutting forces hinders full-scale applications of these ceramic [2] [120]. Micro EDM technology takes care of the precision in machining in very small dimension (micron level). Resistance-capacitance (RC) electrical power supply to create low spark energy for the removal of small units of material is the principal strategy behind the technology of micro EDM process [48] [121].

The spark is produced by the dielectric breakdown of the fluid between the electrodes (tool and work-piece). The discharge energy generated during this process causes the material to be melted and vaporized in EDM [122]. In micro-EDM, a similar phenomenon is believed to happen only at a much smaller gap and during a much shorter time but with a higher energy density [123].

The presence of hard but electrically conducting phases like TiN and TiB_2 in a structurally important insulating ceramic matrix-like Al_2O_3, Si_3N_4, etc. increase the electrical conductivity and subsequent EDM machining of the composite. Very little information on the micro-EDM of ceramics could be available in the literature. Kumar et al. [124] have machined conducting SiC ceramics with micro-EDM and concluded that the performance characteristics of µ-EDM are mainly governed by the plasma channel radius controlled by the discharge energy.

5.1 **Process parameters and their range**

The experimental procedure of ED milling is discussed in section 3.3.2. The electrode rotation speed (S) in rpm, gap voltage (V) in volt and capacitance (C) in microfarad were considered as control factors while material removal rate (MRR) in mm^3/min and EWR in mm^3/min are taken as response parameters. The control factors and their ranges are shown in table 5.1 based on literature review and machine capability. For this study, 20 experiments designed with three control factors with their three levels.

Table 5.1 ED milling parameters

No.	**Parameters (unit)**	**Values**
1	Speed (rpm)	500,800,1100
2	Capacitance (µF)	0.01,0.1,0.4
3	Voltage (volt)	80,100,120
4	Electrode	Tungsten
5	Electrode diameter	500 micron
6	Channel length	5mm
7	EDM oil	De-aromatized Hydrocarbon Fluid

5.2 **Design of experiments**

Response surface methodology (RSM) has been used in parameter optimization of micro ED-milling of the TiN-Al_2O_3 ceramic composite. An attempt has been made to create microchannels of 500 µm depth and 5 mm length in the ceramic-composite with the help of tungsten rod electrodes (diameter 500 µm) by micro electro-discharge milling (µ-ED Milling). All the machining experiments were performed on a hybrid µ-EDM (DT-110i) machine (Mikrotools, Singapore). Schematic diagram of the equipment assembly is presented in chapter 3 (Fig. 3.6). Response surface methodology (RSM) with a series of 20 experiments was adopted with three input parameters to study the machinability of this ceramics. The experimental details are shown in Table 5.2. Twenty microchannels of 5 mm length and 500 µm × 500 µm cross-section were generated with the micro ED-milling method as shown in Fig. 5.2. De-aromatized hydrocarbon was used as the dielectric fluid whose properties are enlisted in Table 3.7.

Table 5.2 Experimental details and responses

Run	**Spindle speed (rpm)**	**Voltage (volt)**	**Capacitance value in µF**	**MRR (mm^3/min)**	**EWR (mm^3/min)**	**Overcut (mm)**
1	800	100	0.1	0.036585	0.002356	0.047785
2	1100	80	0.4	0.054022	0.00453	0.042755
3	1100	120	0.4	0.060274	0.006710	0.03873
4	500	120	0.01	0.016152	0.003850	0.04577
5	1100	80	0.01	0.007009	0.005950	0.001495
6	800	100	0.1	0.035658	0.00249	0.00781
7	500	80	0.4	0.035767	0.002389	0.019615
8	500	80	0.01	0.013783	0.00155	0.034705
9	800	100	0.01	0.038760	0.00217	0.04577
10	800	100	0.1	0.040179	0.00259	0.029675
11	1100	100	0.1	0.013377	0.00437	0.029675
12	800	100	0.1	0.056890	0.00266	0.0337

13	500	120	0.4	0.106383	0.00339	0.029675
14	500	100	0.1	0.022796	0.00294	0.03672
15	800	100	0.1	0.035629	0.002204	0.047785
16	800	100	0.4	0.113136	0.00326	0.034705
17	1100	120	0.01	0.015085	0.004270	0.019615
18	800	100	0.1	0.035942	0.002978	0.034705
19	800	120	0.1	0.089463	0.003093	0.006115
20	800	80	0.1	0.044643	0.003030	0.04577

5.3 **An empirical model for performance measures**

Defining the analytic model for advanced ceramics for micromachining is very difficult due to the presence of nonconductive phase in composite and complexity in machinability. Therefore empirical modeling of MRR and EWR with multi variable regression modeling was established and ANOVA was performed to examine it statistically.

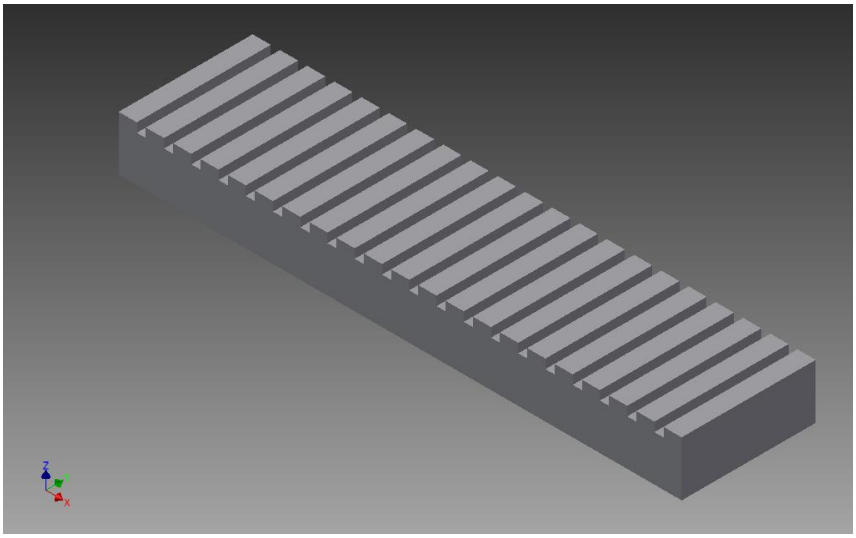

Figure 5.1 3D model of microchannels on composite

The significant control factors were detected and the interaction effects of these control factors on performance measure were investigated. The CAD model of microchannels is shown in Fig. 5.1 and the actual image of microchannels on TiN-Al_2O_3

ceramic-composite are given in Fig. 5.2. The response parameters were analyzed by Design-Expert software®. Adequacy of the model has been checked by various tests like analysis of variance (ANOVA), the sequential model sum of the square, lack of fit and model summary.

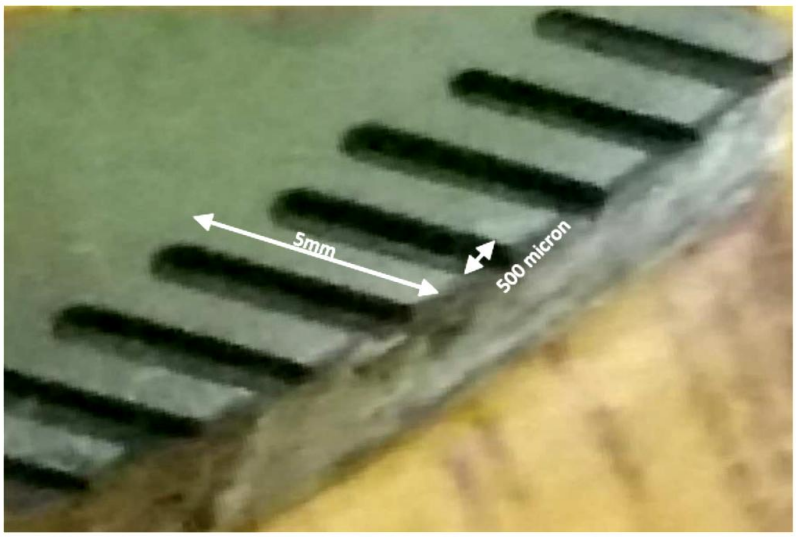

Figure 5.2 Micro-channels of dimensions (500 microns × 500 microns) and of 5 mm in length

5.3.1 ANOVA results for the material removal rate and electrode wear rate

The analysis of variance (ANOVA) for MRR is shown in Table 5.3 and for EWR is shown in Table 5.4. ANOVA results are analyzed by design expert software®. Determination-coefficients were calculated for checking the quality of fitting of the model for MRR and EWR as shown in Table 5.3 and Table 5.4. Determination coefficients for MRR (R^2 = 87.16%) and for EWR (R^2 = 93.05%) indicate the high significance of the developed models as it is showing close agreement with the determination coefficient and the significance of the given model. The Value of Prob >F Value less than 0.0500 indicates the significant model terms. For MRR, the regression model is significant as the P-value is 0.002. The P-value for voltage is 0.018, for capacitance 0.00 and for speed × speed is 0.002, which indicates the significance of these terms.

Table 5.3 ANOVA results for material removal rate (MRR)

Source	DOF	Sum of square	Mean sum of square	F value	P-value
Regression	9	0.014745	0.001638	7.54	0.002
Voltage	1	0.001746	0.001746	8.04	0.018
Capacitance	1	0.007773	0.007773	35.79	0.000
Speed × speed	1	0.001661	0.003850	17.73	0.002
Capacitance×Capacitance	1	0.001149	0.001149	5.29	0.044
Residual error	10	0.002172	0.002172		
Lack of fit	5	0.001820	0.000364	5.18	0.058
Pure error	5	0.000351	0.000070		
Total	19	0.016916			
S	0.0147361		Press	0.0213735	
R-Sq	87.16%		R-sq adj	75.61%	

Table 5.4 ANOVA results for electrode wear rate (EWR)

Source	DOF	Sum of square	Mean sum of square	F value	P value
Regression	9	1.375E-005	1.528E-006	14.88	0.0001
Speed	1	7.728E-006	7.728E-006	75.27	0.0001
Voltage	1	8.667E-007	8.667E-007	8.44	0.0157
capacitance	1	1.274E-006	1.274E-006	12.41	0.0055
Speed × speed	1	1.720E-006	1.720E-006	16.75	0.0022
Residual error	10	1.027E-006	1.027E-007		
Lack of Fit	5	6.690E-007	1.338E-007	1.87	0.2543
Pure Error	5	3.578E-007	7.155E-008		
Total	19	1.478E-005			
S	0.00032		Press	4.5689567691621e-006	
R-sq	93.05 %		R-sq adj	86.80%	

From ANOVA result, the capacitance is come out to the most significant terms followed by voltage for MRR. For EWR, the regression model is significant as the P-value is 0.001. The significant terms for EWR are speed and voltage that hold P values as 0.0001 and 0.0157.

5.4 **Validation of the models**

The sequential sum of the square, lack of fit test and model summary statics test were performed. The F-Value for individual control factor term is determined as the term mean square divided by the residual mean square.

High F-values (14.92 and 14.88) and low lack of fit values (5.18 and 1.87) show the high significance of the regression model for the MRR and EWR (Table 5.3 and Table 5.4). The normal probability plot of the residual for MRR (Fig 5.3) and EWR (Fig. 5.4) indicates that residual fall within six-sigma limits and form almost straight line representing that the errors are normally distributed.

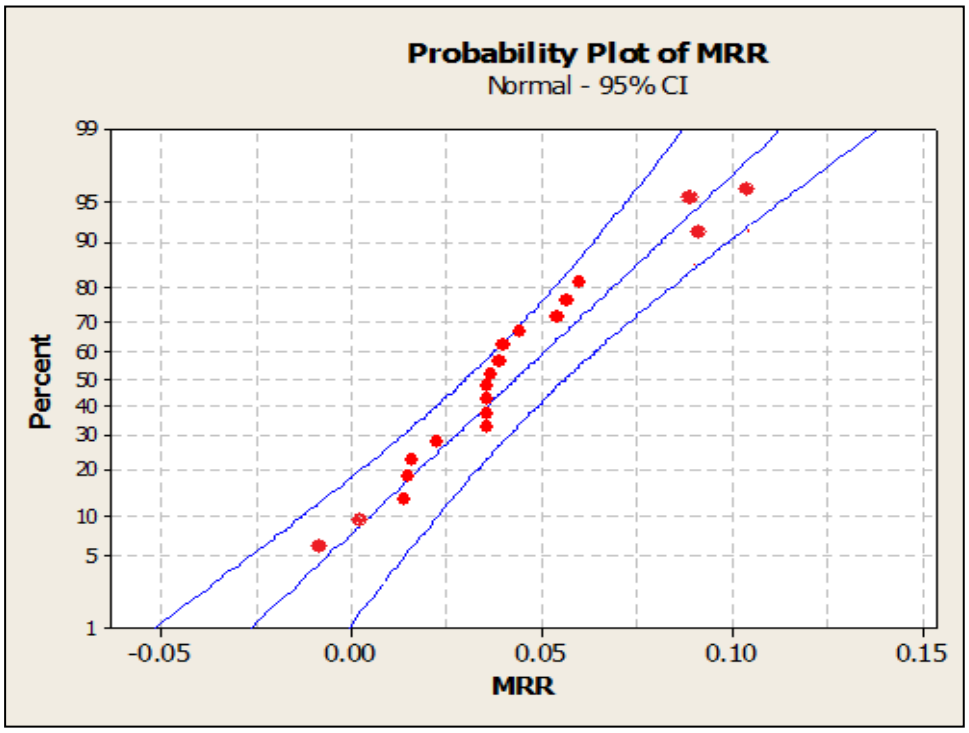

Figure 5.3 Probability plot for MRR

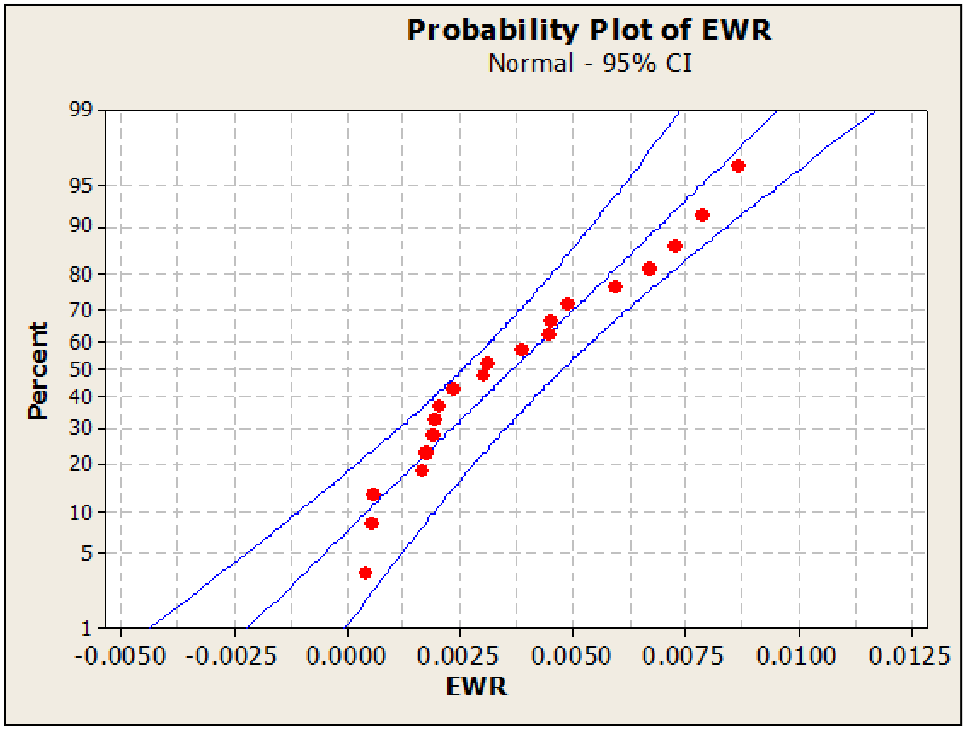

Figure 5.4 Probability plot for EWR

The empirical relation between the response parameters and control factors are expressed by the second-order polynomial equation 5.1 and 5.2.

The equations are:

MRR $= 0.0463 + (0.00081 \times S) - (0.00621 \times V) - (0.21139 \times C) - (4.15 \times 10^{-7} \times$ S2 +2.887×10−5 ×V2+0.0204×C2+0.00041×V×C …………... (5.1)

EWR =

$0.0316178 - (1.33264 \times 10^{-5} \times S) - (3.28437 \times 10^{-4} \times V) - (0.00438857 \times C) +$ $(0.000282318 \times S^2$ ………………………………………………………...…… (5.2)

The response and predicted values are shown in Table 5.5 and their graphs are shown in Fig. 5.5 and Fig. 5.6. The predicted values of MRR and EWR are showing the same pattern as experimental values.

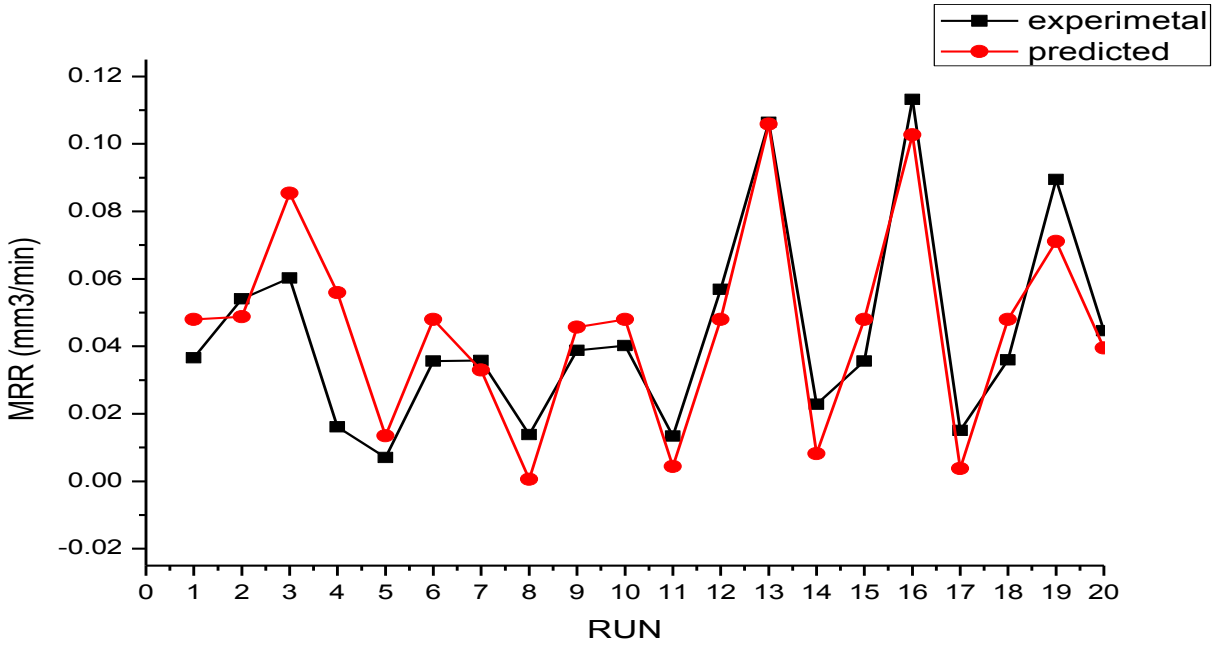

Figure 5.5 Experimental and predicted values of MRR

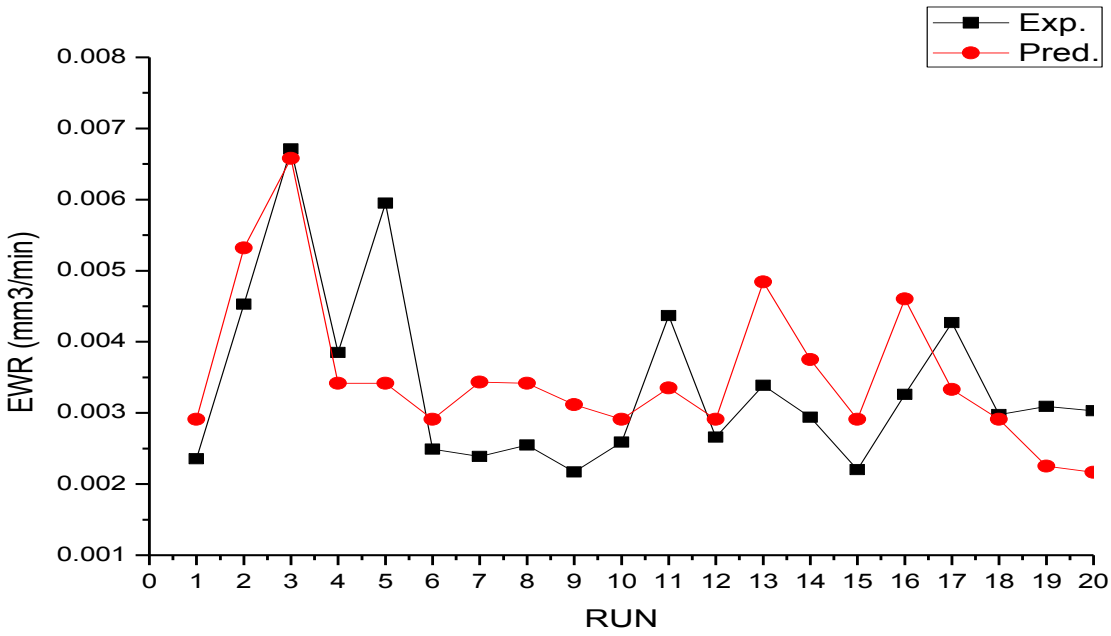

Figure 5.6 Experimental and predicted values of EWR

Table 5.5 Experimental and predicted values of response parameters

Run	**MRR (mm^3/min)**	**EWR (mm^3/min)**	**Predicted MRR (mm^3/min)**	**Predicted EWR (mm^3/min)**
1	0.036585	0.002356	0.048000	0.0053955
2	0.054022	0.00453	0.048785	0.0068326
3	0.060274	0.006710	0.085355	0.0068326
4	0.016152	0.003850	0.055895	0.000041
5	0.007009	0.005950	0.013435	0.0011378
6	0.035658	0.00249	0.048000	0.0053955
7	0.035767	0.002389	0.032950	0.0068326
8	0.013783	0.00155	0.000590	0.002214
9	0.038760	0.00217	0.045690	0.0016334
10	0.040179	0.00259	0.048000	0.0053948
11	0.013377	0.00437	0.004400	0.0062302
12	0.056890	0.00266	0.048000	0.0053955
13	0.106383	0.00339	0.105845	0.0068326
14	0.022796	0.00294	0.008220	0.0062302
15	0.035629	0.002204	0.048000	0.0053955
16	0.113136	0.00326	0.102650	0.0062302
17	0.015085	0.004270	0.003795	0.0068326
18	0.035942	0.002978	0.048000	0.0053955
19	0.089463	0.003093	0.071090	0.0062302
20	0.044643	0.003030	0.039460	0.0062302

5.5 **Results and discussion**

5.5.1 **Influence of control factors on the material removal rate**

The influence of control factors could be understood by the main effect plot. It is a plot of the means at each level of factors. The magnitude of various main effects and relative

strength can be compared with these plots. Since MMR is desired to be maximized, the S/N ratio is calculated by "Larger is Better" equation 5.3.

$$\left(\frac{S}{N}\right) ratio_{MRR} = 10 \log_{10} \frac{\sum_{i=1}^{n} \frac{1}{Yi^2}}{n} \quad \text{..... (5.3)}$$

Where n= number of replications

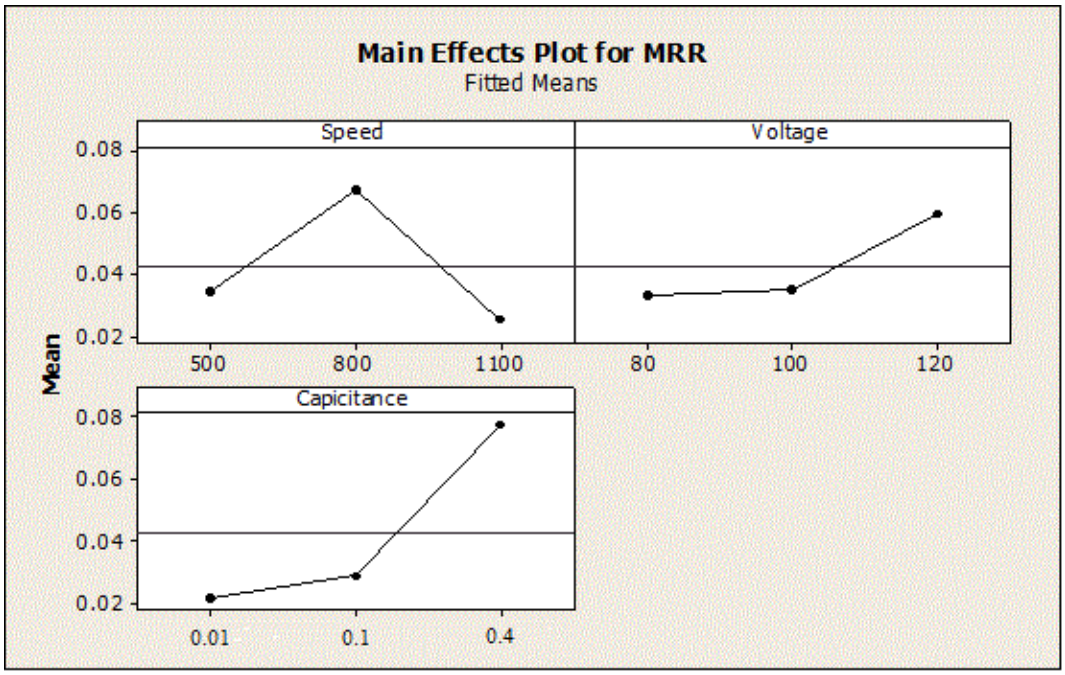

Figure 5.7 Main effects plot for MRR

From the above graph, it can be seen that the highest MRR is achieved at 800 rpm speed, 120 volt gap voltage, and 0.4 µF capacitance. The main effect plot for MRR indicates that Capacitance has the highest signal to noise ratio thus comes out to be the most significant parameter followed by voltage. MRR is highest at the maximum value of capacitance as high capacitance value indicates high discharge energy

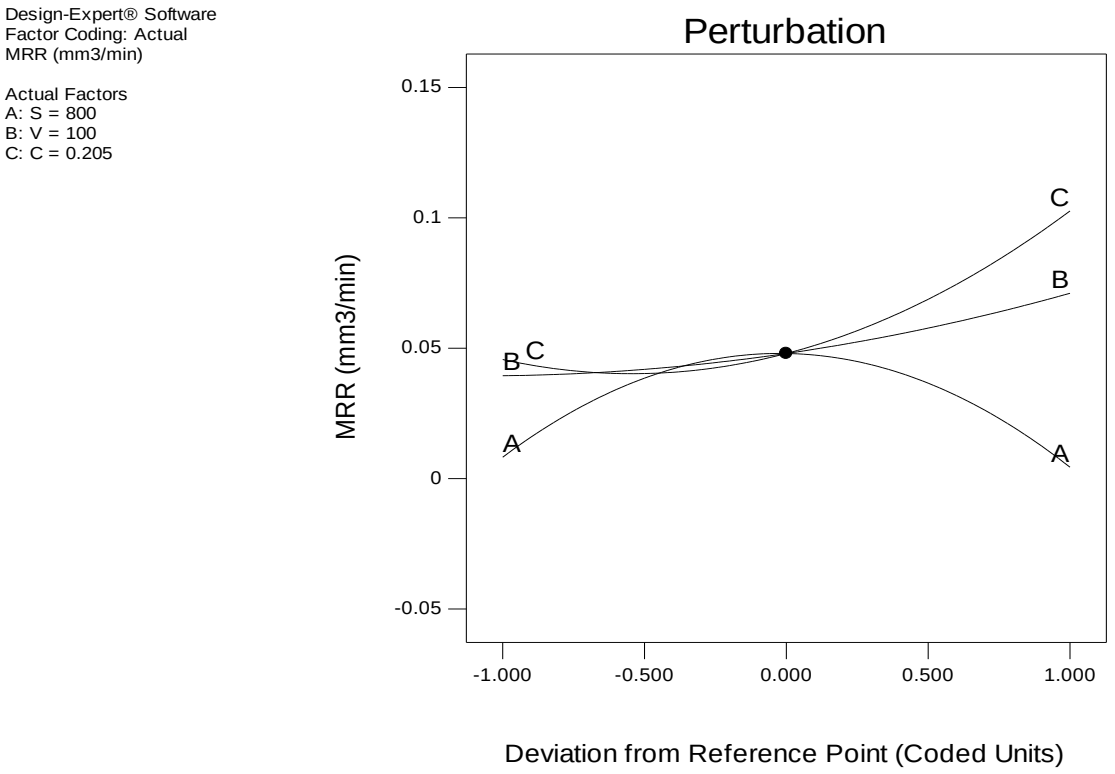

Figure 5.8 Perturbation curve for MRR

Perturbation plot for MRR shows the comparative effects of significant input parameters on MRR. Design-Expert software was used for plotting the perturbation of the input parameter shown in Fig. 5.8. For all the factors reference point is taken as midpoint (coded value). A steep slope for capacitance (C) and the input voltage (B) shows that MRR is sensitive to capacitance and voltage. A relatively less slop of electrode rotation speed shows that it has less effect in improving the MRR.

It is clear from ANOVA results (Table 5.3) that both linear and quadratic models are significant for MRR. Significant model terms are voltage (V), Capacitance (C), the square term of speed (S×S) and the square term of capacitance (C×C).

The response surface curve in Fig. 5.9, 5.10, 5.11 are showing the interactive effects of voltage, capacitance, and electrode rotation speed on MRR. Fig. 5.9 shows the effect of applied voltage and electrode rotation speed of MRR while keeping all other parameters

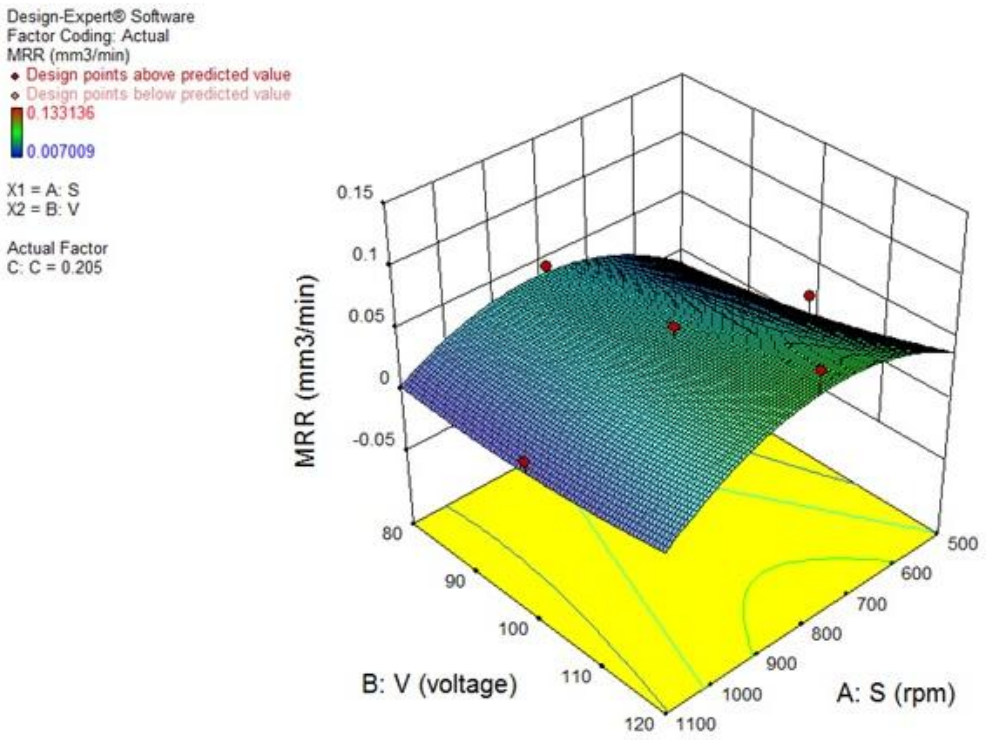

Figure 5.9 Response surface showing the interactive effect of applied voltage (V) and electrode rotation speed (S) for MRR

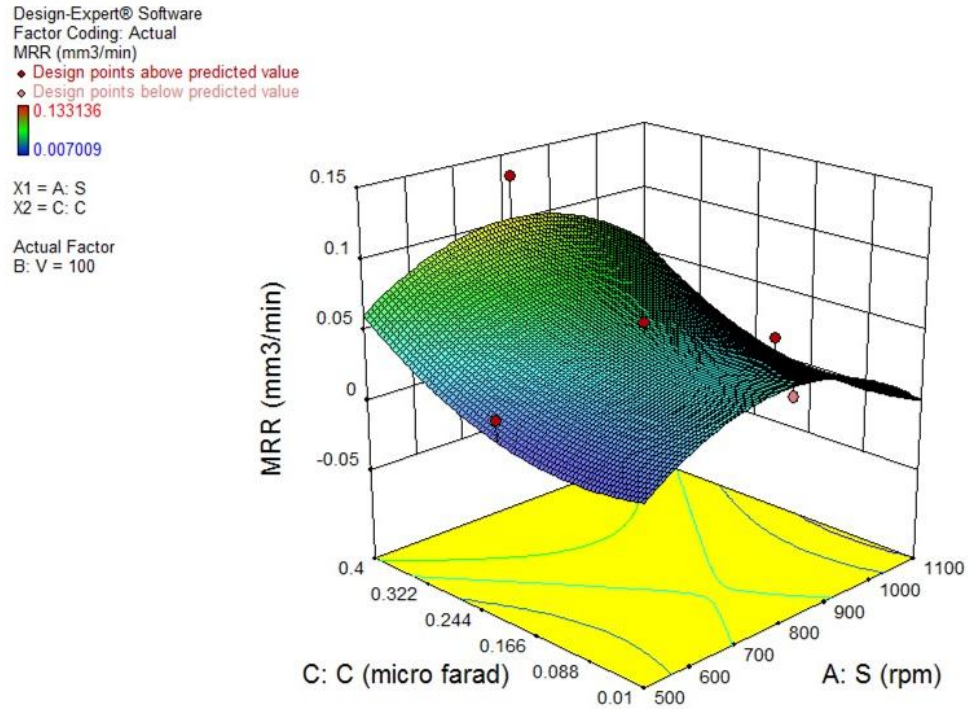

Figure 5.10 Response surface showing the interactive effect of capacitance(C) and electrode rotation speed (S) for MRR

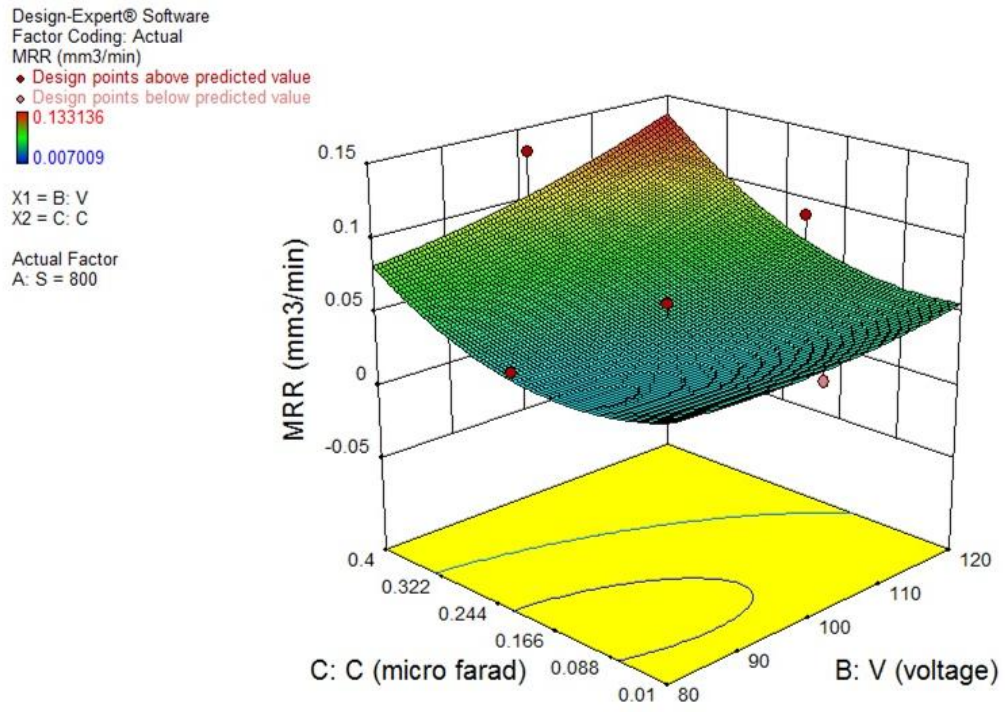

Figure 5.11 Response surface showing the interactive effect of capacitance (C) and applied voltage (V) for MRR

at middle value as indicated in plots. It illustrates that MRR increases with increase in the applied voltage that attributed to the fact that MRR is dependent on the discharge energy. Fig. 5.11 also shows that the improvement in MRR with the increase of capacitance value. The reason for the improvement in MRR is the increase in the discharge energy that can be calculated as $0.5\ CV^2$. Fig. 5.11 and 5.12 also show the improvement of MRR with electrode rotation speed. Electrode rotation speed indicates the milling effect in this hybrid process. As the electrode rotation speed increase the MRR is also increasing. Fig. 5.12 shows the combined effect of voltage and capacitance.

The effect of capacitance is more prominent at a higher value of capacitance. High capacitance and high voltage produce high discharge energy that leads to higher MRR due to the presence of hard abrasives (Al_2O_3) in the composite that requires a higher temperature for melting and vaporizing the composite.

5.5.2 **Influence of control factors on the electrode wear rate**

The value of EWR is desired to minimize, The S/N ratio for EWR is calculated by "Smaller is Better" equation 5.4. The main effect plot (Fig. 5.12) for electrode wear shows that capacitance holds rank one followed by speed and voltage. Higher capacitance and higher speed lead to more EWR. Here capacitance is the most influencing parameter followed by electrode rotation speed that indicates at higher speed and higher capacitance, discharge energy is high enough to wear out the electrode.

$$\left(\frac{S}{N}\right) ratio_{EWR} = \log_{10} \frac{\sum_{i=1}^{n} Yi^2}{n} \quad \text{..... (5.4)}$$

Where n= number of replications

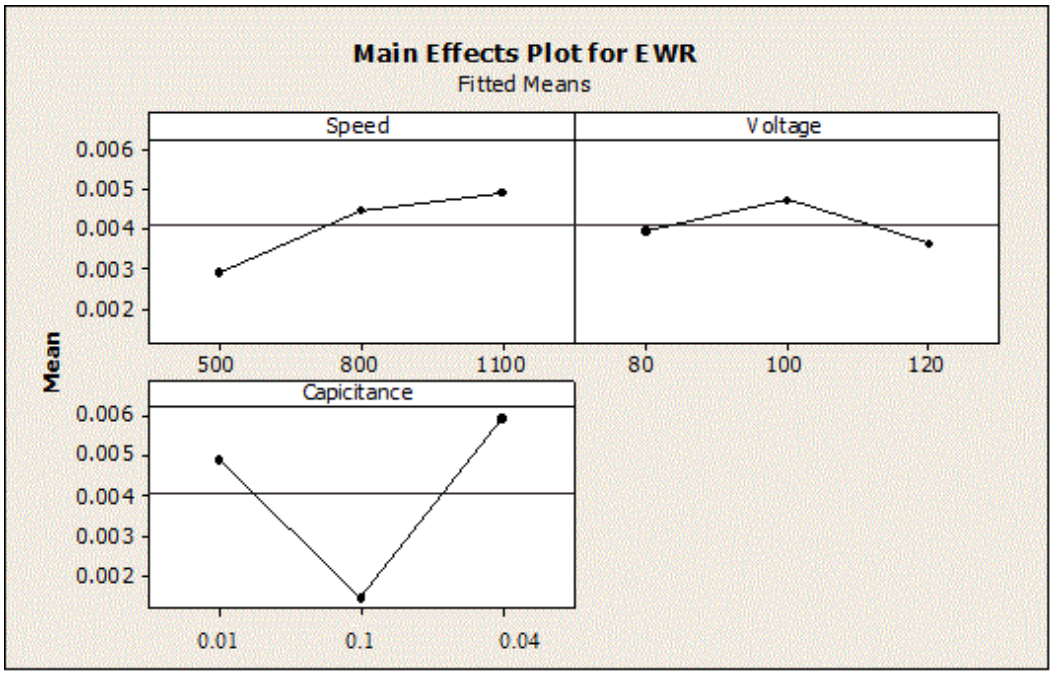

Figure 5.12 Main effects plot for EWR

Fig. 5.13, 5.14 and 5.15 are showing the surface plot for EWR. Fig. 5.13 shows that the EWR increases more with the rotational speed than with the voltage. The effect of capacitance is more prominent at a higher value of capacitance. High capacitance and high voltage produce high discharge energy that leads to higher MRR due to the presence

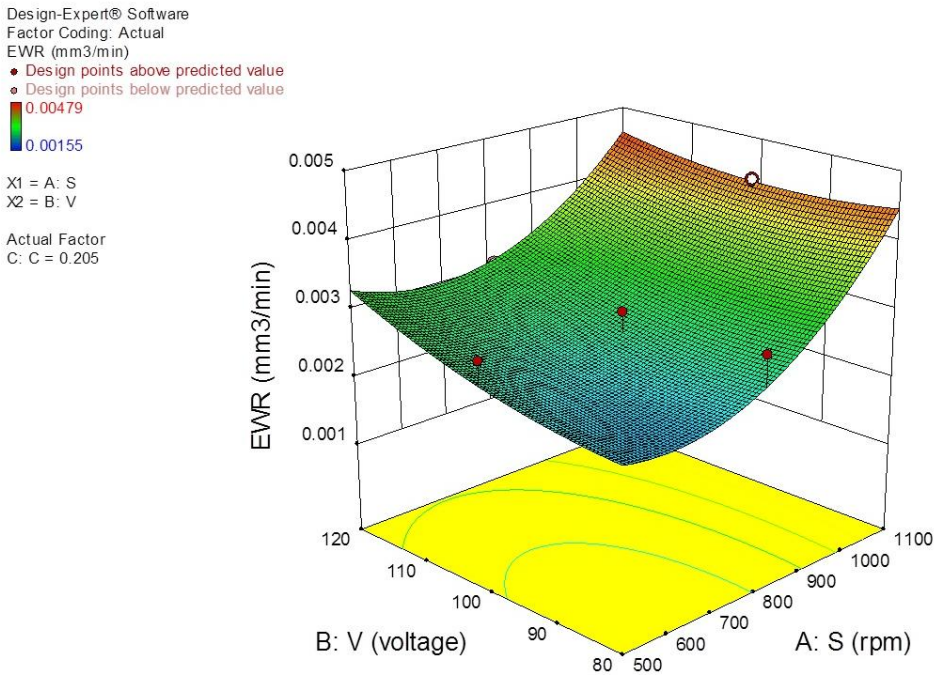

Figure 5.103 Response surface plot for EWR with applied voltage (V) and electrode-rotation speed (S)

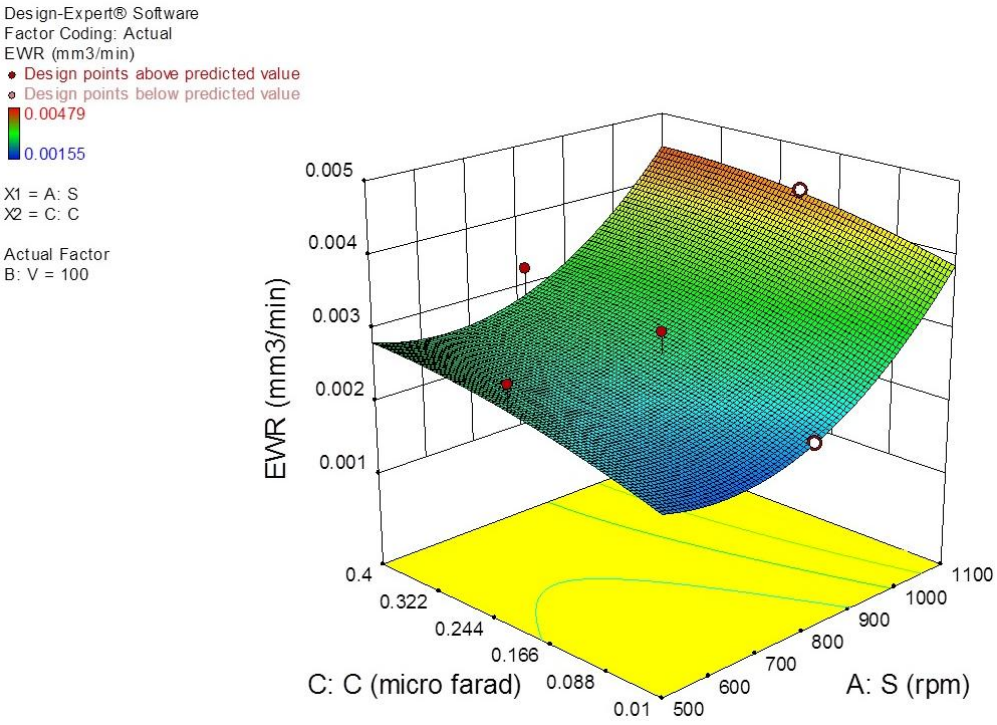

Figure 5.114 Response surface plot for EWR with capacitance (C) and electrode rotation speed (S)

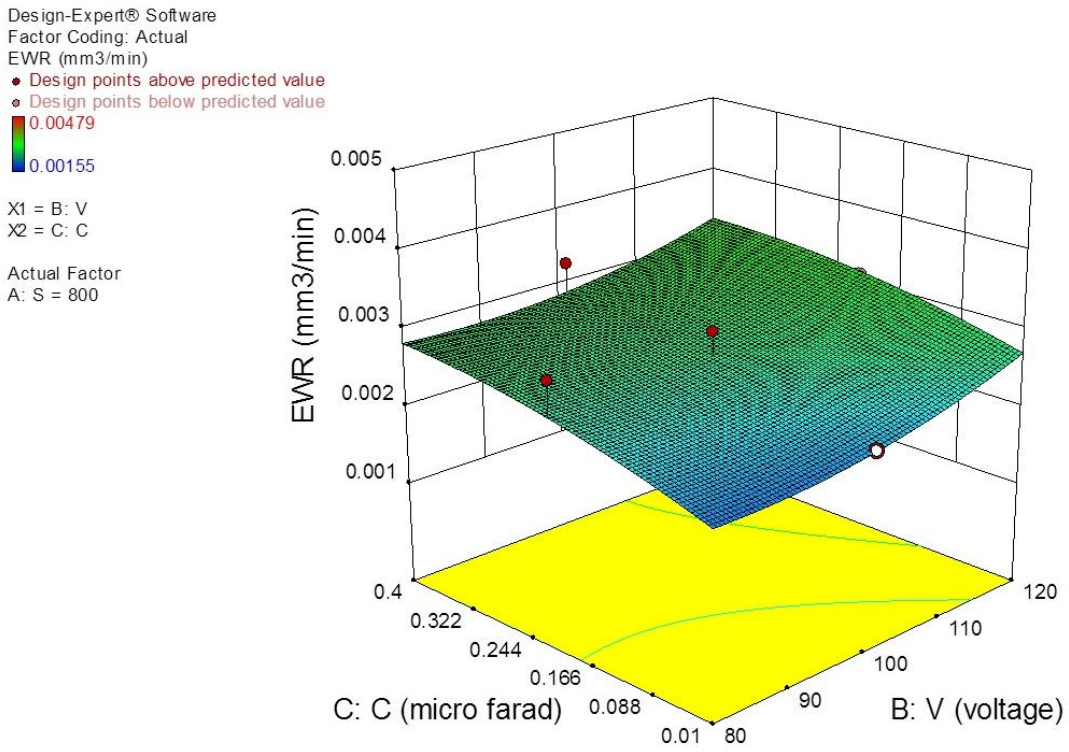

Figure 5.125 Response surface plot for EWR with capacitance (C) and voltage (V)

of hard abrasives (Al_2O_3) in the composite that requires a higher temperature for melting and vaporizing the composite. Fig. 5.14 shows, the combination of high electrode rotation speed and capacitance lead to higher EWR values. The low increment in EWR with voltage is observed at low speed but there is a sharp increment in EWR with high electrode rotational speed as shown in Fig. 5.15.

5.5.3 **Influence of control factors on overcut**

In EDM, the electric spark occurs between the two nearest points on the positive and negative electrode in the presence of dielectric. Thus machining may occur on the periphery of micro features that leads to overcut.

Overcut cannot be prevented as it is inherent to the EDM process, it only is controlled by a suitable parameter setting. The effects of various control parameters are shown in Fig. 5.16. As shown in Fig. 5.16 (a), the overcut tends to increase with the increase in the value of electrode rotation speed.

This is due to the fact that by increasing the rotation speed, the centrifugal force increases that lead to the removal of debris from interelectrode gap (IEG) and place them inside gap

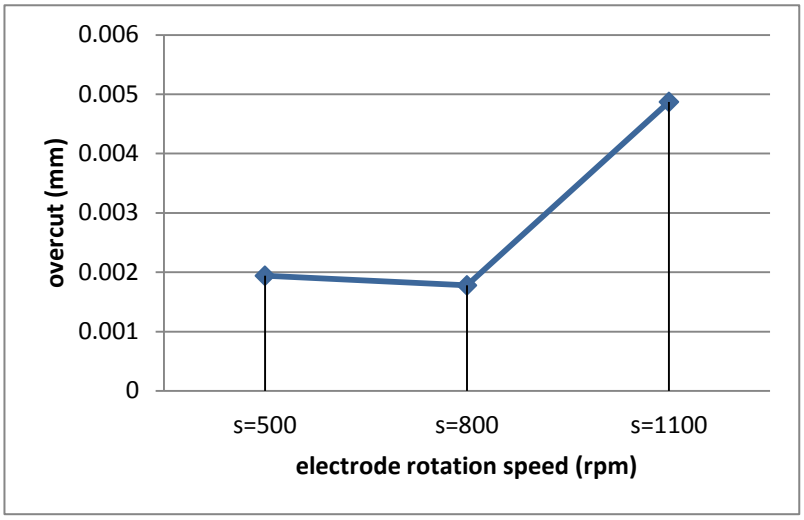

(a) Effect of increase in rotation speed

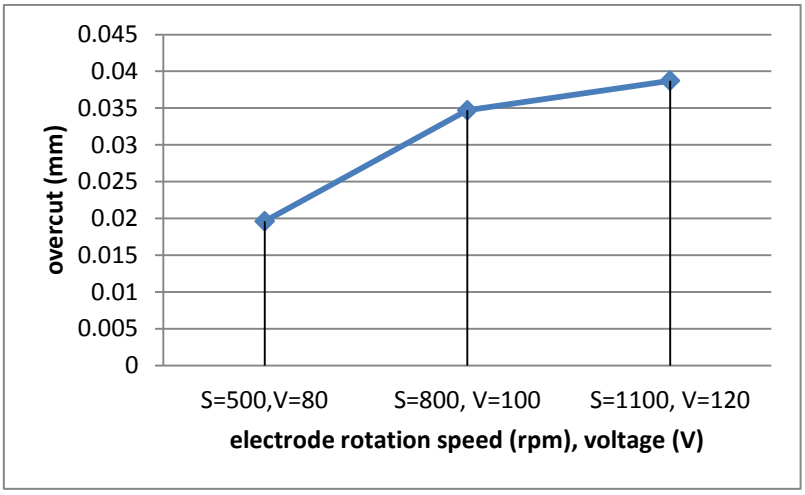

(b) Effect of increase in rotation speed and voltage at high capacitance (C=0.4 µF)

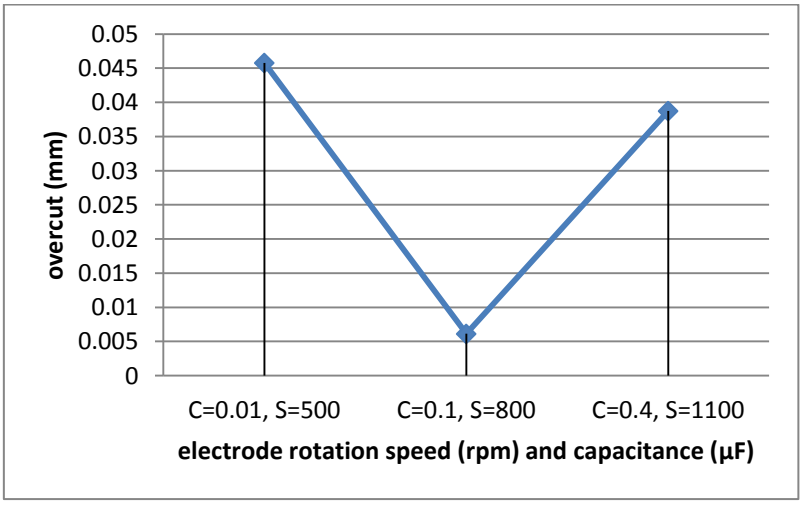

(c) Effect of increase in capacitance and speed at high voltage (V=120 V)

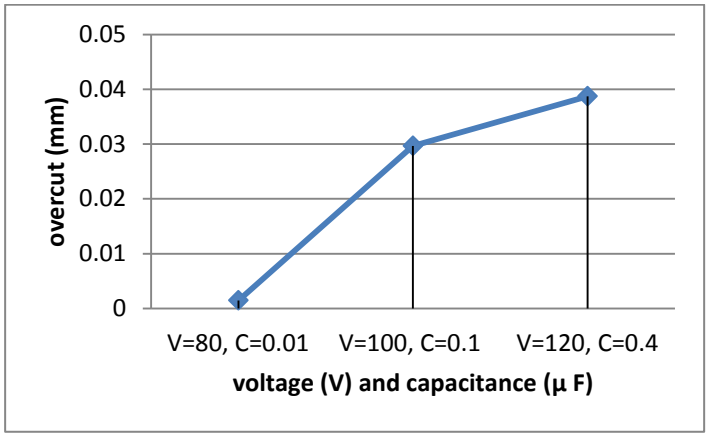

(d) Effect of increase in voltage and capacitance at high speed (S=1200 rpm)

Figure 5.136 Influence of control factors on overcut

thus leads to side spark. This phenomenon increases with the increase in speed and leads to more overcut. Fig. 5.16 (b) is showing the effect of voltage with electrode rotation speed. The graph is showing that the increase in overcut (OC) with combined increased in speed and voltage. The first reason behind the increase of over cut is an increase in centrifugal force on debris and another reason which leads to increasing overcut is an increase in discharge energy. More discharge energy tends to remove more material from the channel walls.

As higher voltage leads to having more overcut thus at a high voltage setting the overcut is studied. Fig. 5.16 (c) is showing the effect of an increase in capacitance and speed at high voltage. High capacitance and high speed lead to an increase in discharge energy thus more active pulses in the wall gap that result in increasing the size of the crater on the sidewalls of the tool electrode and workpiece. Thus generating discharge between them, and, as a result, OC is highest at high capacitance value 0.4µF and minimum at 0.1µF. Fig. 5.16 (d) is showing the effect of an increase in voltage and capacitance at high speed. The combination of high discharge energy and high speed leads to more removal of sidewall surface thus more overcut.

5.5.4 Mechanism of material removal

5.5.4.1 Field Emission Scanning Electron Microscope images for machining surface

Overall, the optimization analysis (Fig. 5.9 - 5.15) shows that MRR is the highest when Capacitance and Voltage are high. The reason for the improvement in MRR is the increase in discharge energy (~$1/2CV^2$). High capacitance (C) and voltage (V) produced very high discharge energy which causes spalling in the ceramic thus leading to high MRR. However, too much rotation of the rod electrode reduces the MRR after reaching a maximum value. Fig. 5.17(a) shows the FESEM micrographs of the machined surface at 0.01 µF (low energy level) and 0.4 µF (high energy level) with a constant electrode rotation speed of 1000 rpm and voltage 100 V.

Material removal is the consequence of interaction of discharge plasma with the surface of workpiece materials generally used as cathodes. However, the characterization of plasma formed during the micro EDM of Titanium metal workpiece had shown that low capacitance and tool electrode gap could produce a plasma temperature as high as 6170 K [125].

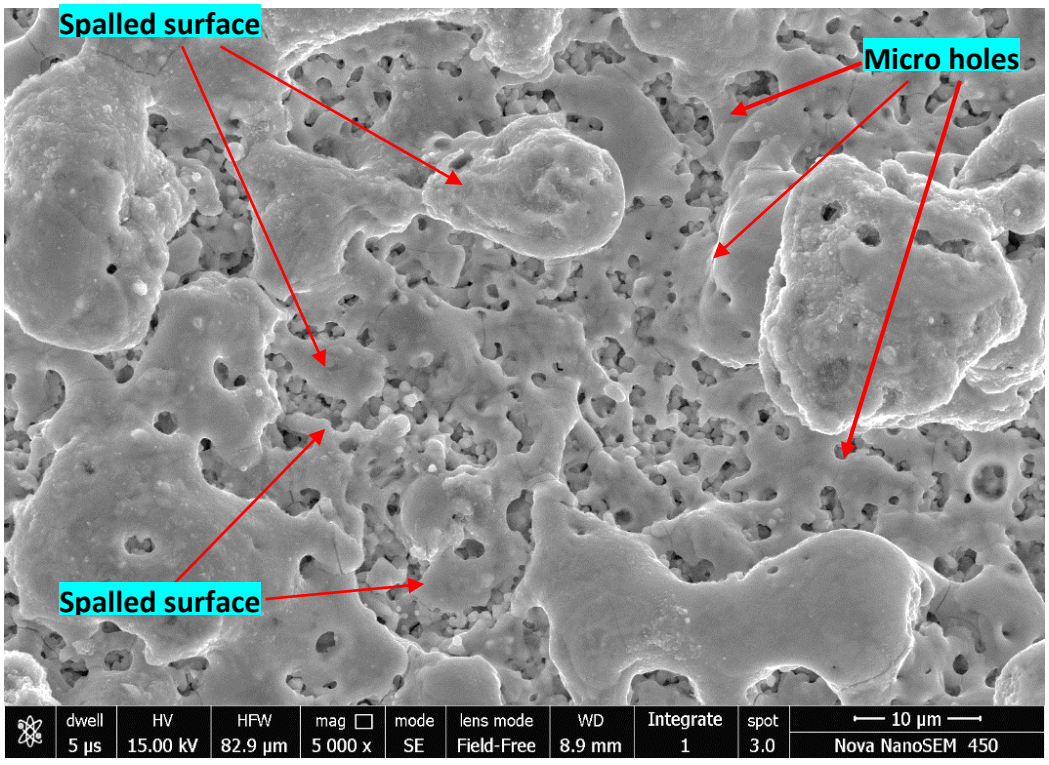

(a) At 0.01 µF

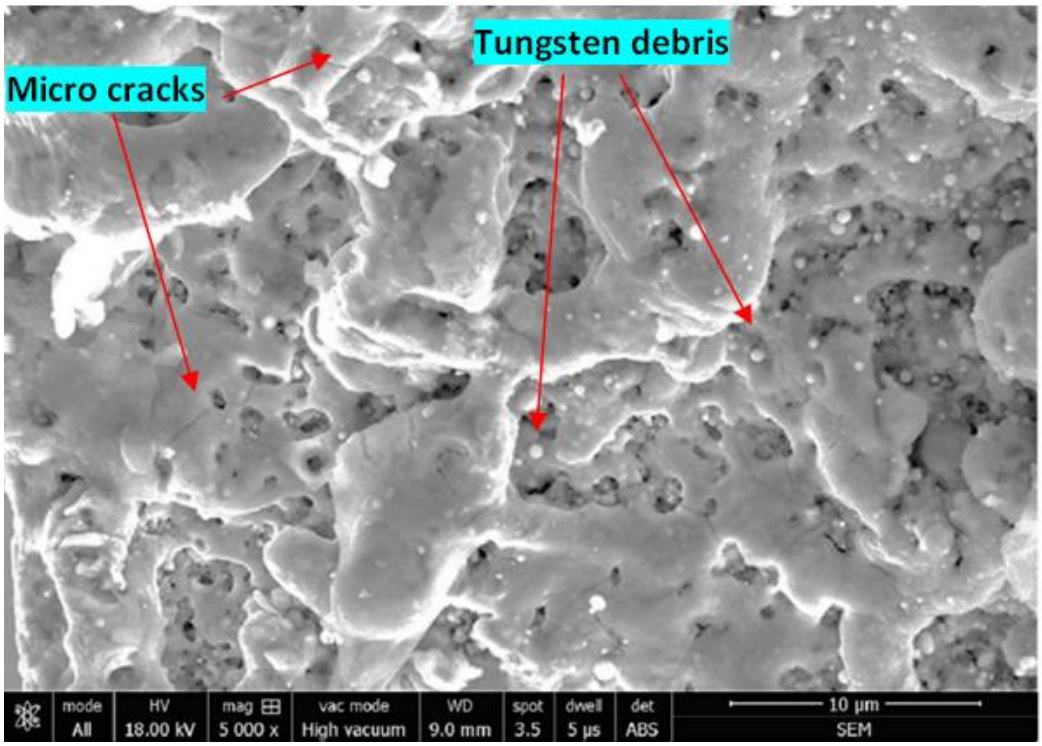

(b) At 0.1 µF

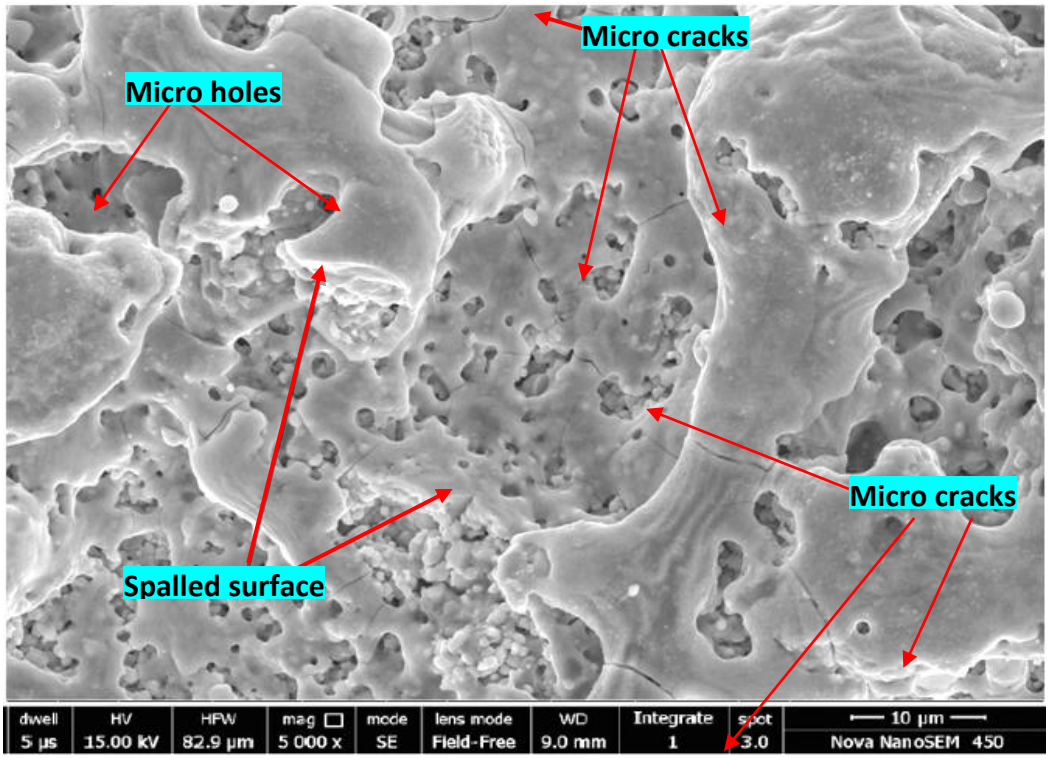

(b) At 0.4 µF

Figure 5.147 FESEM micrograph of the machined surface

It may, therefore, be possible that high melting point of ceramics will need high discharge energy of the plasma for the melting and erosion of the surface of the composite in the present study. Gas bubble formation within the melt (micro-holes in Fig 5.17) formed by the oxidation of TiN at high temperature. Some areas of spalling could also be noticed in the micrographs are due to the presence of non-conducting Al_2O_3 phase in the material. Important feature noticed after comparing Fig. 5.17 (a) and Fig. 5.17 (b) is that the vertical cracks in the re-solidified surface layers are mostly observed in the samples machined under high capacitance {Fig. 5.17 (b)} and consequently high discharge energy. Such vertical microcracks will propagate and meet the horizontal cracks present sub-surface and remove the whole material under the spalled zone [126] [82].

Thus, the parameters could be optimized to have both rough and fine machining regime. Electrode Wear Rate (EWR) is the other output response studied in the present work. EWR during EDM had earlier been found to be dependent on the shape and materials as well as the current, elapsed time of the pulse and flushing pressure [19]. Dependence of EWR on electrode rotation speed along with capacitance is an interesting observation in the present study [Fig. 5.14 and Fig. 5.15]. The debris from the workpiece surface accumulates in the gap between the electrode and the workpiece which is very small in micro-EDM. High rotation speed should flush out the debris but at the same time erodes the electrode at a much higher rate. Therefore, the primary reason for the highest electrode wear in case of highest rotation speed and discharge energy is the higher abrasive erosion rate of the electrode by the debris formed from the workpiece surface. Therefore, the reason for the optimal value of the rotation speed on MRR could be explained by the fact that high EWR deforms the shape of the tool and reduces the diameter of the rod near the tip. Consequently, the material removal becomes less due to lower plasma volume [Fig. 5.14 and Fig. 5.15].

5.5.5 **EDS analysis of machined surface**

Energy-Dispersive X-Ray Spectroscopy (EDS) is used to find the chemical composition of machined surface down to a size of few microns as shown in Fig. 5.18 and color Mapping of constituents present on the surface is present Fig. 19. In this, a micro pit is

focused and micro pit along with a surrounded area is studied. Table 5.6 shows the presence of Al, Ti and O, and N in the surface of µ-EDM samples.

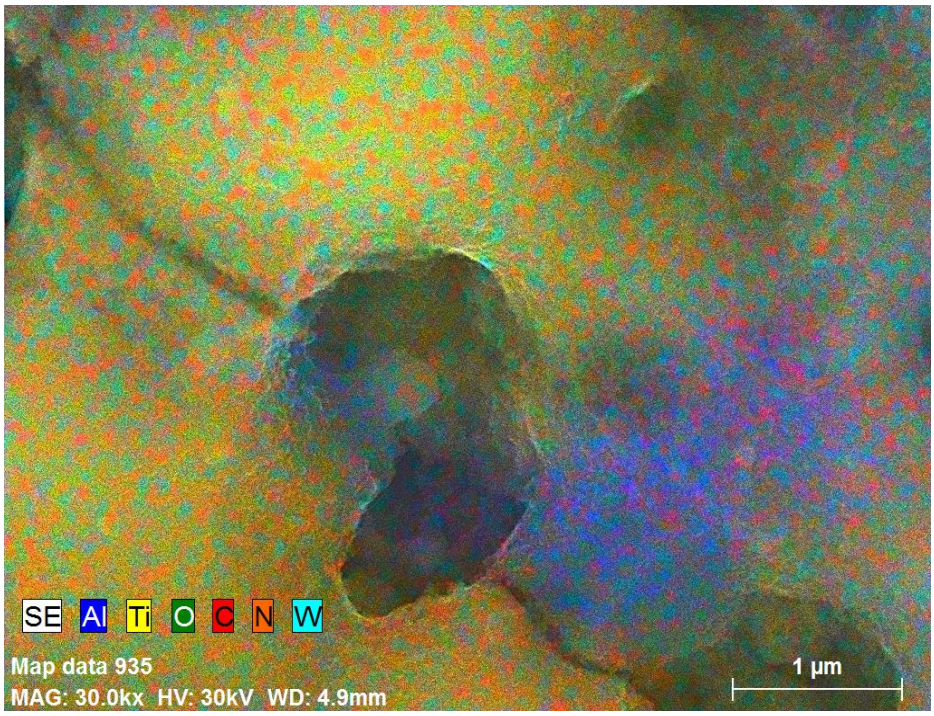

Figure 5.18 SEM image of ED milling surface for EDS

Table 5.6 EDS data for machined surface by ED milling

Elements			**µ-EDM (S=1100 rpm, C= 0.1 µF, V=100 volt)**		
Name	Atomic number	series	Unn. Wt.%	C.norm. Wt.%	C. Atom. Wt.%
Ti	22	K-series	57.80	48.39	24.77
O	8	K-series	29.75	24.91	38.15
Al	13	K-series	15.31	12.81	11.64
W	74	L-series	0.83	0.70	0.09
C	6	K-series	9.34	7.82	15.96
N	7	K-series	6.42	5.37	9.40

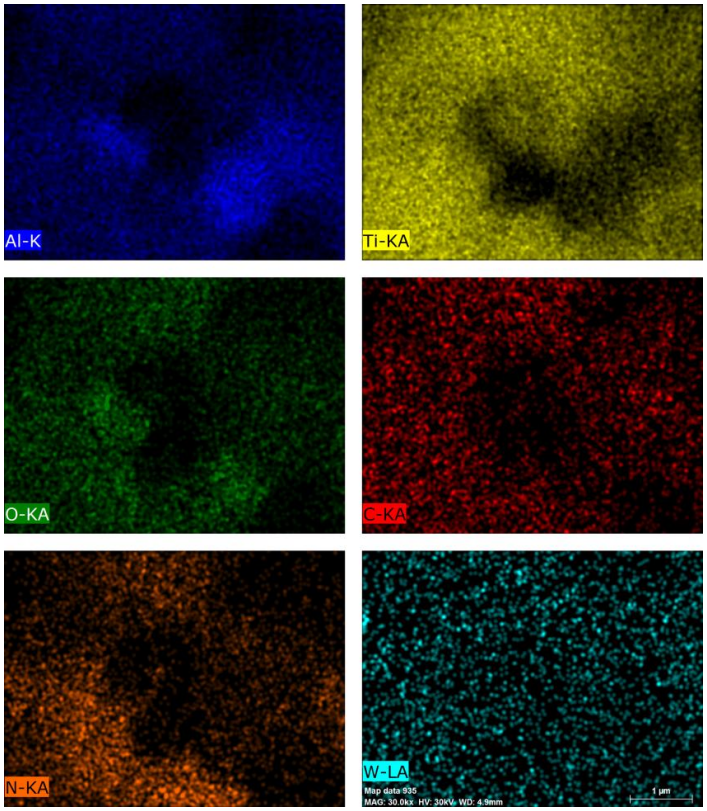

Figure 5.19 Color mapping of elements on ED Milling surface

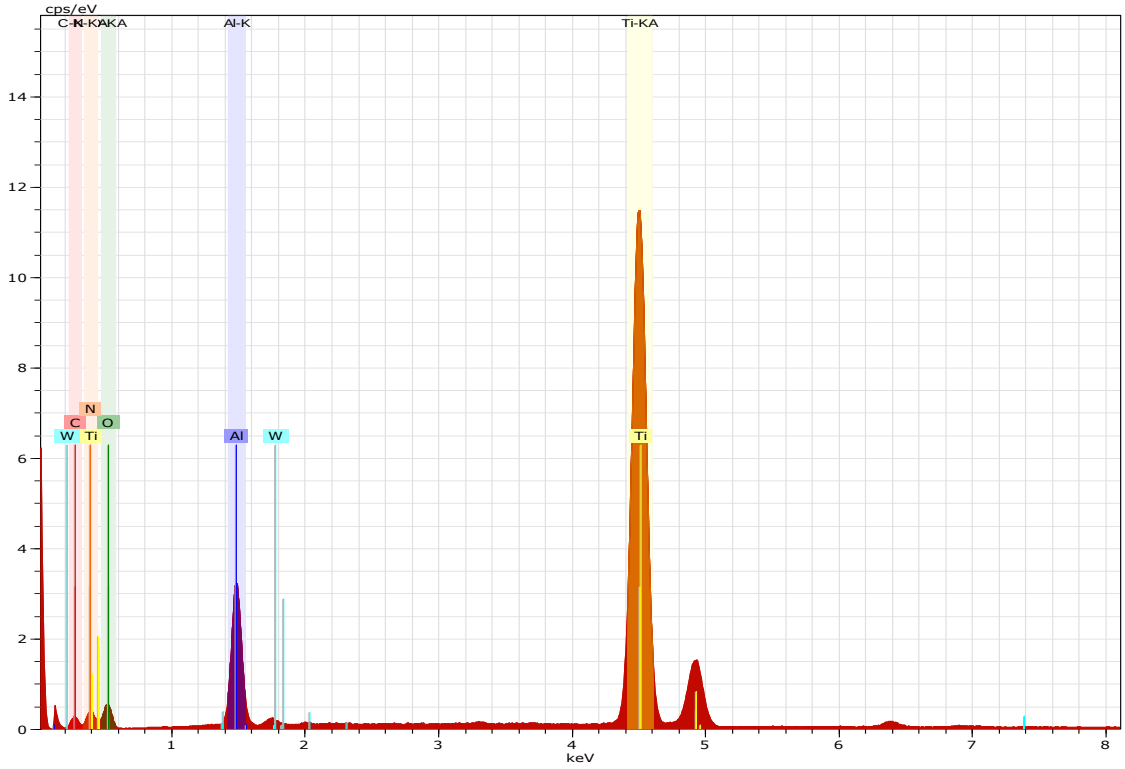

Figure 5.20 EDS plot for machined surface by ED Milling

The topography of the samples is different from those of oxidized samples under ambient conditions indicating the formation of amorphous Ti-Al-O-N phase during the quenching under the EDM machining conditions. However, the presence of nitrogen in the melt indicates that either the penetration of electron beam to much deep inside the surface acquiring the information from the subsurface region of the melt is actually a Ti-Al-O-N quaternary system. The high amount of carbon in the surface originated from the dielectric breakdown of the organic liquid The EDS spectrum is portrayed as a plot of x-ray counts vs. energy (in keV) in. Energy peaks correspond to the various elements in the sample as shown in Fig. 5.20.

5.6 **Summary**

In the present chapter, the fabrication of microchannels on TiN-Al_2O_3 ceramic-composite, which has the potential applications in micro devices such as microchemical reactors and high-temperature heat exchangers; is accomplished by µED-milling both in the rough and fine machining regime. RSM reveals, the dependence of MRR primarily on the high electrical discharge energy derived from capacitance and applied voltage while the EWR depends mainly on the rotation speed of the tool. Material removal mechanism and surface damage of machined TiN-Al_2O_3 ceramic-composite, electroconductive, and chemically inert ceramic-composite have been also analyzed from field emission scanning electron micrographs (FESEM). Analysis of the topology of the surfaces machined at different capacitances by FESEM shows the appearance of amorphous re-solidified layer devoid of granular features and having vertical cracking arising out of high cooling rate due to the circulation of dielectric fluid. Some areas in the crater zone show brittle fracture due to spalling. The vertical cracks caused by thermal quench helps to remove the materials in large quantities by coalescence with the horizontal cracks. An optimum capacitance and voltage led to smooth surfaces after machining due to the stability of the electrical discharge. However, the evidence of an increase in electrode wear coupled with the decrease in the material removal and with the increased rotation speed indicates an abrasive erosion of the electrode by the high quantity of debris formed from the TiN-Al_2O_3 ceramic-composite workpiece present in the IEG. Evidence of electrode material migration could be confirmed from the presence of tiny tungsten

globules on the surface. EDS results show the presence of Ti-Al-O-N phase on the machined surface of the material along with tungsten. This experimental study could help practicing engineers to develop micro-channel based miniaturized products of TiN-Al_2O_3 ceramic-composite.

6. EXPERIMENTAL INVESTIGATION OF SIC POWDER MIXED MICRO-ELECTRO-DISCHARGE MACHINING OF TiN-Al_2O_3 CERAMIC-COMPOSITE FOR HIGH ASPECT RATIO MICRO HOLES

In the present scenario, there is a demand for the miniaturizing the products of materials that are of lightweight and possess high mechanical properties. Metal matrix composite (MMC), ceramic matrix composite (CMC) are fit in the present requirements of material that is applicable in the aerospace, defense, and automotive industries as discussed in chapter 2. They have superior mechanical properties like high toughness, hot hardness, low density to weight ratio and high stiffness. Micro-Electro-discharge machining (μEDM), a well-known process of the non-contact type of machining is playing an important role in machining such hard to machine materials as machining rate is not affected by the strength and the hardness. A further enhancement of the EDM process could be done by hybridizing the process. In present work powder, mixed μ-EDM is studied for knowing the effects of SiC powder inclusion in the dielectric as assisting electrodes on geometric characteristics of microfeatures. Micro features are generated that could be used in microchemical reactors and Micro-electro-mechanical system (MEMS) is one of the widely used applications of microfeatures. Micro features like micro holes, micro-channels, fins are also needed in products to resist wear and to increase the heat transfer rate [127].

6.1 Process parameters and their range

The input parameters taken in this study are spindle speed (S), voltage (V), powder concentration (C) and responses are material removal rate (MRR), electrode wear rate (EWR), radial overcut (ROC), and a taper angle (α). The different concentrations of powder in the dielectric fluid are shown in Fig. 6.1. The optimal parameter settings for the responses are determined with the help of statistical analyses.

All the experiments are performed on Hybrid μ-EDM (DT-110i) machine (Mikrotools, Singapore) shown in Fig. 3.4 and power mixed μ-EDM set up is shown in Fig. 6.2. Response surface methodology (RSM) with a series of 20 experiments is adopted to study the powder mixed Electro-discharge machining (PM-μEDM). De-

aromatized hydrocarbon fluid is used as dielectric fluid (Table 3.7) and silicon carbide powder of 120 mesh size is used as an assisted electrode. PMμ-EDM has been applied to machine Titanium-Nitride Aluminium Oxide ceramic-composite

Table 6.1 Input process parameters

Process Parameter Range		**Constant Process Parameter**	
Spindle speed (S)	900, 1200, 1500 RPM	Tool Electrode	Tungsten (ø=500μm)
Voltage (V)	90, 110, 130 Volt	Machine Feed	1.5 mm/min
Concentration (C)	2, 4,6 g/litre	Capacitance (C)	0.1 μF

6.2 **Design of experiments**

All the experiments were performed according to the response surface methodology (RSM) of central composite design (CCD) with three control factors and two response parameter Material Removal Rate (MRR) and Electrode Wear Rate (EWR).

(a) 2 g/l

(b) 4 g/l

(c) 6 g/l

Figure 6.1 Di-electric fluid with various powder concentrations

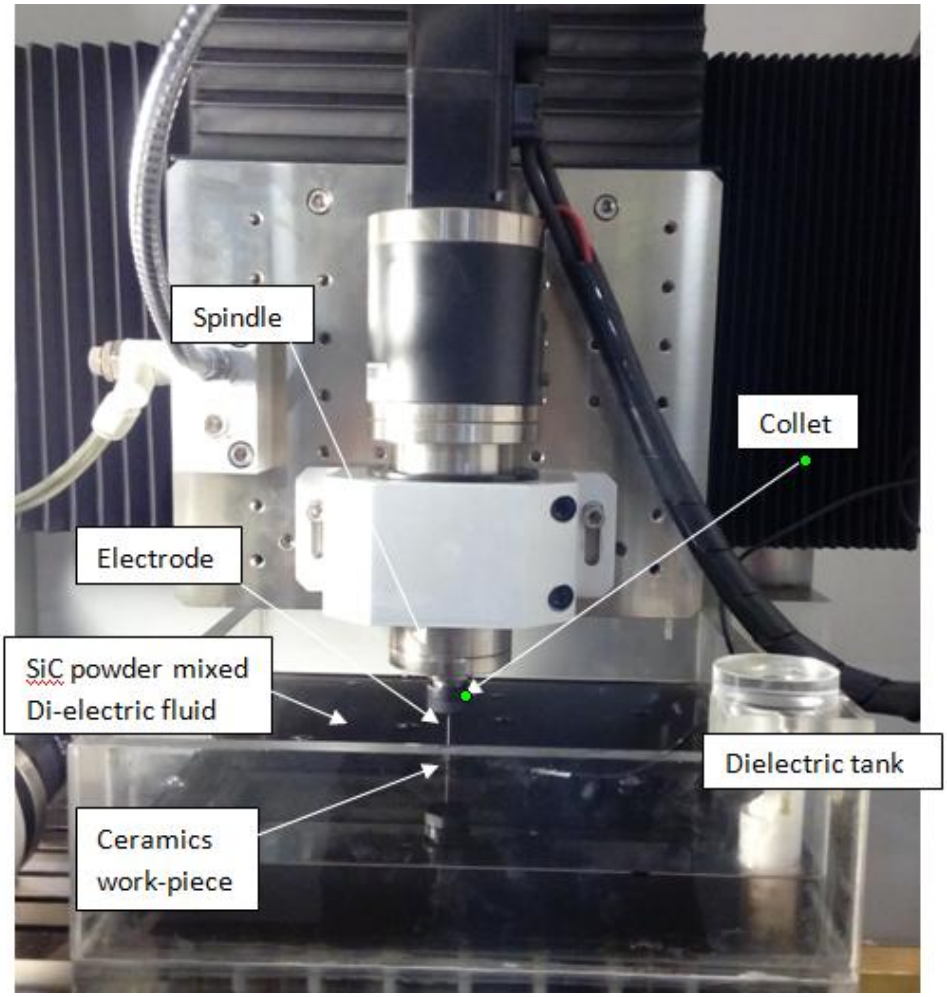

Figure 6.2 SiC powder mixed micro-EDM setup

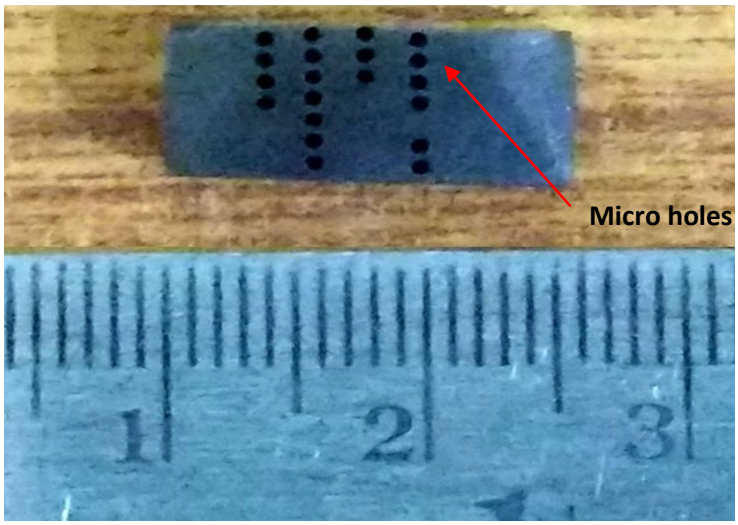

Figure 6.3 Micro-holes fabricated in work-piece

The geometric characteristics of micro-holes i.e. Radial Overcut (ROC) and Taper Angle (TA) are also observed, The details of input and output parameters are given in Table 6.1. The micro-holes on advanced ceramics workpiece are shown in Fig. 6.3 and response parameters are written in Table 6.2.

Table 6.2 Design matrix with the standard order of input parameters and responses

Std	**run**	**Speed**	**Voltage**	**Concentration of SiC**	**MRR**	**EWR**	**Radial overcut**	**Taper Angle**
		rpm	Volt	g/l	mm^3/min	mm^3/min	Micro-meter	Degree
10	1	1736	115	4	0.0243991	0.02314	31.35	8.18
8	2	1600	130	6	0.0317044	0.045137	33.525	9.11
9	3	1063	115	4	0.0244295	0.034677	30.82	5.77
3	4	1200	130	2	0.0235972	0.038406	33.19	6.92
2	5	1600	100	2	0.0230973	0.020576	37.375	9.9
17	6	1400	115	4	0.0279957	0.027495	28.885	2.418
1	7	1200	100	2	0.0317044	0.024904	32.21	6.54
20	8	1400	115	4	0.0290168	0.023727	30.225	5.38
16	9	1400	115	4	0.0299924	0.04867	30.535	5.12
15	10	1400	115	4	0.0318588	0.030144	33.395	5.47
14	11	1400	115	7	0.0327083	0.03191	33.87	5.04
11	12	1400	90	4	0.0277189	0.047335	26.555	3.99
4	13	1600	130	2	0.0283325	0.05672	33.63	4.66
5	14	1200	100	6	0.0361418	0.021102	30.8	6.64
12	15	1400	140	4	0.0292474	0.033107	30.745	8.15
13	16	1400	115	0	0.0335853	0.021636	32.89	4.63
18	17	1400	115	4	0.0282239	0.011697	30.77	9.35
19	18	1400	115	4	0.0301305	0.02314	32.08	6.84
7	19	1200	130	6	0.0284833	0.045137	33.17	3.24

6	20	1600	100	6	0.0324559	0.024677	32.36	5.67

6.3 **Influence of process parameter on MRR**

6.3.1 **ANOVA results for the material removal rate**

ANOVA results for MRR are given in Table 6.3. The Model F-value of 3.16 implies the model is significant. There is only a 4.36 % chance that an F-value this large could occur due to noise. Values of "Prob > F" less than 0.0500 indicate model terms are significant. In this case, C, AB, A^2, C^2 are significant model terms.

Table 6.3 ANOVA for MRR in response surface quadratic model

Source	Sum of Squares	DOF	Mean Square	F Value	p-value Prob > F	Remarks
Model	1.715E-004	9	1.906E-005	3.16	0.0436	significant
A (Tool rotation Speed)	1.410E-006	1	1.410E-006	0.23	0.6390	
B (Voltage)	5.557E-006	1	5.557E-006	0.92	0.3594	
C (Powder Concentration)	3.101E-005	1	3.101E-005	5.15	0.0466	significant
AB (tool rotation speed×voltage)	5.125E-005	1	5.125E-005	8.51	0.0154	significant
A^2 (tool rotation $speed^2$)	3.876E-005	1	3.876E-005	6.44	0.0295	significant
C^2 (powder $concentration^2$)	3.019E-005	1	3.019E-005	5.01	0.0491	significant
Residual	6.023E-005	10	6.023E-006			
Lack of Fit	4.991E-005	5	9.981E-006	4.84	0.0543	not significant
Pure Error	1.032E-005	5	2.064E-006			
Total	2.317E-004	19				

Values greater than 0.1000 indicates the model terms are not significant. The "Lack of Fit F-value" of 4.84 implies there is a 5.43 % chance that a "Lack of Fit F-value" this large could occur due to noise. The probability plot (Fig. 6.4) also shows that errors are normally distributed. In probability plot, all the residuals fall within six sigma limit.

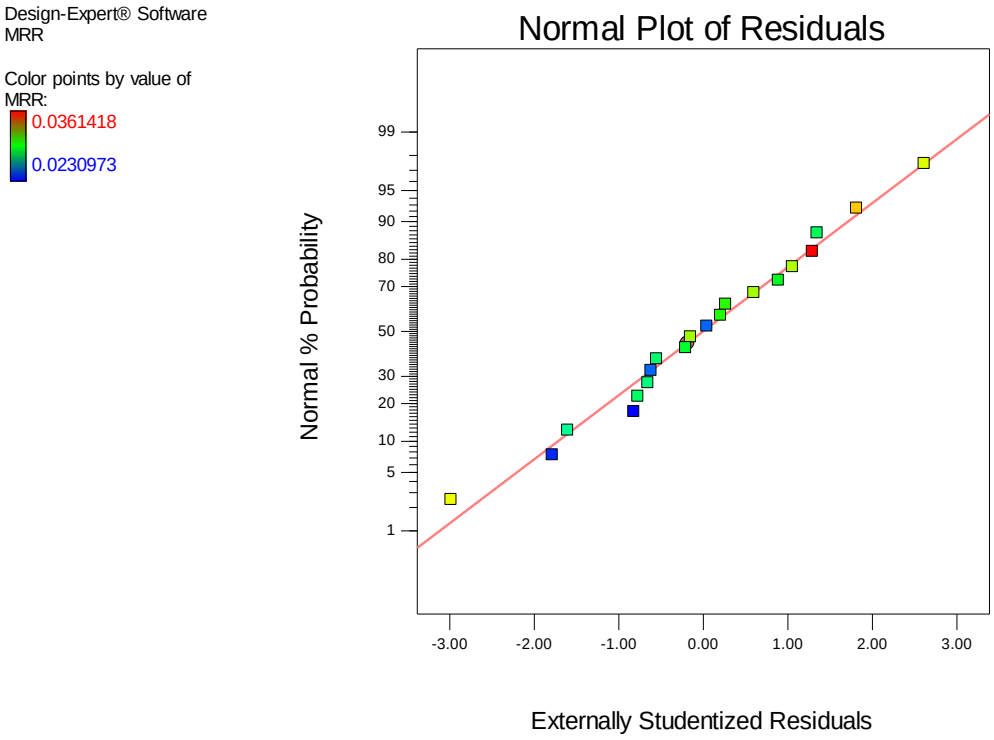

Figure 6.4 Probability plot for MRR

Fig. 6.5, 6.6 and 6.7 are showing the surface plot of MRR with voltage (V), electrode rotation speed (S) and powder concentration. The Surface plot shows that MRR increases with the increase of gap voltage and powder concentration. High voltage leads to high discharge energy thus more MRR. The high concentration of SiC particles and rotation speed also leads to high MRR showing the hybrid effect of the process. The Perbutation curve for MRR shown in Fig. 6.8, indicates that the concentration of SiC particles has a significant influence on MRR.

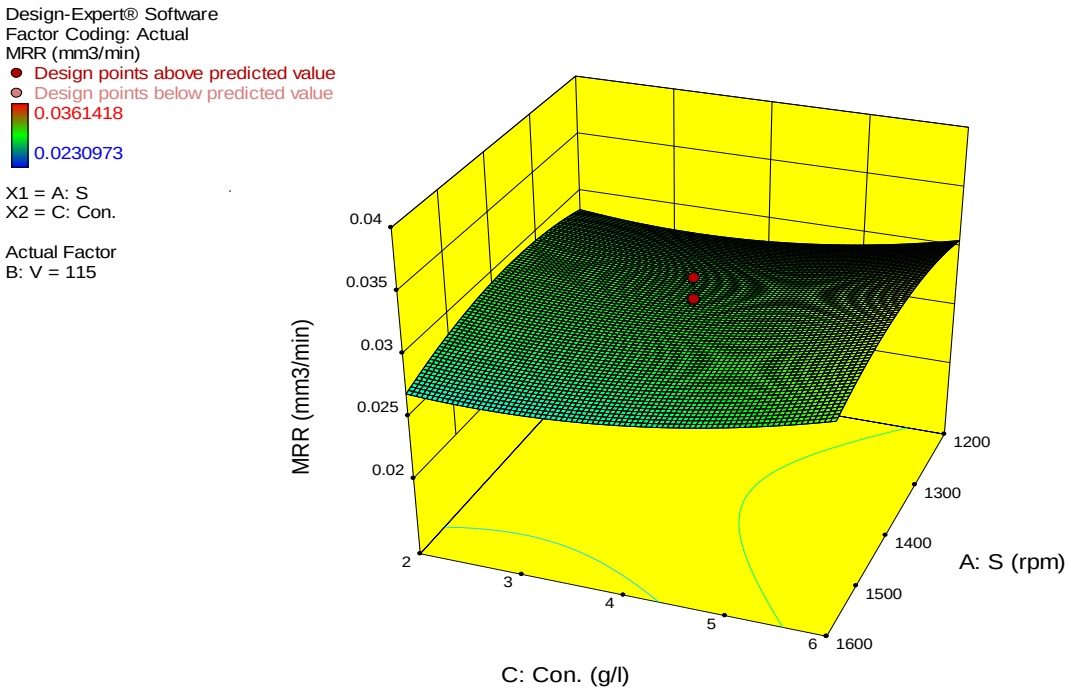

Figure 6.5 Surface plot for MRR between electrode rotation speed (S) and powder concentration

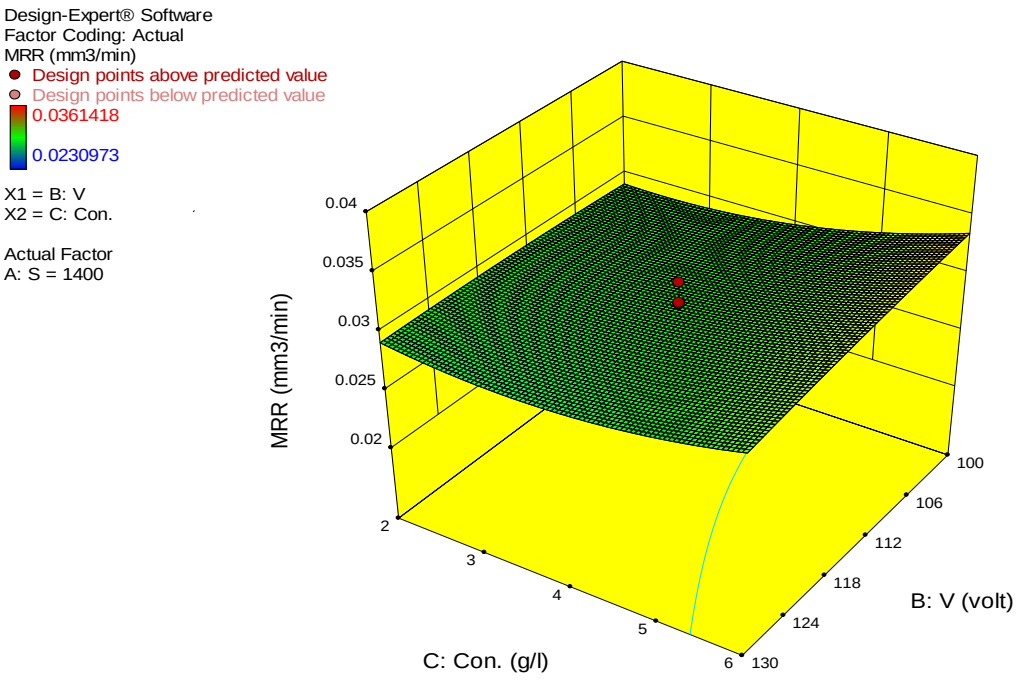

Figure 6.6 Surface plot for MRR between voltage (V) and powder concentration (C)

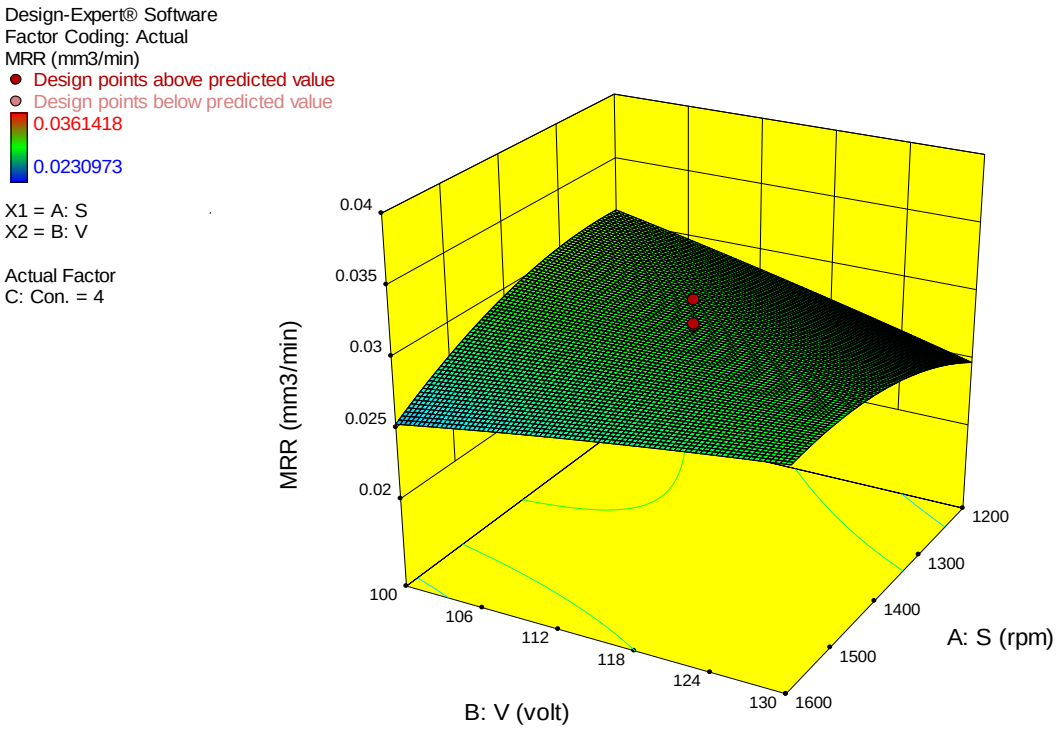

Figure 6.7 Surface plot for MRR between electrode rotation speed(S) and voltage(V)

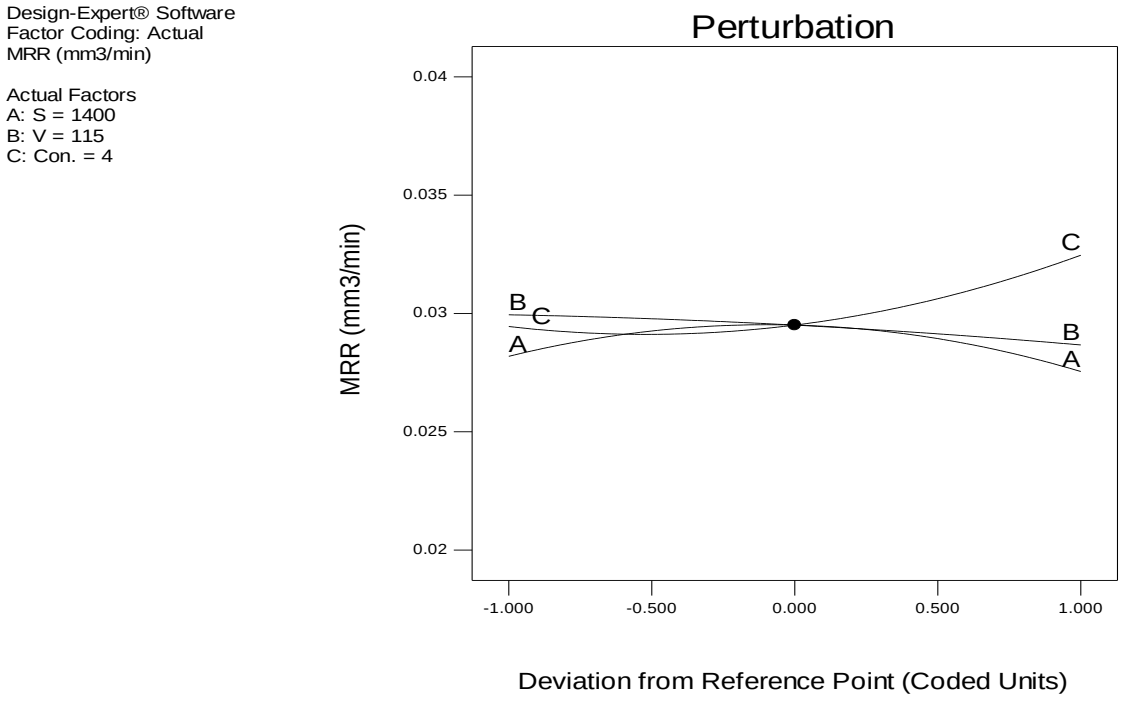

Figure 6.8 Perturbation curve for MRR

6.3.2 An empirical model for performance measures

Regression equations for MRR from this study (Equation 6.1) shown that linear and quadratic both models terms are significant and Powder concentration (C) comes out to be a most influencing parameter. The equation in terms of actual factors can be used to make predictions about the response for given levels of each factor. Here, the levels are specified in the original units for each factor.

Regression equation for MRR

$MRR=0.095801+ (1.47642E^{-5})\times S- (1.2237E^{-3})\times V- (2.1814E^{-3})\times C+ (8.4372E^{-7})\times S\times V - (4.0499E)-(8\times S)^2 +(3.6685E)-4\times C^2$ …………………………………………………….. (6.1)

6.4 Comparison of the response parameter of μ-EDM and PMμ-EDM

The Comparison of response parameters of μ-EDM and PMμ-EDM is presented in Table 6.4. In Fig. 6.5 and Fig. 6.9, It is observed that MRR is significantly improved with the inclusion of SiC powder. This is due to the enlargement of the discharge gap along with the dispersion of discharging energy. The continuous sparking occurs as added SiC particles caused high conductivity [128].

Table 6.1 Comparison of response parameters of micro -EDM and powder mixed micro-EDM

Ex. Run	**Micro-EDM (without SiC powder)**				**PMμ-EDM (with SiC powder)**			
	MRR	EWR	ROC	TA	MRR	EWR	ROC	TA
1	0.003845	0.000116	64.05	12.62	0.0243991	0.02314	31.35	8.18
2	0.004837	8.82E-05	59.6	14.83	0.0317044	0.045137	33.525	9.11
3	0.005058	0.000143	64.55	10.95	0.0244295	0.034677	30.82	5.77
4	0.005233	0.000329	67.25	11.68	0.0235972	0.038406	33.19	6.92
5	0.004978	0.000217	67.6	12.93	0.0230973	0.020576	37.375	9.9

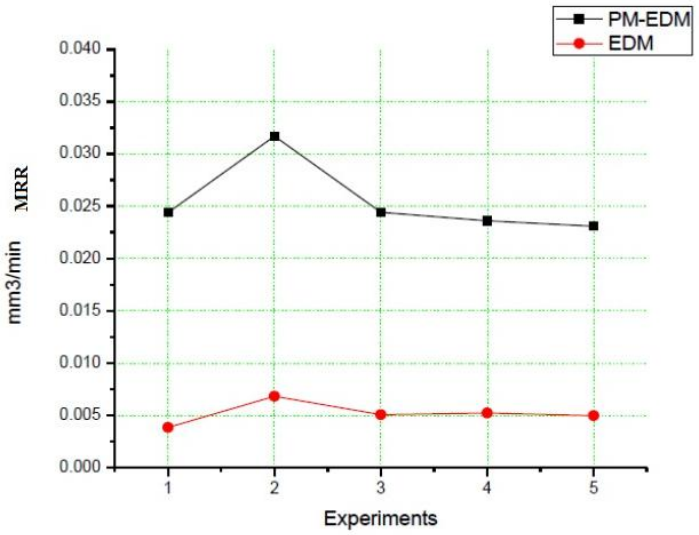

Figure 6.9 Plot of MRR in micro EDM and Powder mixed micro EDM

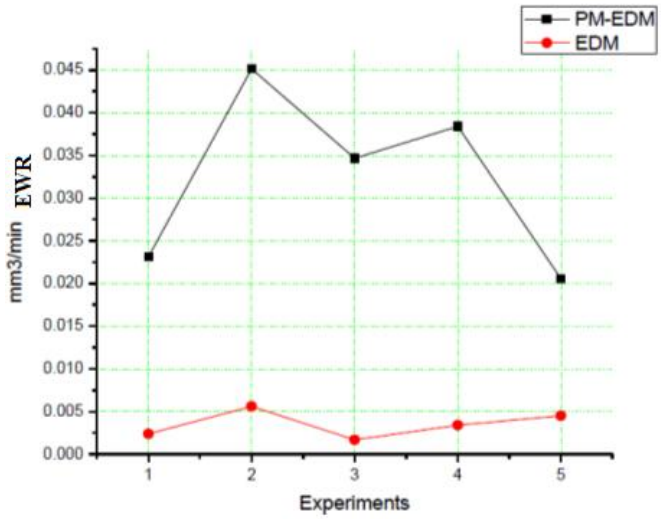

Figure 6.10 Plot of EWR in micro-EDM and powder mixed micro EDM

On the other hand, EWR is also increased as indicated in Fig. 6.10. The reason behind this may be high wear of electrode tip at high temperature. For good machining operation, both the geometric characteristics should have least values. Fig. 6.11 and Fig. 6.12 are showing that both the geometric characteristics exhibit similar trends. Lower values in ROC and TA are due to less machining time in PMμ-EDM compared to μ-EDM. The

internal surface of the fabricated hole encounters the spark for less time in case of PM-µEDM, resulting in less damage to the periphery surface walls. Fig. 6.13 is showing magnified image of cross action of drilled hole by µ-EDM and PM µ-EDM.

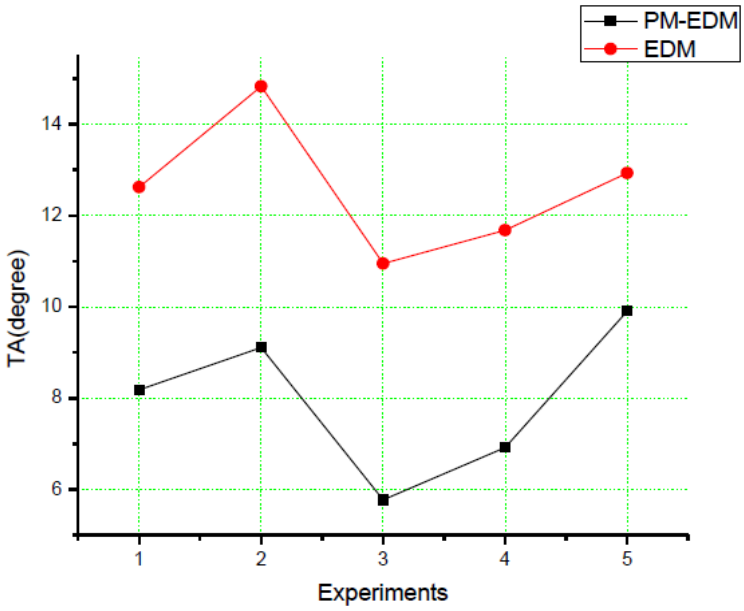

Figure 6.11 Plot of Taper-angle in micro EDM and powder mixed micro EDM

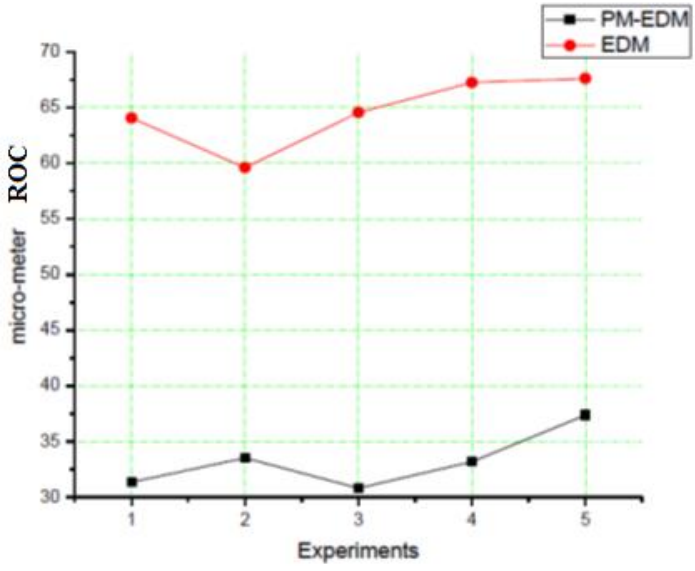

Figure 6.12 Plot of radial overcut in micro-EDM and powder mixed micro EDM

EWR increase because continuous sparking leads to wear of electrode tip due to high temperature in PM-micro-EDM. The difference in diameter is less in PM µ-EDM that results in low taper angle.

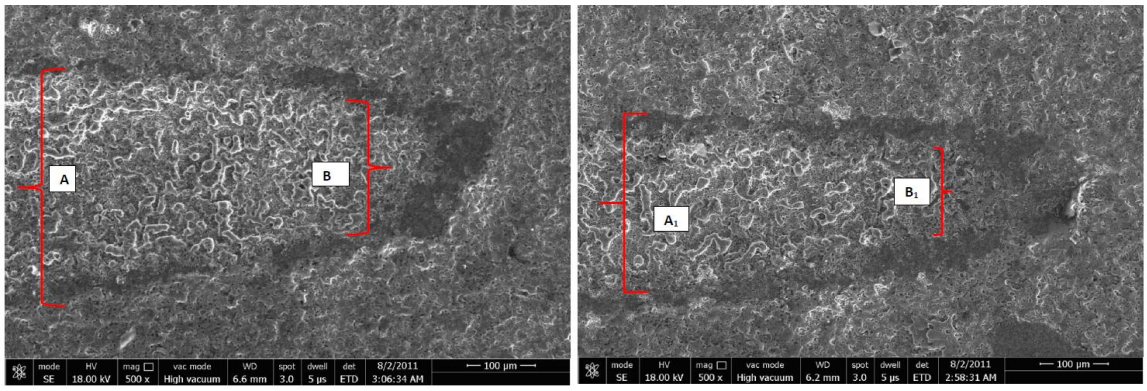

(a) µ-EDM **(b) PM µ-EDM**

Figure 6.13 Comparison of hole shape micro EDM and powder mixed micro EDM

6.5 Results and discussion

6.5.1 Influence of control factors on the material removal rate and electrode wear rate

The main effect curve for MRR and EWR are shown in Fig. 6.14.

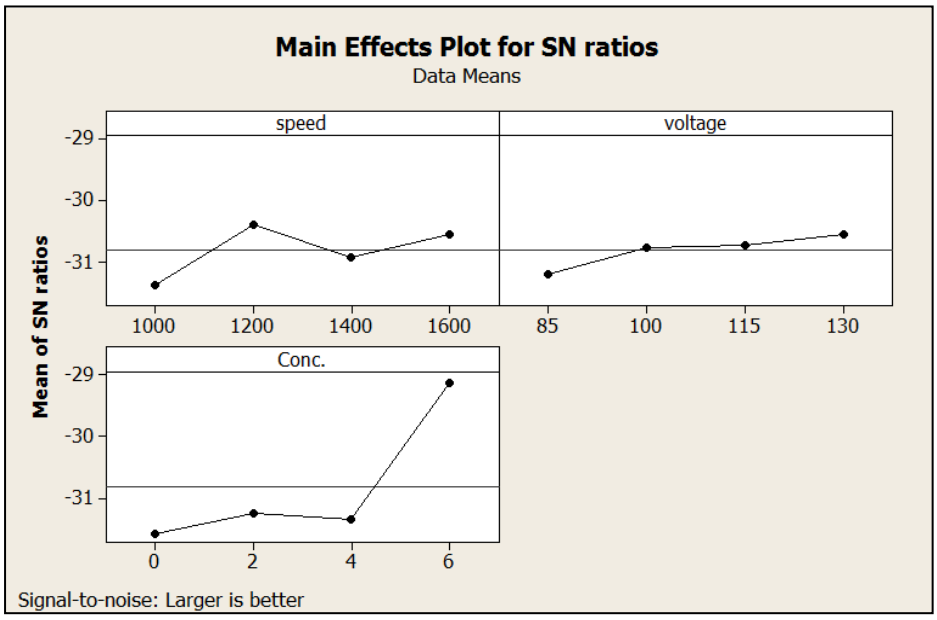

(a) For MRR

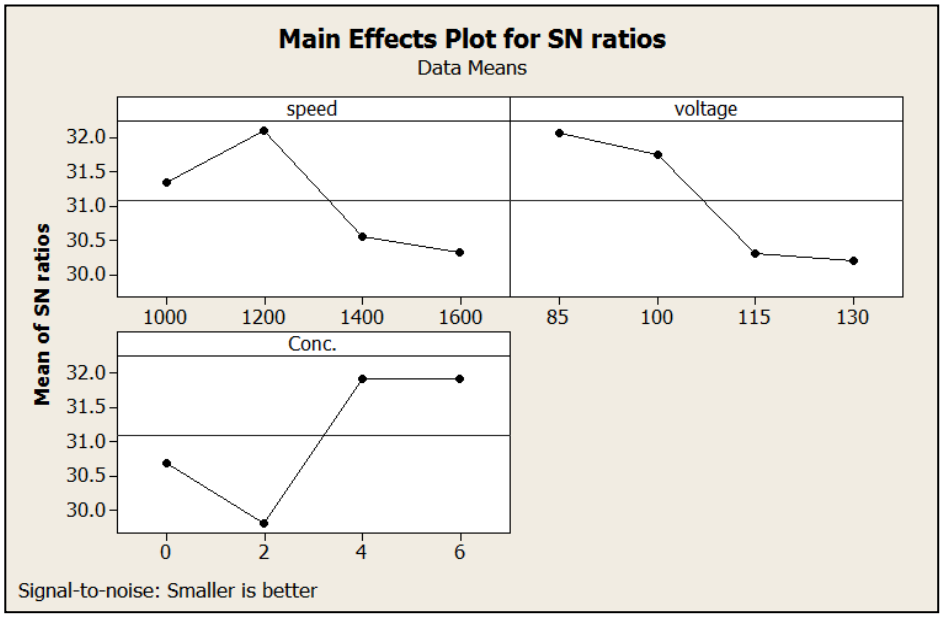

(b) for EWR

Figure 6.14 Main effects plots

The MRR plot in Fig. 6.14(a) indicates a high concentration of SiC powder, MRR is highest. The high concentration of particles leads to low discharge gap, high conductivity thus producing a continuous spark that resulting in high MRR. On the other hand, EWR is also high at high concentration of SiC powder as shown in Fig. 6.14 (b). As explained earlier high concentration of SiC powder leads to continuous sparking that result in a rise in the temperature of tool-tip. The high temperature of tool-tip augments the erosion of the tool thus leads to higher EWR.

6.5.2 **Effects of tool rotation speed on the machined surface**

Separate experiments were carried out under constant capacitance (0.1 µF), voltage (100 V) and SiC concentration (6 g/l) to observe the effect of tool rotation speed on the topography of the machined surface. The results show that the surface becomes rough when the electrode rotation speed is increased above 1000 rpm (Fig. 6.15).

The roughness of the surface is usually the result of high material removal caused by high discharge energy. The increase of electrode rotation speed causes an increase inhomogeneity of the liquid suspension and consequently higher discharge energy. Thus, the milder grinding regime could be ensured with speed reduction (1000 rpm).

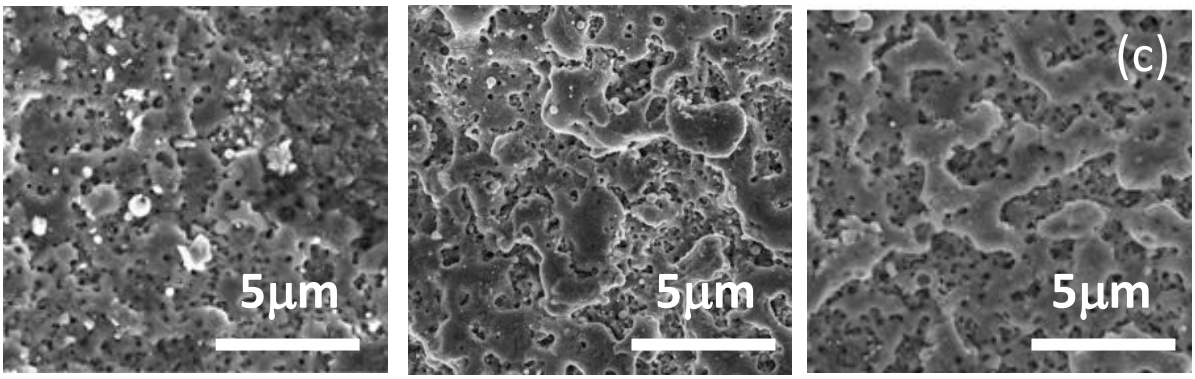

(a) 1000 rpm **(b) 1200 rpm** **(c) 1400 rpm.**

Figure. 6.15 SEM micrographs of the machined surface of samples at different speeds of tol rotations; Machining was carried out with 0.1 µF capacitance, 100 V voltage, and SiC concentration, 6 g/l

6.6 Mechanism of material removal

6.6.1 Field Emission Scanning Electron Microscope images for machining

Fig. 6.16 shows the formation of molten material pools spread across the surface with spalled surfaces existing as craters in between the metal pools. Vertical micro-cracks are formed on the re-solidified melt during cooling on the machined surface probably due to thermal stresses arising out of dissimilar thermal expansion coefficients of the melt and underlying substrates.

Material removal, therefore, took place by the removal of the spalled mass (flakes) created by the progression of the horizontal cracks created underneath the vertical microcracks showed in Fig. 6.17 and Fig. 6.18 as described in earlier studies [82] [126]. Formation of micropores took place by the evolution of gas bubbles generated by the oxidation reaction of TiN high temperature. Small white spheres spread across the whole surface are formed by the melting evaporation and condensation of the tungsten electrode used in the present study. The white color of the spheres indicates the higher atomic number of the chemical elements present in the spherical particles and, therefore, represents Tungsten in the present case. These globules are mostly deposited to the craters and caused by material migration from the electrode to the surface of the work-piece.

Most important observation obtained from Fig. 6.16 and 6.17 are that the surface roughness indicated by the height of the crest of the discharge crater is much less in sample machined by PMμ-EDM than that of the sample machined by μ-EDM [87].

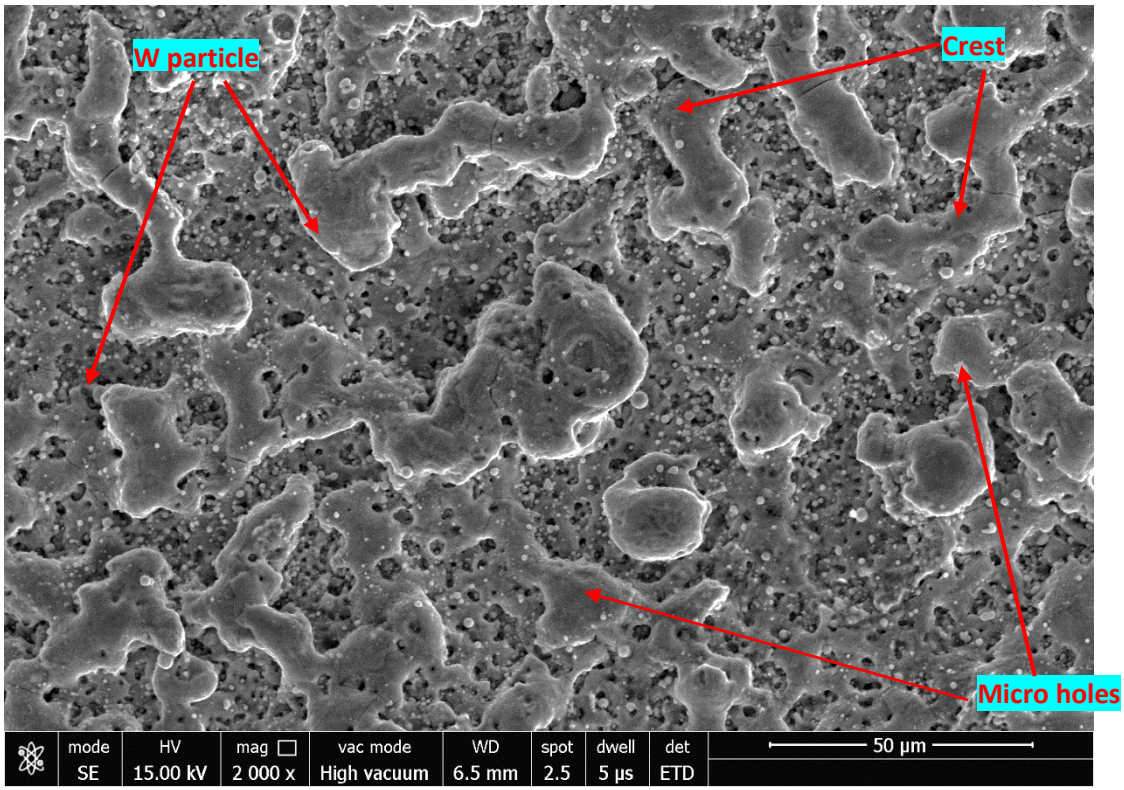

Figure 6.16 Microstructure of TiN-Al_2O_3 surface μ-ED machined at speed= 1200 rpm, voltage 100 volt and capacitance = 0.1 micro-farad

PMμ-EDM makes the discharge breakdown much easier as it enlarges the discharge gap and widens the discharge passes [87].

Consequently, evenly distributed shallow cavities were generated due to stable discharge. Another reason for lower roughness is the erosion of the crest materials by high-speed rotation of the liquid dispersion containing hard abrasive SiC particles surrounding the electrode and within the gap between the electrode and the micro-hole wall. Impact of SiC particles disentangle loosely held flakes and erodes the crest materials similar to the proposition made earlier [129].

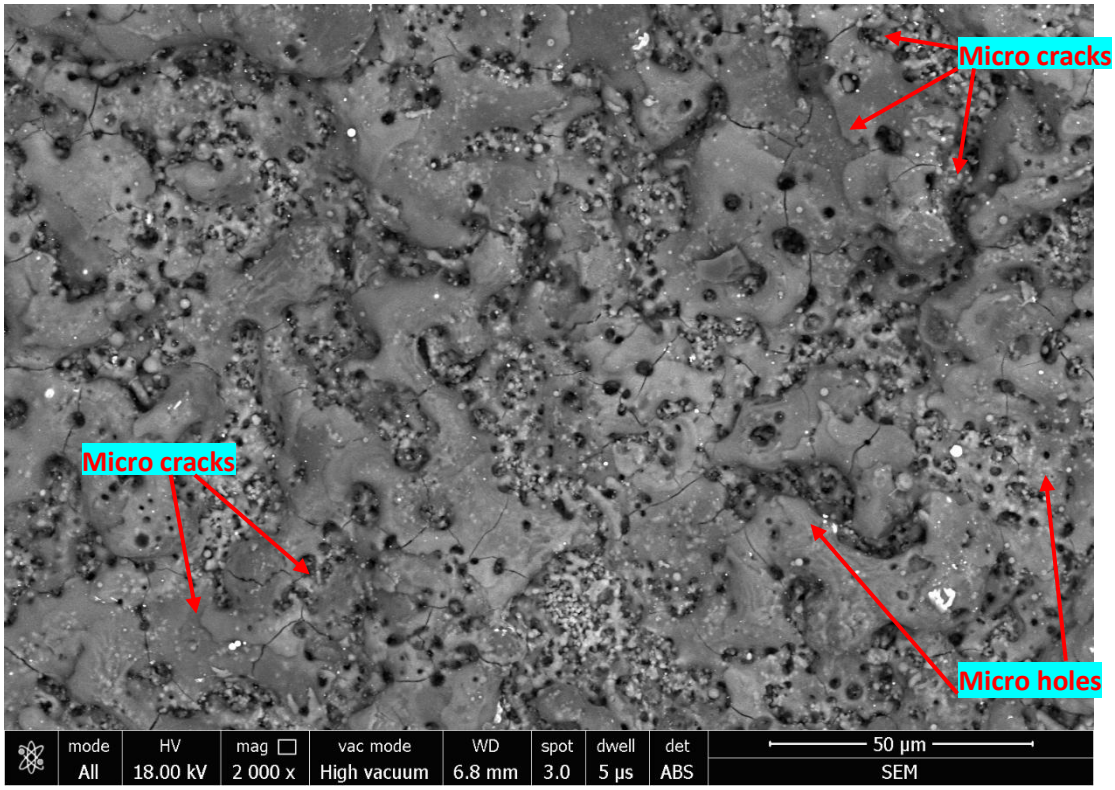

Figure 6.17 Microstructure of TiN-Al_2O_3 surface Powder mixed micro-EDM machined at speed= 1200 rpm, voltage= 100 volt and capacitance =0.1 µF and SiC powder concentration = 6 g/l

6.7 Comparison of the machined surface of µ-EDM and PM-µEDM

The topography of the machined surfaces as exhibits from Fig. 6.18 shows the formation of molten material pools spread across the surface with spalled surfaces existing as craters in between the metal pools. The solidified molten mass looks like a glass phase formed by the high cooling rate.

The vertical micro-cracks are formed on the re-solidified melt during cooling on the machined surface probably due to the thermal stress arising out of dissimilar thermal expansion coefficients of the melt and underlying substrates. Material removal, therefore, took place by the flushing of the spalled mass (flakes) created by the progression of the horizontal cracks created underneath the vertical microcracks [130] [126]. In SEM micrographs height of the crest of the discharge, the crater is slightly less in the sample machined by PMµ-EDM than that of the sample machined by µ-EDM alone.

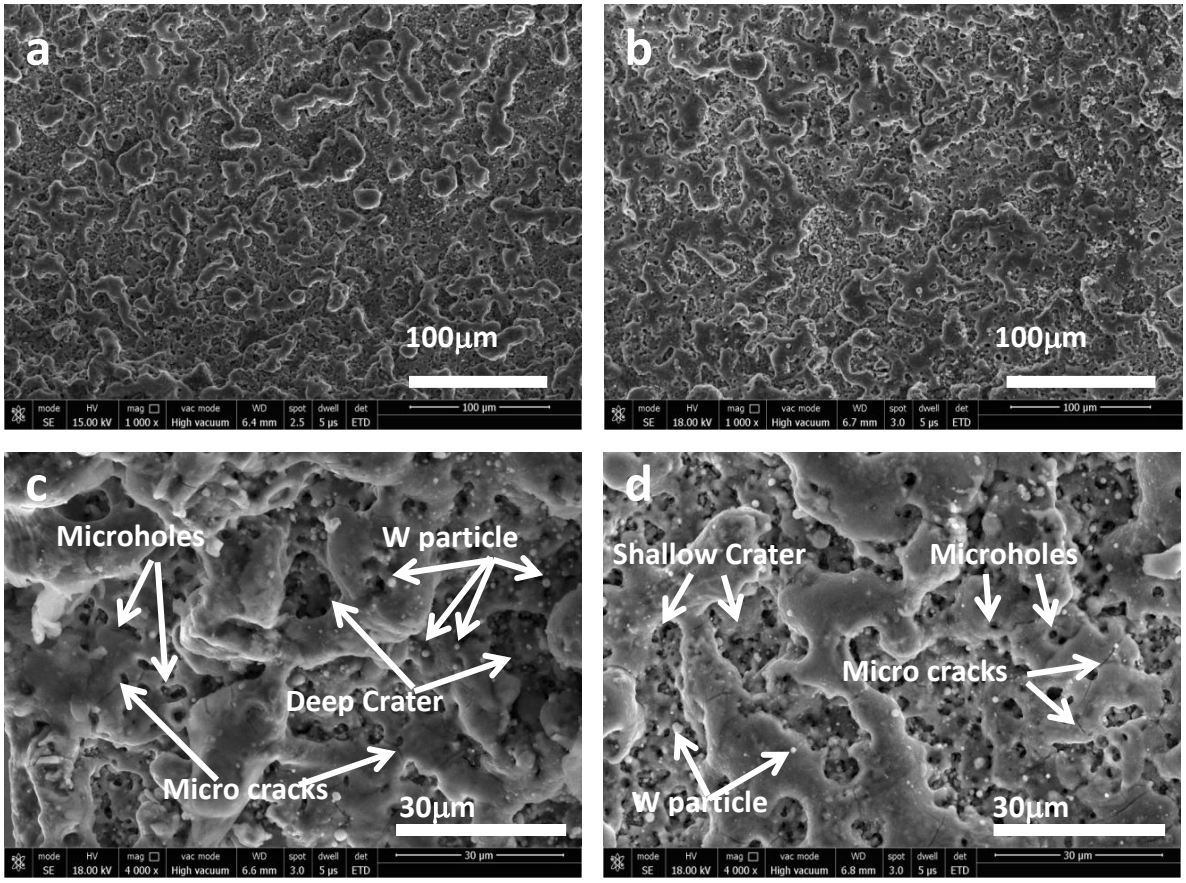

Figure 6.18 SEM micrographs of TiN-Al_2O_3 composite surface machined at tool rotation speed – 1200 rpm, voltage -100 V and capacitance – 0.1µF under (a) µ-EDM and (b) PMµ-ED at SiC concentration, 6 g/l. (c) and (d) are higher magnification micrographs of (a) and (b) respectively.

PMµ-EDM makes the discharge breakdown much easier as it enlarges the discharge gap and widens the discharge passes. Evenly distributed shallow cavities were generated due to stable discharge as a consequence of powder addition. Impact of SiC particles should disentangle loosely held flakes and erodes the crest materials.

Formation of micropores took place by the evolution of gas bubbles generated by the oxidation reaction of TiN high temperature. Thermal micro-cracking in the melt (Fig. 6.18) indicates differential volume change between the surface and interior of the glass associated with rapid cooling of the molten mass by the flow of the dielectric and heat conduction.

Table 6.2 Results of EDS for machined surface by Powder mixed micro-EDM and micro-EDM

Elements		**PM µ-EDM With SiC powder (S=1200 rpm, C= 0.1 µF, V=100 volt)**			**µ-EDM Without SiC powder (S=1100 rpm, C= 0.1 µF, V=100 volt)**		
Name	Atomic number	Unn. Wt.%	C.norm. Wt.%	C. Atom. Wt.%	Unn. Wt.%	C.norm. Wt.%	C. Atom. Wt.%
Ti	22	51.11	42.39	22.32	57.80	48.39	24.77
O	8	45.77	37.96	59.82	29.75	24.91	38.15
Al	13	22.67	18.80	17.57	15.31	12.81	11.64
W	74	0.74	0.62	0.08	0.83	0.70	0.09
Si	14	0.28	0.23	0.21	-	-	-
C	6	-	-	-	9.34	7.82	15.96
N	7	-	-	-	6.42	5.37	9.40

Small white spheres spread across the whole surface are formed by the melting evaporation and condensation of the tungsten electrode used in the present study. The white color of the spheres indicates the higher atomic number of the chemical- elements present in the spherical particles and, therefore, should represent Tungsten in the present case as observed from the EDS analysis of the machined surfaces of under two µ-EDM and (b) PMµ-EDM is (Table 6.5, Fig.6.19).

Table 6.5 and Fig. 6.19 shows the presence of Al, Ti and O and N in the surface of µEDM samples without SiC powder addition while no trace of N could be visible in PM-µEDM sample although almost similar EDM parameters were used. Moreover, the topography of the samples is different from those of oxidized samples under ambient conditions [14] indicating the formation of amorphous Ti-Al-O-N phase during the quenching under the EDM machining conditions. However, the presence of nitrogen in the melt indicates that either the penetration of electron beam to much deep inside the surface acquiring the information from the subsurface region of the melt is actually a Ti-Al-O-N quarternary

system. The high amount of carbon in the surface originated from the dielectric breakdown of the organic liquid.

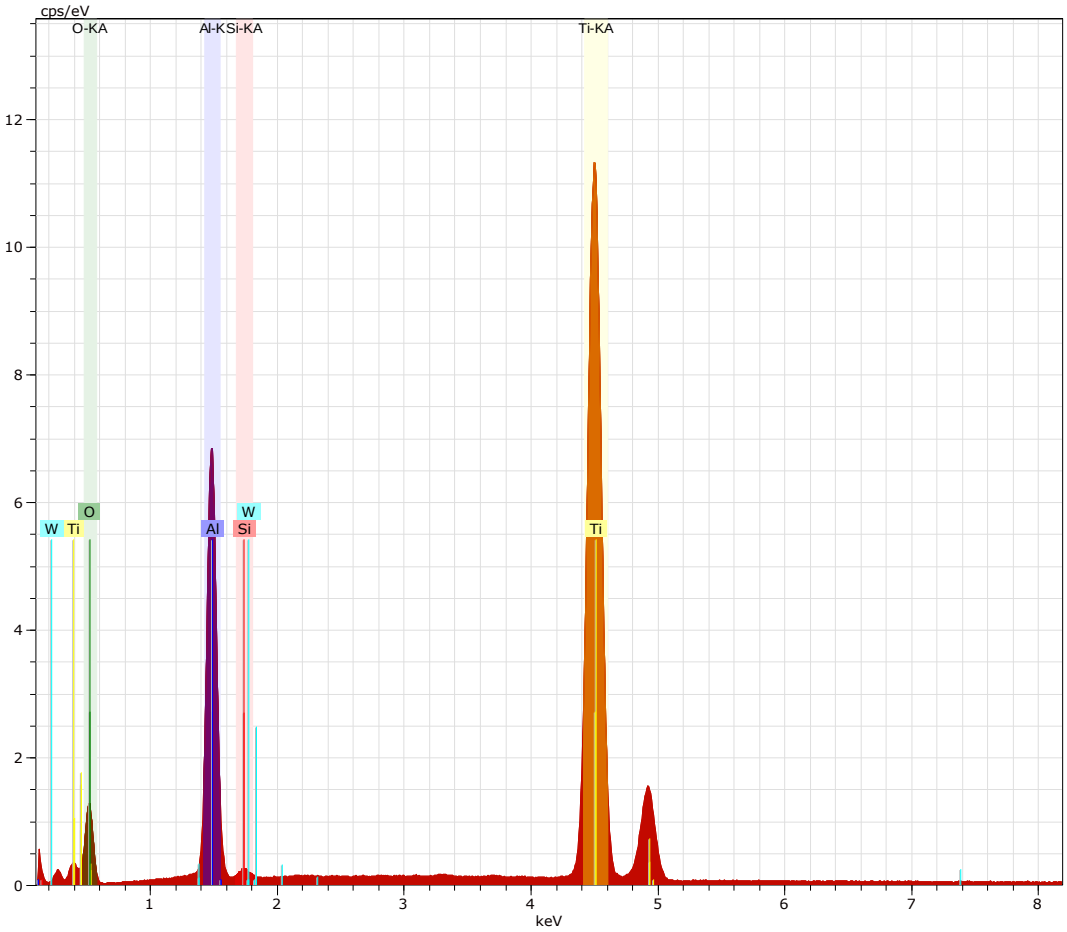

Figure 6.19 EDS results for powder mixed micro-EDM

In PM- μ-EDM process the temperature of plasma might be higher and intense and, therefore, oxidized the melt. Presence of higher amount of oxygen on the surface (Table 6.6 Fig. 6.20) precludes the formation of Ti-Al-O-N glass in samples processed by PM-μ-EDM. The absence of carbon in these samples is also due to the oxidation at a higher temperature under the PM-μ-EDM conditions. The chemical composition of the amorphous phase formed on the surface does not correspond to Tialite (Al_2TiO_5) either. White globules are mostly located on the craters and caused by material migration from the electrode to the surface of the workpiece as observed [83]. Globules were formed by melting, evaporation, and condensation of the tungsten electrode used during the spark.

Figure 6.20 EDS color mapping of machined surface PM micro-EDM

6.8 Material removal mechanism of TiN-Al_2O_3 ceramic-composite in µ-EDM

The material removal process in TiN-Al_2O_3 ceramic-composite by µ-EDM shows the two principal mechanisms i.e. melting and thermal spalling, An illustration of mechanism is shown in Fig. 6.21.. As discussed the characterization of plasma formed on the machined surface during the micro EDM indicates that low capacitance and small tool electrode gap could produce a plasma temperature as high as 6170 K.

Thus at low capacitance value (low discharge energy), gas bubbles within the melt are formed by oxidation of TiN. Some areas of spalling are also noticed during the study that is due to the presence of non-conducting Al_2O_3 phase in the material. At high discharge energy, it is noticed that the presence of vertical cracks in the re-solidified surface layers increases in the sample. Such vertical microcracks can propagate and meet the horizontal cracks present on sub-surface and may remove the whole material under the spalled zone leading to rough machining. Thus, the µ-EDM could be used for

machining of advanced ceramic-composite for both rough and fine machining regime and material removal takes place through thermal spalling as well as melting.

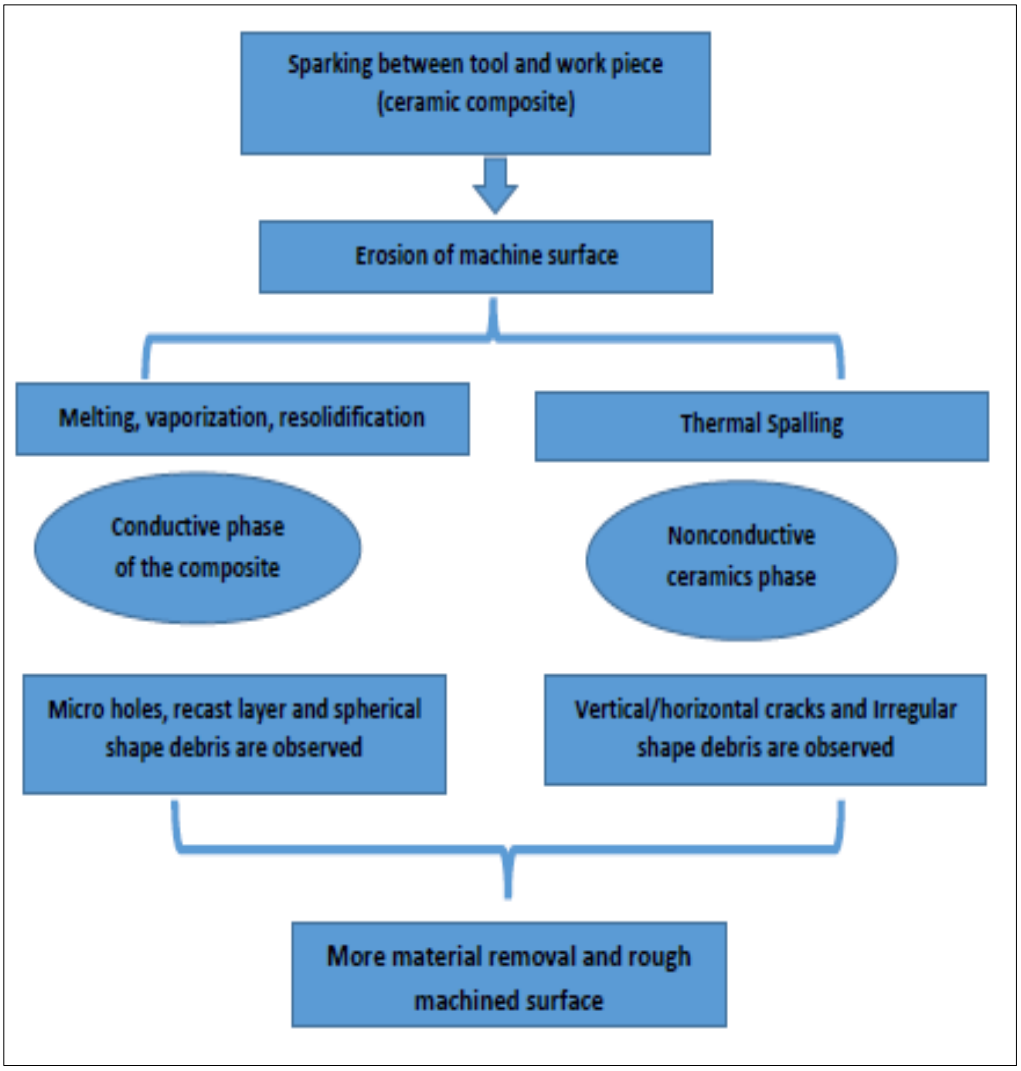

Figure 6.21 Illustration of the material removal process of TiN-Al_2O_3 ceramic-composite by micro-EDM

6.9 Summary

PMμ-EDM of reaction bonded conductive TiN-Al_2O_3 ceramic-composite has been performed with SiC power as an admixture (assisting electrode). The results prove the feasibility of machining this difficult to machine ceramic-composite by PMμ-EDM. Micro-Electro-discharge machining (μ-EDM) is one of the promising manufacturing processes especially in the generation of precise and complex geometrical shapes on difficult to machine materials. The machining characteristics in μ-EDM are highly

dependent on the dielectric's performance. A further enhancement in response parameters and surface quality can be done by adding powders in the dielectric. The presence of foreign particles reduces the insulating strength of the dielectric fluid and increases the spark frequency between the tool and workpiece. As a result, the spark becomes continuous and stable leading to higher material removal rate (MRR) and improved quality of the machined surface. As compared to μ-EDM, in PMμ-EDM the improvement in machining efficiency in terms of Material Removal Rate (MRR) is 6.5 times (increase), geometric characteristics in terms of Taper Angle (TA) is 2 times (decrease) and Radial Overcut (ROC) is 1.5 times (decrease). However, EWR is 1.8 times (increases) as compared to the μ-EDM process. The effect of SiC powder on the machined surface is also analyzed by the scanning electrode microscope where thermal cracking (Spalling) and melting are found to be the prominent mechanisms of material removal. The results prove the feasibility of machining this difficult to machine ceramic-composite by PMμ-EDM.

7. Conclusions

In this chapter, a summary of the main conclusions and accomplishment that are drawn from experimental and theoretical studies undertaken on hybrid micromachining of TiN-Al_2O_3 ceramic-composite.

7.1 Preliminary Experiments

Based on the preliminary experiments, the following conclusions are made:

1. The machining process parameters chosen for the preliminary experiments on modified Electronica®) ZNC ENC-35 electro-discharge machine with diamond abrasive grinding wheel setup were Pulse on-time, pulse off time, duty factor, depth of cut, peak current, feed rate, and wheel rotation speed. Based on the preliminary test, the range of these parameters was selected.for further experimental study.
2. The machining process parameters chosen for the preliminary experiments on hybrid micro EDM (DT-110i®) were input voltage, capacitance, electrode rotation speed, electrode feed rate, feed rate in x, y-direction, and powder concentration. For fabrication of microchannels, spindle speed, voltage, capacitance were taken as variable parameters and feed rate in x and z-axis was kept constant. For fabrication of micro holes, voltage, spindle speed, and powder concentration were taken as variable parameters and feed rate, and capacitance was kept constant. Based on the preliminary test, the range of parameters for various experimental studies was selected.

7.2 Diamond grinding assisted electro-discharge machining of TiN-Al_2O_3 ceramic-composite

1. Diamond grinding-assisted electro-discharge (DGA-ED) machining proves to be a good machining process for conductive ceramic composites like TiN-Al_2O_3.
2. The empirical model for material removal rate for TiN-Al_2O_3 ceramic has been developed by using RSM, and it shows that the most significant parameter affecting MRR is the rotation speed of the grinding wheel, followed by the pulse on-time (t_{on}) and duty factor (DF).

3. The model is a reliable representative of experimental results, and it can be placed within standard uncertainty that is 3.69%. For multi-influencing parameters, the highest material removal rate is 0.37220 mg /min at wheel rotation speed of 1200 rpm (constant wheel diameter and width), 150 μs pulse on-time (t_{on}), and 3 A current.
4. The optimization plot shows that the grinding wheel rotation speed and pulse on time (t_{on}) have a positive influence on the material removal rate and the composite design desirability is 97.85 %.
5. The surfacing of the TiN-Al_2O_3 ceramic composite is done for the fabrication of microfeatures and 2.54 μm average surface roughness (Ra) value is achieved at 1200 RPM.
6. Surface cracks, flakes, and a molten pool of ceramics are visible in the SEM micrographs of the machined surface which indicates that thermal spalling, i.e., brittle fracture, along with decomposition of ceramics and melting is taking place during the machining process. It is also observed that at higher speed, the recast layer is removed due to the grinding effect.

7.3 Micro-electro-discharge milling of TiN-Al_2O_3 ceramic-composite for micro-channels fabrication

1. Fabrication of microchannels on TiN-Al_2O_3 ceramic-composite considering its potential application in a micro-chemical reactor and high-temperature heat exchanger could be accomplished by μ-ED milling both in the rough and fine machining regime.

2. Response Surface Methodology (RSM) reveals the dependence of material removal rate (MRR) primarily on the high electrical discharge energy created by the capacitance and applied voltage while the electrode wear rate (EWR) depends on the rotational speed of the tool.

3. Analysis of the topology of the surfaces machined at low and high capacitance by FESEM shows that vertical cracking of the re-solidified layer takes place mainly when the capacitance discharge is very high. The vertical cracking created by the discharge helps to remove the material in large quantities during the dielectric flush.

4. The evidence of the electrode wear increase coupled with the decrease of the material removal with the increased rotation speed indicates an abrasive erosion of the electrode by the high quantity of debris formed from the workpiece present in the dielectric medium.

7.4 SiC powder mixed micro-electro-discharge machining of TiN-Al_2O_3 ceramic-composite for high aspect ratio micro holes

1. The SiC Powder concentration in dielectric has come out to be the most influencing parameter in the machining of the TiN-Al_2O_3 ceramic composite among the three inputs – powder concentration, voltage and rotation speed. Next important parameter is voltage while rotation speed has an optimal value with the least significance to MRR.
2. Both linear and quadratic terms are significant in the empirical model developed for the material removal rate of TiN-Al_2O_3 ceramic composite by using Response Surface Methodology. MRR is improved with powder inclusion in the dielectric. Geometric characteristics i.e. Taper angle (TA) and radial overcut (ROC) decrease in PMμ-EDM as compared to μ-EDM.
3. The machining performance of PMμ-EDM on TiN-Al_2O_3 composite is well understood by experimental study and it is concluded that PMμ-EDM possesses the good potential for machining difficult to machine ceramics for micro features like micro holes, microchannels, etc. considering its application in the micro heat exchanger and micro-chemical reactor.
4. The topography of the machined surface reveals the presence of micro-cracks and microbubbles in the solidified melt surface. Areas of brittle fracture could also be observed on the machined surface. Mechanism of material removal is therefore melting and spallation of the ceramic composite followed by brittle fracture. Formation of microspores is due to the evolution of gas bubbles due to the oxidation of TiN materials at high temperature.
5. Internal surfaces of micro-holes generated by μ-EDM and PMμ-EDM are also observed by scanning electrode microscopy and a significantly low taper angle is observed with PMμ-EDM as compared to μ-EDM. It is also observed that electrode material deposition on the machined surface is significantly less. PMμ-

EDM makes the discharge breakdown much easier as it enlarges the discharge gap and an evenly distributed cavity forms as a result of the stable discharge.

After conducting all experimentations, it is found that Diamond grinding assisted Electro-discharge machining (DGA-EDM) shows better material removal rate as compared to EDM and diamond grinding, for surfacing of the samples. The MRR improves threefold by hybridizing diamond grinding with EDM. The surfaces generated by DGA-EDM are found to be suitable for developing micro features by hybrid μ-EDM. For the fabrication of micro-channels, micro ED milling is selected and it is found that high discharge energy i.e. a combination of high capacitance and high voltage leads to better MRR. Further process enhancement is done by PM μ-EDM by the inclusion of SiC powder in the dielectric fluid. It is found that not only MRR is improved in this process but geometrical characteristics i.e. taper angle and radial overcut are also found to improve. The mechanism of material removal is also different in TiN-Al_2O_3 ceramic-composite than that of metal. Thermal spalling is found to be the dominant mechanism of material removal than melting and vaporization. Thus, in conclusion, experimental results show that DGA-EDM and hybrid μ-EDM are suitable methods for surfacing and machining respectively on TiN-Al_2O_3 ceramic-composite. Successful fabrication of micro features such as micro blind holes, micro holes, and microchannels will pave the way for developing micro-reactors out of TiN-Al_2O_3 ceramic-composite.

7.5 **Research contribution**

This work will contribute in the knowledge of hybrid-EDM machining of newly developed Titanium Nitride Aluminium oxide (TiN-Al_2O_3) ceramic-composite by putting forward the experiment based study on the complexities associated with the process during machining and optimization of process parameters. Fabrication of micro-features on one of the most challenging classes of materials and studies on the effect of process parameters on geometric characteristics of micro-features with regard to its application in the micro-chemical reactor has been done. The experimental investigation was performed in preparing the finished surface and fabricating micro features like holes, microchannels, high aspect ratio micro holes in very hard to machine advance ceramics TiN-Al_2O_3.

- For surfacing on TiN-Al_2O_3 ceramics composite, DGAEDM process worked successfully and achieved more MRR as compared to EDM or diamond grinding. DGAED Machined samples are more finished as compare to Diamond-grind samples and on an average 2.54 μm average surface roughness (Ra) value is achieved.
- For fabrication of microchannels in TiN-Al_2O_3 ceramics composite, ED milling successfully works and the optimum parametric study was done.
- Introducing SiC powder in dielectric fluid encouraged the continuous spark thus more MRR is achieved during fabrication of high aspect ratio holes. The geometrical characteristics of holes improve i.e. radial overcut, taperness is also less as compared to holes drilled by EDM process.
- To the best of the author's knowledge, no study has been conducted elsewhere on this workpiece for generating microchannels and for generating high aspect ratio micro holes.

7.6 **Scope for future work**

This research work is focused on generating microfeature and parametric studies are also done for various hybrid EDM processes. Hybrid EDM enables machining based on specific applications. Few directions for further research are listed below-

- Study on further improvement in electrode wear during PM-μEDM.
- Further process enhancement can be done by "on-machine fabrication" of the tool and "on-machine measurement" technique for achieving maximum accuracy.
- Study of microreactor fabrication of TiN-Al_2O_3 ceramic composite using hybrid EDM process could be done.
- Study on the fabrication of micro-tool insert of TiN-Al_2O_3 ceramic composite using hybrid EDM process could be done.

References

[1] Y. K. LOK and T. C. LEE, "Processing of Advanced Ceramics Using the Wire-Cut EDM Process," Journal of materials Processing Teclmology, vol. 63, pp. 839-843, 1997.

[2] B. Bhattacharyya, B. N. Doloi and S. K. Sorkhel, "Experimental investigations into electrochemical discharge machining (ECDM) of non-conductive ceramic materials," Journal of Materials Processing Technology, vol. 95, no. 1-3, pp. 145-154, 1999.

[3] A. Schubert, H. Zeidler, R. Kühn, M. Hackert-Oschätzchen, S. Flemmig, and N. Treffkorn, "Investigation of ablation behavior in micro-EDM of nonconductive ceramic composites ATZ and Si_3N_4-TiN," in 18th CIRP Conference on Electro Physical and Chemical Machining, Procedia CIRP 42 , 727 – 732, 2016.

[4] D. Bhaduri, A. S. Kuar, S. Sarkar, S. K. Biswas and S. Mitra, "Electro Discharge Machining of Titanium Nitride-Aluminium Oxide," Materials and Manufacturing Processes, vol. 24, no. 12, pp. 1312–1320,, 2009.

[5] R. Baghel, H. S. Mali and S. K. Biswas, "Parameter Optimization of Diamond Grinding Assisted EDM of TiN-Al_2O_3 Ceramics using Taguchi Method," in 6th International & 27th All India Manufacturing Technology, Design and Research Conference, College of Engineering, Pune, Maharashtra, INDIA, 2016.

[6] C. J. Luis, I. Puertas and G. Villa, "Material removal rate and electrode wear study on the EDM of silicon carbide," Journal of Materials Processing Technology, vol. 164–165, p. 889–896, 2005.

[7] M. Lassettre and J. O. EVERHART, "Stress-strain relationship in ceramics," Journal of The American Ceramic Society, vol. 29, no. 9, pp. 261-266, 1946.

[8] M. Lassettre and J. O. Everhart, "Stress-strain relationship in ceramics," Journal of American Ceramic Society, vol. 29, no. 9, pp. 261-266, 1946.

[9] V. Ghiasi, H. Omar and Z. B Md, "A New Model of Microcracks Propagation in Granite Rock," Australian Journal of Basic and Applied Sciences, vol. 12, no. 4, 2010.

[10] G. E. Dieter, Metallurgy and Metallurgical Engineering Series, McGRAW-HILL Book company, New York Toronto London, 1961.

[11] N. Mohd Abbas, D. G. Solomon, and M. F. Bahari, "A review on current research trends in electrical discharge machining," International Journal of Machine Tools & Manufacture, vol. 47, p. 1214–1228, 2007.

[12] H. Kim, K. Matsumaru, A. Takata and K. Ishizaki, "Reduction of ceramic machining defects by regulated force feeding grinding system," Advances in technology of materials and materials processing, vol. 6, no. 2, pp. 290-297, 2004.

[13] A. Schubert, H. Zeidler, M. Hahn, M. Hackert-Oschätzchen and J. Schneider, "Micro-EDM milling of electrically nonconducting zirconia ceramics," in The Seventeenth CIRP Conference on Electro Physical and Chemical Machining (ISEM), Procedia CIRP, 2013 (297 – 302).

[14] J. Mukerji and S. K. Biswas, "Synthesis, Properties, and Oxidation of Alumina-Titanium Nitride Composites," Journal of the American Ceramic Society, vol. 73, no. 1, pp. 142-145, 1990.

[15] N. Mohd Abbas, D. G. Solomon, and M. F. Bahari, "A review on current research trends in electrical discharge machining (EDM)," International Journal of Machine Tools & Manufacture, vol. 47, p. 1214–1228, 2007.

[16] R. Ji, Y. Liu, Y. Zhang and F. Wang, "Machining performance of silicon carbide ceramic in end electric discharge milling," International Journal of Refractory Metals and Hard Materials, pp. 117-122, 29 (2011).

[17] M. A. Norliana, D. G. Solomon and M. F. Bahari, "A review on current research trends in electrical discharge machining (EDM)," International Journal of Machine Tools & Manufacture, vol. 47, pp. 1214-1228, 2007.

[18] Y. Fukuzawa, N. Mohri, H. Gotoh, and T. Tani, "Three-dimensional machining of insulating ceramics materials with electrical discharge machining," Transactions of Nonferrous Metals Society of China, vol. 19, no. 1, pp. 150-156, 2009.

[19] Y. Pachaury and P. Tandon, "An overview of electric discharge machining of ceramics and ceramic-based composites," Journal of Manufacturing Processes, vol. 25, p. 369–390, 2017.

[20] K. K. Saxena, S. Agarwal and S. K. Khare, "Surface characterization, material removal mechanism and material migration study of micro EDM process on conductive SiC," in 18th CIRP Conference on Electro Physical and Chemical Machining, Procedia CIRP, 2016.

[21] I. Puertas, C. J. Luis, and G. Villa, "Spacing roughness parameters study on the EDM of silicon carbide," Journal of Materials Processing Technology, vol. 164–165, p. 1590–1596, 2005.

[22] K. Liu, E. Ferraris, J. Peirs, B. Lauwers and D. Reynaerts, "Micro EDM process investigation of Si_3N_4-TiN ceramic composites for the development of micro fuel-based power unit," International Journal of Manufacturing Research, vol. 3, no. 1, 2008.

[23] K. Gupta and N. K. Jain, "On surface integrity of miniature spur gears manufactured by wire electrical discharge machining," The International Journal of Advanced Manufacturing Technology, vol. 72, no. 9-12, pp. 1735-1745, 2014.

[24] R. Kumar and I. Singh, "Productivity improvement of micro EDM process by

improvised tool," Precision Engineering, vol. 51, pp. 529-535, 2018.

[25] Y. Ziada and P. Koshy, "Rotating Curvilinear Tools for EDM of Polygonal Shapes with Sharp Corners," CIRP Annals, vol. 56, no. 1, pp. 221-224, 2007.

[26] R. Baghel, H. S. Mali and S. K. Biswas, "Study of Vibration Assisted Micro Electro-Discharge Milling of Titanium Nitride-Aluminium Oxide Composite," in Proceedings of 6th International & 27th All India Manufacturing Technology, Design, and Research Conference, Coep, Pune, 2016.

[27] A. Sabur, M. Y. Ali, M. A. Maleque and A. A. Khan, "Investigation of Material Removal Characteristics in EDM of Nonconductive ZrO_2 Ceramic," Procedia Engineering, vol. 56, pp. 696-701, 2013.

[28] D. D. DiBitonto, "Theoretical models of the electrical discharge machining process. I. A simple cathode erosion model," Journal of Applied Physics, vol. 66, no. 9, 1998.

[29] D. DiBitonto, P. T. Eubank, M. R. Patel, and M. A. Barrufet, "Theoretical models of the electrical discharge machining process. I. A simple cathode erosion mode," Journal of applied physics, vol. 66, no. 9, pp. 4095-4103, 1989.

[30] K. Obwald, S. Schneider, L. Hensgen, A. Klink and F. Klocke, "Experimental investigation of energy distribution in continuous sinking EDM," CIRP Journal of Manufacturing Science and Technology, vol. 19, pp. 36-43, 2017.

[31] R. Landfried, F. Kern, and R. Gadow, "Electrically conductive ZTA–TiC ceramics: Influence of TiC particle size on material properties and electrical discharge machining," International journal of refractory metals and hard materials, vol. 49, pp. 334-338, 2015.

[32] I. Puertas and C. J. Luis, "A study on the electrical discharge machining of conductive ceramics," Journal of Materials Processing Technology, Vols. 553-554, p. 1033–1038, 2004.

[33] J. M. Hoffmann, "Ceramic application in the automotive industry," Institute of applied materials - ceramics in mechanical engineering, 2011.

[34] B. Lauwers, K. K. Brans, W. Liu, J. Vleugels, S. Salehi and K. Vanmeensel, "Influence of the type and grain size of the electro-conductive phase on the Wire-EDM performance of ZrO2 ceramic composites," CIRP Annals - Manufacturing Technology, vol. 57, pp. 191-194, 2008.

[35] B. Lauwers, J. P. Kruth, W. Liu, W. Eeraerts, B. Schacht and P. Bleys, "Investigation of material removal mechanisms in EDM of composite ceramic materials," Journal of Materials Processing Technology, vol. 149, p. 347–352, 2004.

[36] L. Melk, M.-L. Antti and M. Anglada, "Material removal mechanisms by EDM of

zirconia reinforced MWCNT nanocomposites," Ceramics International, vol. 42, no. 5, pp. 5792-5801, 2016.

[37] F. Zeller, C. Müller, P. Miranzo and M. Belmonte, "Exceptional micromachining performance of silicon carbide ceramics by adding graphene nanoplatelets," Journal of the European Ceramic Society, vol. 37, no. 12, pp. 3813-3821, 2017.

[38] S. Tripathy and D. K. Tripathy, "Surface Characterization and Multi-response optimization of EDM process parameters using powder mixed dielectric," in the 5th International Conference of Materials Processing and Characterization (ICMPC 2016), Materials today proceedings, 2017.

[39] M. A. Singh, D. K. Sarma, O. Hanzel, J. Sedlácek and P. Sajgalík, "Machinability analysis of multi-walled carbon nanotubes filled alumina composites in wire electrical discharge machining process," Journal of the European Ceramic Society, vol. 37, p. 3107–3114, 2017.

[40] O. Flaño, Y. Zhao, M. Kunieda and K. Abe, "Approaches for improvement of EDM cutting performance of SiC with foil electrode," Precision Engineering, vol. 49, pp. 33-40, 2017.

[41] A. Torres, C. J. Luis, and I. Puertas, "EDM machinability and surface roughness analysis of TiB2 using," Journal of Alloys and Compounds, vol. 690, pp. 337-347, 2017.

[42] S. S. Sidhu and P. S. Bains, "Study of the Recast Layer of Particulate Reinforced Metal Matrix Composites machined by EDM," in 5th International Conference of Materials Processing and Characterization, Materials Today: Proceedings, 2017.

[43] R. Bamber, R. Morrell, C. Waldon, and M. Shannon, "Design substantiation of ceramic materials on fusion reactor confinement boundaries," Fusion Engineering and Design, vol. 125, pp. 283-289, 2017.

[44] H. Gotoh, T. Tani, and N. Mohri, "EDM of Insulating Ceramics by Electrical Conductive Surface Layer Control," in 18th CIRP Conference on Electro Physical and Chemical Machining, Procedia CIRP, 2016.

[45] H.-K. Yoo, J.-H. Ko, K.-Y. Lim, W. T. Kwon, and Y.-W. Kim, "Micro-electrical discharge machining characteristics of newly developed conductive SiC ceramic," Ceramics International, vol. 41, p. 3490–3496, 2015.

[46] R. Bajaj, A. K. Tiwari and A. R. Dixit, "Current trends in electric discharge machining using micro and nanopowder materials- A Review," in 4th International Conference on Materials Processing and Characterization, Materials Today: Proceedings, 2015.

[47] H. Marashi, A. A. D. Sarhan and M. Hamdi, "Employing Ti nano-powder dielectric to enhance surface characteristics in electrical discharge machining of

AISI D2 steel," Applied Surface Science, vol. 357, pp. 892-907, 2015.

[48] J. Qian, F. Yang, J. Wang, B. Lauwers, and D. Reynaerts, "Material removal mechanism in the low-energy micro-EDM process," CIRP Annals, vol. 64, no. 1, pp. 225-228, 2015.

[49] M. Kolli and A. Kumar, "Effect of dielectric fluid with surfactant and graphite powder on Electrical Discharge Machining of titanium alloy using Taguchi method," Engineering science and technology, An international journal, vol. 18, no. 4, pp. 524-535, 2015.

[50] G. Talla, D. K. Sahoo, S. Gangopadhyay, and C. K. Biswas, "Modeling and multi-objective optimization of powder mixed electric discharge machining process of aluminum/alumina metal matrix composite," Engineering Science and Technology, an International Journal, vol. 18, pp. 369-373, 2015.

[51] R. Landfried, F. Kern, and R. Gadow, "Electrically conductive ZTA–TiC ceramics: Influence of TiC particle size on material properties and electrical discharge machining," International Journal of Refractory Metals and Hard Materials, vol. 49, pp. 334-338, 2015.

[52] V. Aggarwal, S. Singh Khangura and R. K. Garg, "Parametric modeling and optimization for wire electrical discharge machining of Inconel 718 using response surface methodology," International Journal of advanced manufacturing technology, vol. 79, pp. 31-47, 2015.

[53] S.-L. Chen, M.-H. Lin, G.-X. Huang and C.-C. Wang, "Research of the recast layer on implant surface modified by micro-current electrical discharge machining using deionized water mixed with titanium powder as dielectric solvent," Applied Surface Science 311, vol. 311, pp. 47-53, 2014.

[54] M. Kunieda, Y. Zhao and K. Abe, "Study of EDM cutting of single crystal silicon carbide," Precision Engineering, vol. 38, pp. 92-99, 2014.

[55] P. J. Liew, J. Yan, and T. Kuriyagawa, "Fabrication of deep micro-holes in reaction-bonded SiC by ultrasonic cavitation-assisted micro-EDM," International Journal of Machine Tools and Manufacture, vol. 76, pp. 13-20, 2014.

[56] C. Zhang, "Effect of wire electrical discharge machining (WEDM) parameters," Ceramics International, no. 1, pp. 1-6, 2014.

[57] Y. Zhao, M. Kunieda and K. Abe, "Study of EDM cutting of single crystal silicon carbide," Precision Engineering, vol. 38, pp. 92-99, 2014.

[58] P. J. Houa, Y. F. Guo, L. X. Sun and G. Q. Deng, "Simulation of temperature and thermal stress filed during reciprocating traveling WEDM of insulating ceramics," in The Seventeenth CIRP Conference on Electro Physical and Chemical Machining, Procedia CIRP, 2013.

[59] P. J. Liew, J. Yan, and T. Kuriyagawa, "Carbon nanofiber assisted micro electro-discharge machining of reaction-bonded silicon carbide," Journal of Materials Processing Technology, vol. 213, pp. 1076-1087, 2013.

[60] D. Hanaoka, Y. Fukuzawa, C. Ramirez, P. Miranzo, M. I. Osendi and M. Belmonte, "Electrical discharge machining of ceramic / carbon nanostructure composites," Procedia CIRP, vol. 6, pp. 95-100, 2013.

[61] F. Q. Hu, F. Y. Cao, B. Y. Song, P. J. Hou, Y. Zhang, K. Chen and J. Q. Wei, "Surface properties of SiCp/Al composite by powder-mixed EDM," in The Seventeenth CIRP Conference on Electro Physical and Chemical Machining, Procedia CIRP, 2013.

[62] Y. P. Delgado, K. Bonny, P. De Baets, P. D. Neis, O. Malek, J. Vleugels and B. Lauwers, "Impact of wire-EDM on dry sliding friction and wear of WC-based and ZrO2-based composites," Wear, vol. 271, pp. 1951-1961, 2011.

[63] E. Ferraris, D. Reynaerts and B. Lauwers, "Micro-EDM process investigation and comparison performance of Al_2O_3 and ZrO_2 based ceramic composites," CIRP Annals, vol. 60, no. 1, pp. 235-238, 2011.

[64] S. Mitra, S. Sarkar, G. Paul, D. Bhaduri, and S. Biswas, "Pareto optimization of electro-discharge machining of Titanium nitride- aluminium oxide composite material using a genetic algorithm," Advanced Materials Research, Vols. 264-265, pp. 985-990, 2011.

[65] A. Sommers, Q. Wang, X. Han, C. T. Joen, Y. Park and A. Jacobi, "Ceramics and ceramic matrix composites for heat exchangers in advanced thermal systems—A review," Applied Thermal Engineering, vol. 30, no. 11-12, pp. 1277-1291, 2010.

[66] S. Lopez-Esteban, C. F. Gutierrez-Gonzalez, G. Mata-Osoro, C. Pecharroman, L. A. Diaz, R. Torrecillas and J. S. Moya, "Electrical discharge machining of ceramic/semiconductor/metal nanocomposites," Scripta Materialia, vol. 63, pp. 219-222, 2010.

[67] S. Clijsters, K. Liu, D. Reynaerts and B. Lauwers, "EDM technology and strategy development for the manufacturing of complex parts in SiSiC," Journal of Materials Processing Technology, vol. 210, pp. 631-641, 2010.

[68] L. Liu, D. Reynaerts and B. Lauwers, "Influence of the pulse shape on the EDM performance of Si3N4–TiN ceramic composite," CIRP Annals, vol. 58, no. 1, pp. 217-220, 2009.

[69] K. M. Patel, P. M. Pandey and P. Venkateswara Rao, "Surface integrity and material removal mechanisms associated with the EDM of Al2O3 ceramic composite," International Journal of Refractory Metals & Hard Materials, vol. 27, pp. 892-899, 2009.

[70] S. Kumar, R. Singh, T. P. Singh and B. L. Sethi, "Surface modification by electrical discharge machining: A review," Journal of Materials Processing Technology, vol. 209, no. 8, pp. 3675-3687, 2009.

[71] C. F. Hua, Y. C. Zhou and Y. W. Bao, "Material removal and surface damage in EDM of Ti3SiC2 ceramic," Ceramics International, vol. 34, no. 3, pp. 537-541, 2008.

[72] Y. H. Liu, X. P. Li, R. J. Ji, L. L. Yu, and H. F. Zhang, "Effect of the technological parameter on the process performance for electric discharge milling of insulating Al2O3 ceramic," Journal of materials processing technology, vol. 208, pp. 245-250, 2008.

[73] B. Lauwers, J. P. Kruth and K. Brans, "Development of Technology and Strategies for the Machining of Ceramic Components," Annals of the CIRP, vol. 56, no. 1, pp. 225-228, 2007.

[74] C. J. Luis and I. Puertas, "Methodology for developing technological tables used in EDM processes of conductive ceramics," Journal of Materials Processing Technology, vol. 189, pp. 301-309, 2007.

[75] R. Kumar, A. Singh, and I. Singh, "Electric discharge hole grinding in hybrid metal matrix composite," Materials and Manufacturing Processes, vol. 32, pp. 127-134, 2017.

[76] M. S. Rayat, S. S. Gill, R. Singh, and L. Sharma, "Fabrication and machining of ceramic composites — A review on current scenario," Materials and Manufacturing processes, vol. 32, no. 13, pp. 1451-1474, 2016.

[77] R. Goyal, S. Singh, and H. Kumar, "Performance evaluation of cryogenically assisted electric discharge machining (CEDM) process," Materials and Manufacturing Processes, vol. 1, pp. 1-11, 2017.

[78] G. S. Prihandana, M. Mahardika, M. Hamdi, Y. S. Wong and K. Mitsui, "Effect of micro-powder suspension and ultrasonic vibration of dielectric fluid in micro-EDM processes—Taguchi approach," International Journal of Machine Tools and Manufacture, vol. 49, no. 12-13, pp. 1035-1041, 2009.

[79] R. Baghel, H. S. Mali and S. K. Biswas, "Parametric optimization and surface analysis of diamond grinding-assisted EDM of TiN-Al2O3 ceramic composite," The International Journal of Advanced Manufacturing Technology, vol. 1, pp. 1-10, 2018.

[80] Y.-F. Chen and Y.-C. Lin, "Surface modifications of Al–Zn–Mg alloy using combined EDM with ultrasonic machining and addition of TiC particles into the dielectric," Journal of Materials Processing Technology, vol. 209, no. 9, pp. 4343-4350, 2009.

[81] W. S. Zhao, Q. G. Meng, and Z. L. Wang, “The application of research on powder mixed EDM in rough machining,” Journal of Materials Processing Technology, vol. 129, no. 1-3, pp. 30-33, 2002.

[82] C. S. Trueman and J. Huddleston, “Material removal by spalling during EDM of ceramics,” Journal of the European Ceramic Society, vol. 20, no. 10, pp. 629-1635, 2000.

[83] P. J. Liew, J. Yan, and T. Kuriyagawa, “Experimental investigation on material migration phenomena in micro-EDM of reaction-bonded silicon carbide,” Applied Surface Science , vol. 276, pp. 731-743, 2013.

[84] T. T.Öpöz and H. Yaşar, “Particle migration and surface modification on Ti6Al4V in SiC powder mixed electrical discharge machining,” Journal of Manufacturing Processes, vol. 31, pp. 744-758, 2018.

[85] M. Shabgard and B. Khosrozadeh, “Investigation of carbon nanotube added dielectric on the surface characteristics and machining performance of Ti–6Al–4V alloy in EDM process,” Journal of Manufacturing Processes, vol. 25, pp. 212-219, 2017.

[86] B. Singh, J. Kumar, and S. Kumar, “Influences of Process Parameters on MRR Improvement in Simple and Powder-Mixed EDM of AA6061/10%SiC Composite,” Materials and Manufacturing Processes, vol. 30, no. 5, pp. 303-312, 2015.

[87] H. Marashi, D. M. Jafarlou, A. A. Sarhan and M. Hamdi, “State of the art in powder mixed dielectric for EDM applications,” Precision Engineering, vol. 46, pp. 11-33, 2016.

[88] D. R. Unune and H. S. Mali, “Parametric modeling and optimization for abrasive mixed surface electro discharge diamond grinding of Inconel 718 using response surface methodology,” The International Journal of Advanced Manufacturing Technology, vol. 93, no. 9-12, p. 3859–3872, 2017.

[89] B. T. Long, N. H. Phan, N. Cuong, and V. S. Jatti, “Optimization of PMEDM process parameter for maximizing material removal rate by Taguchi’s method,” The International Journal of Advanced Manufacturing Technology, vol. 87, no. 5-8, p. 1929–1939, 2016.

[90] P. Peças and E. Henriques, “Effect of the powder concentration and dielectric flow in the surface morphology in electrical discharge machining with a powder-mixed dielectric (PMD-EDM),” The International Journal of Advanced Manufacturing Technology, vol. 37, no. 11-12, p. 1120–1132, 2008.

[91] S. Assarzadeh and M. Ghoreishi, “A dual response surface-desirability approach to process modeling and optimization of Al2O3 powder-mixed electrical discharge machining (PMEDM) parameters,” The International Journal of

Advanced Manufacturing Technology, vol. 64, no. 9-12, p. 1459–1477, 2013.

[92] S. Assarzadeh and M. Ghoreishi, "Investigating surface properties of OHNS die steel after electrical discharge machining with manganese powder mixed in the dielectric," The International Journal of Advanced Manufacturing Technology, vol. 64, no. 9-12, p. 1459–1477, 2013.

[93] Z. He, Y. Li, Q. Zhang and H. Wang, "Capillary microchannel- based microreactors with highly durable ZnO/TiO2 nanorod arrays for rapid, high efficiency and continuous- flow photocatalysis," Applied Catalysis B: Environmental, vol. 93, pp. 376-382, 2010.

[94] P. Watts and C. Wiles, "Recent advances in synthetic micro reaction technology," Chemical Communications, no. 5, pp. 443-467, 2007.

[95] V. Hessel, H. Lowe, and S. Hardt, Chemical micro process engineering: Fundamentals, modeling and reactions, Isbn:978-3-527-60537-8. Wiley-VCH, 2006.

[96] J. Jin and N.-T. Nguyen, "Manipulation schemes and applications of liquid marbles for micro total analysis systems," Microelectronic Engineering, vol. 197, pp. 87-95, 2018.

[97] R. M. Guijt and A. Manz, "Miniaturised total chemical-analysis systems (μTAS) that periodically convert chemical into electronic information," Sensors and Actuators B: Chemical, vol. 273, pp. 1334-1345, 2018.

[98] X. Chen, Y. Cheng, T. Li, and Y. Cheng, "Characteristics and applications of plasma assisted chemical processes and reactors," Current opinion in chemical engineering, vol. 17, pp. 68-77, 2017.

[99] Y. Takeuchi, C. Park, K. Noborio, Y. Yamamoto and S. Konishi, "Heat transfer in SiC compact heat exchanger," Fusion engineering and design, vol. 85, pp. 1266-1270, 2010.

[100] L. Xia and Y. Chan, "Investigation of the enhancement effect of heat transfer using microchannel," in The 7th International Conference on Applied Energy, Energy Procedia, 75,912 – 918, 2015.

[101] M. J. AlamKhan, M. R. Hasan and M. A. H. Mamun, "Flow Behavior and Temperature Distribution in Micro-Channels for Constant Wall Heat Flux," in 5th BSME International Conference on Thermal Engineering, Procedia Engineering, 56,350-356, 2013.

[102] A. Sommers, Q. Wang, X. Han, C. T. Joen, Y. Park and A. Jacobi, "Ceramics and ceramic matrix composites for heat exchangers in an advanced thermal systems-A review," Applied. Thermal Engineering, vol. 30, pp. 1277-1291, 2010.

[103] V. Nagarajan, Y. Chen, Q. Wang and T. Ma, "CFD modeling and simulation of

sulfur trioxide decomposition in ceramic plate-fin high-temperature heat exchanger and decomposer," International Journal of Heat and Mass Transfer, vol. 80, p. 329–343, 2015.

[104] S. K. S. Yadav, V. Yadava and V. L. Narayana, "Experimental study and parameter design of electro-discharge diamond grinding," The International Journal of Advanced Manufacturing Technology, vol. 36, no. 1-2, pp. 34-42, 2008.

[105] H. Kumar, "Development of mirror-like surface characteristics using nanopowder mixed electric discharge machining (NPMEDM)," The International Journal of Advanced Manufacturing Technology, vol. 76, no. 1-4, p. 105–113, 2015.

[106] S. K. Biswas and J. Mukerji, "Synthesis, Properties, and Oxidation of Alumina-Titanium Nitride Composites," J.Am.Ceram.Soc., 1990.

[107] S. Mahapatra and A. Patnaik, "Parametric Optimization of Wire Electrical Discharge Machining (WEDM) Process using Taguchi Method," J. of the Braz. Soc. of Mech. Sci. & Eng, 2006.

[108] H. S. Mali, D. Unune and S. Tiwari, "Modelling and prediction of material removal rate in electrical discharge diamond surface grinding process of Inconel-718," in 5th International and 26th All India. Manufacturing Technology, Design, and Research Conference, 2014.

[109] D. R. Unune, V. P. Singh and H. S. Mali, "Experimental Investigations of Abrasive Mixed Electro Discharge Diamond Grinding of Nimonic 80A," Materials and Manufacturing Processes, vol. 3, no. DOI: 10.1080/10426914.2015.1090598, pp. 1718-1723, 2015.

[110] S. K. S. Yadav and V. Yadava, "Experimental study and parameter design of electro-discharge diamond grinding," The International Journal of Advanced Manufacturing Technology, vol. 36, no. 1-2, pp. 34-42, 2008.

[111] P. Koshy, V. Jain, and G. Lal, "Mechanism of material removal in electrical discharge diamond grinding," International Journal of Machine Tools and Manufacture, vol. 36, no. 10, pp. 1173-1185, 1996.

[112] V. J. G. L. Philip Koshy, "Grinding of cemented carbide with electrical spark assistance," Journal of Materials Processing Technology, vol. 72, pp. 61-68, 1997.

[113] J. Yan and T.-H. Tan, "Sintered diamond as a hybrid EDM and grinding tool for the micromachining of single-crystal SiC," CIRP Annals - Manufacturing Technology, vol. 64, no. 1, pp. 221-224, 2015.

[114] Douglas C. Montgomery, design and analysis of experiments, John Wiley & sons INC, Newyork Chichester Weinheim bresbane Toronto Singapore, 2000.

[115] V. Aggarwal, S. S. Khangura and R. K. Garg, "Parametric modeling and

optimization for wire electrical discharge machining of Inconel 718 using response surface methodology," Int J Adv Manuf Technol (2015) 79:31–47.

[116] L. Xia and Y. Chan, "Investigation of the enhancement effect of heat transfer using microchannel," in The 7th International Conference on Applied Energy, Energy Procedia 75 (912 – 918, 2015.

[117] K. Liu, E. Ferraris, J. Peirs, B. Lauwers and D. Reynaerts, "Micro EDM process investigation of Si3N4-TiN ceramic composites for the development of micro fuel-based power unit," Int. J. Manufacturing Research, vol. 3, no. 1, 2008.

[118] M. J. Alam Khan, M. R. Hasan and M. A. Hasan Mamun, "Flow behavior and temperature distribution in micro-channels for constant wall heat flux," in 5th BSME International Conference on Thermal Engineering, Procedia Engineering 56, 2013.

[119] V. Nagarajan, Y. Chen, Q. Wang and T. Ma, "CFD modeling and simulation of sulfur trioxide decomposition in ceramic plate-fin high-temperature heat exchanger and decomposer," International Journal of Heat and Mass Transfer, vol. 80, p. 329–343, 2015.

[120] Y. K. Lok and T. C. Lee, "Processing of Advanced Ceramics Using the Wire-Cut EDM Process," Journal of Materials Processing Technology, vol. 63, no. 1-3, pp. 839-843, 1997.

[121] A. Asad, M. T. Islam, T. Masaki, M. Rahman, and Y. S. Y.S. Wong, "Analysis of micro-EDM electric characteristics employing plasma property," CIRP Journal of Manufacturing Science and Technology, vol. 20, pp. 36-50, 2018.

[122] V. Schulze, P. Weber, and C. Ruhs, "Increase of process reliability in the micro-machining processes EDM-milling and laser ablation using on-machine sensors," Journal of Materials Processing Technology, vol. 212, no. 3, pp. 625-632, 2012.

[123] B. Shao and R. P. Kamlakar, "Modelling of the crater formation in micro-EDM," in the CIRP Conference on Intelligent Computation in Manufacturing Engineering, Procedia CIRP, 2015.

[124] K. K. Saxena, A. S. Srivastava and S. Agarwal, "Experimental Investigation Into The Micro EDM Characteristics Of Conductive Sic," Ceramic international, vol. 42, no. 1, pp. 1597-1610, 2015.

[125] Nagahanumaiah, J. Ramkumar, N. Gluma, S. G. Kapoor and R. E. DeVor, "Characterization of plasma in micro-EDM discharge using optical spectroscopy," Journal of Manufacturing Processes, vol. 11, no. 2, pp. 82-87, 2009.

[126] B. Lauwers, J. P. Kruth, W. Liu, W. Eeraerts, B. Schacht and P. Bleys, "Investigation of material removal mechanisms in EDM of composite ceramic materials," Journal of Materials Processing Technology, vol. 149, p. 347–352,

2004.

[127] Z. Y. Yu, Y. Zhang, J. Li, J. Luan, F. Zhao, and D. Guo, "High aspect ratio micro-hole drilling aided with ultrasonic vibration and planetary movement of electrode by micro-EDM," CIRP Annals, vol. 58, no. 1, pp. 213-216, 2009.

[128] S. H. Yeo, P. C. Tan, and W. Kurnia, "Effects of powder additives suspended in dielectric on crater characteristics for micro electrical discharge machining," Journal of Micromechanics and Microengineering, vol. 17, no. 11, 2007.

[129] T. Lee and J. Deng, "Mechanical surface treatments of electro-discharge machined (EDMed) ceramic composite for improved strength and reliability," Journal of the European Ceramic Society, vol. 22, no. 4, pp. 545-550, 2002.

[130] C. S. Trueman and J. Huddleston, "Material removal by spalling during EDM of ceramics," Journal of European ceramics society, vol. 1, pp. 1629-1635, 2000.

[131] https://www.aiche.org/academy/webinars/microreactors-discovery-development-and-chemical-engineering-opportunities-29-11-2018

APPENDIX "A" **Study of Vibration Assisted Micro Electro-Discharge Milling of Titanium Nitride-Aluminium Oxide Composite**

In this study, the effects of incorporating the unidirectional vibration in ED machining on Titanium Nitride-Aluminium Oxide ($TiN\text{-}Al_2O_3$) ceramic-composite workpiece are studied. All the experiments are performed on Hybrid μ EDM DT-110i machine. Taguchi L9 algorithm is used to design the experiments. The range of process parameters taken for machining experiments is shown in Table A.1.

Table A.1 Range of input parameters

SN	**Input parameter**	**Unit**	**Range of input parameters**		
1	Capacitance	Micro-fared	0.01	0.1	0.4
2	Spindle speed	RPM	400	600	800
3	Vibration	Hz	10	60	110

To study the effect of vibration on the EDM process, first experiments are performed on EDM followed by vibration assisted EDM at the same parametric setting.

A.1 Experimentations

All the experiments were performed according to the Taguchi L9 orthogonal array design with three control factors and two response parameters, the results observed are shown in Table A.2. Materials removal rate (MRR in mm^3/min) and electrode wear rate (EWR in mm/min) are taken as response parameters. Signal to noise (S/N) ratio is calculated for each response parameter.

Table A.2 Results based on experimental design

Sn.	**Capacitance (Microfarad)**	**Speed (RPM)**	**Vibration (Hz)**	**MRR (mm^3/min)**	**EWR (mm/min)**	**S/N Ratio for MRR**	**S/N Ratio for EWR**

1	0.01	400	10	0.00442	0.00222	-47.0916	53.0729
2	0.01	800	55	0.00704	0.00680	-43.0485	43.3498
3	0.01	1200	110	0.00785	0.00658	-42.1026	43.6355
4	0.1	400	55	0.00469	0.00477	-46.5765	46.4296
5	0.1	800	110	0.01009	0.00949	-39.9222	40.4547
6	0.1	1200	10	0.00849	0.00497	-41.4218	46.0729
7	0.4	400	110	0.00539	0.00614	-45.3682	44.2366
8	0.4	800	10	0.00892	0.00629	-40.9927	44.0270
9	0.4	1200	55	0.00948	0.00674	-40.4638	43.4268

A.2 Results and discussion

A.2.1 Analysis of variance (ANOVA) for MRR and EWR

Analysis of variance (ANOVA) test is performed for each response parameter. If the output parameter has to be maximized, then (S/N) ratio can be calculated by equation A.1. For the MRR (S/N) ratio follows "The Larger the Better" model.

$$\text{(S/N) ratio}_{\text{MRR}} = 10\log_{10}\frac{\sum_{i=1}^{n}\frac{1}{i^2}}{n} \quad \ldots\ldots\ldots\ldots\ldots\ldots\ldots\ldots\ldots\ldots\ldots\ldots\ldots\ldots\ldots \text{(A.1)}$$

n= number of replications

From Table A.3, it is clear that electrode rotation speed has the highest contribution in improving the MRR. The determination coefficient (R^2) indicates the goodness of fit for the model. In this case, the value of the determination coefficient (R^2=0.9802) indicates that only less than 2% of the total variance is not explained by the model. The value of the adjusted determination coefficient (adjusted R^2=0.9207) is also high and close to the determination coefficient, which indicates a high significance of this model. Predicted R^2 is also in good agreement with the adjusted R^2. The (S/N) ratio curve of MRR is shown in Fig. A.1, it indicates the increase in capacitance and speeds the higher MRR can be achieved. Higher vibration leads to better MRR.

Source	DF	Sum of square	Adj SS	Adj MS	F	P
Capacitance	2	5.4707	5.4707	2.7353	4.73	0.175
Speed	2	50.4040	50.4040	25.2020	43.55	0.022
Vibration	2	1.3414	1.3414	0.6707	1.16	0.463
Error	2	1.1575	1.1575	0.5787		
Total	8	58.3736				
S			0.760748			
R-Sq			98.02%			
R-Sq(adj)			92.07%			

Table A.3 ANOVA results for MRR

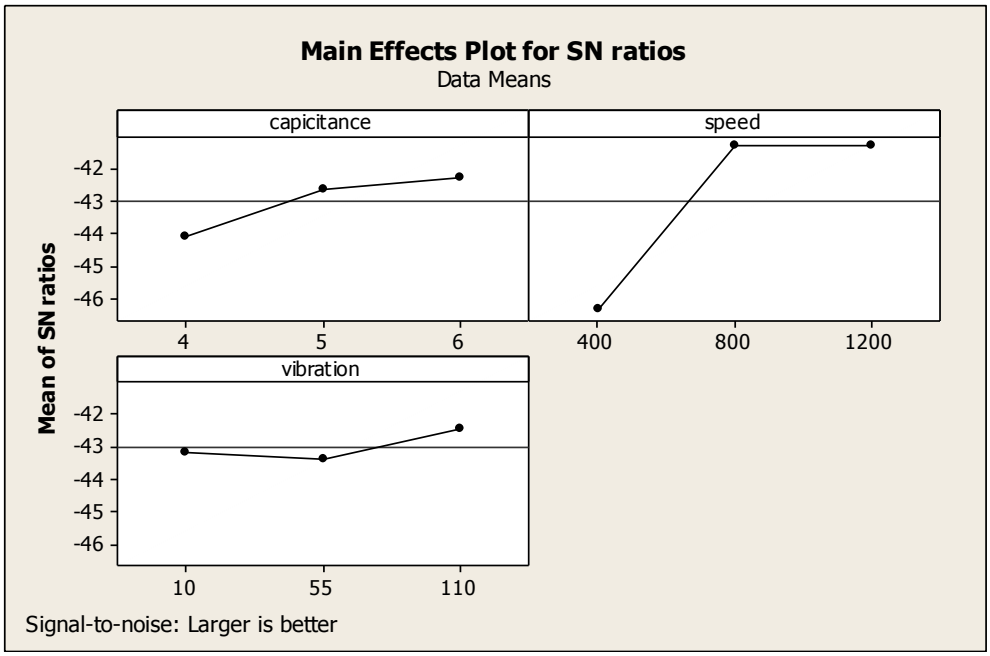

Figure A.1 Main effect plot for MRR

Value of electrode wear should be as lower as possible and if the value of the response parameter has to be minimized then signal to noise ratio can be calculated by the equation A.2.

$$\text{(S/N) ratio}_{EWR} = \log_{10} \frac{\sum_{i=1}^{n} Yi^2}{n} \quad \ldots\ldots\ldots\ldots\ldots\ldots\ldots\ldots\ldots\ldots\ldots\ldots\ldots\ldots \text{(A.2)}$$

n=number of replications

Table A.4 ANOVA results for EWR

Source	**DF**	**Sum of square**	**Adj SS**	**Adj MS**	**F**	**P**
Capacitance	2	13.561	13.561	6.781	6.34	0.136
Speed	2	43.737	43.737	21.868	20.46	0.047
Vibration	2	38.172	38.172	19.086	17.86	0.050
Error	2	2.138	2.138	1.069		
Total	8	97.607				
S			1.03381			
R-Sq			97.81%			
R-Sq(adj)			91.24%			

The shape and size of the electrode are damaged by EDM sparks. This damage is called "electrode wear". EWR is calculated by a change in the length of the electrode in each machine time. From Table A.5, it is clear from observation that vibration and electrode rotation speed has the largest contribution in the EWR.

The determination coefficient (R^2) indicates the goodness of fit for the model. In this case, the value of the determination coefficient (R^2=0.9781) indicates that only less than 3% of the total variance is not explained by the model. The value of the adjusted determination coefficient (adjusted R^2=0.9124) is also high and close to the determination coefficient, which indicates a high significance of the model. The value of probability >F in Table 5 for the model is less than 0.05, which indicates that the model is significant. The (S/N) ratio curve (Fig. A.2) of EWR shows that at low speed and low vibration, electrode wear is less.

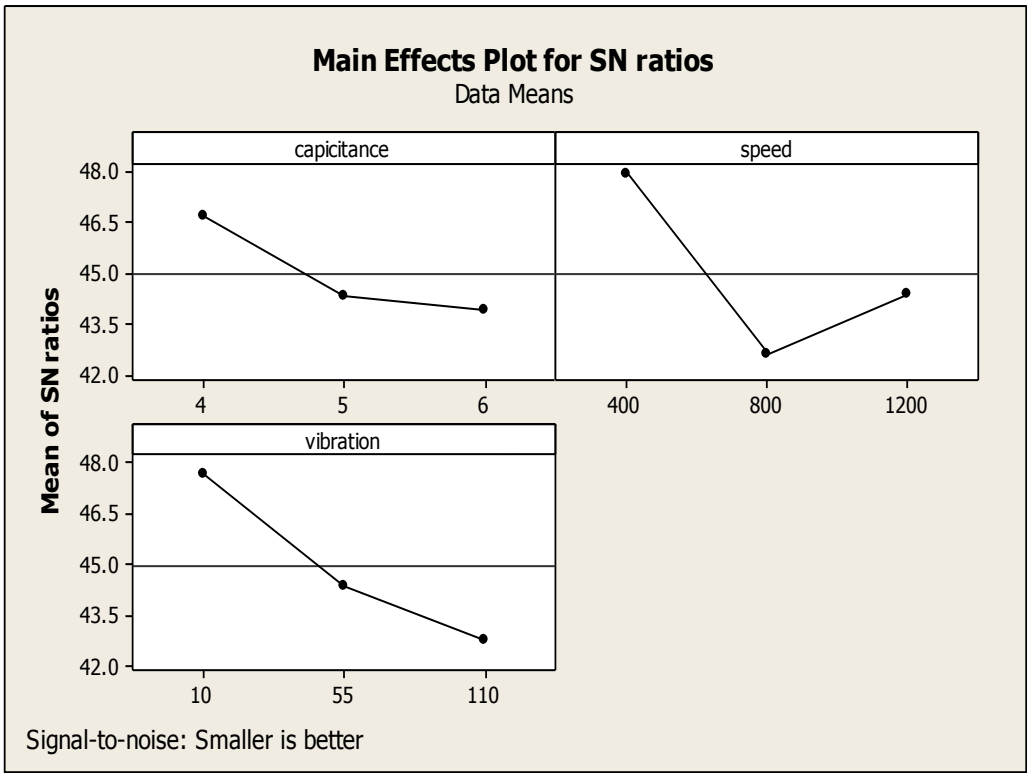

Figure A.2 Main effects plot for EWR

A.2.2 Comparisons of response parameters in micro EDM and vibration-assisted micro EDM

To know the effect of vibration on response parameters like MRR and EWR. A set of experiments is conducted on the same machine and at same parameter setting, but this time without vibration. The results obtained are shown in Table A.5.

Table A.5 Comparison of response parameters of EDM and vibration-assisted EDM process

	Without vibration		**With vibration**	
Sn.	**MRR (mm^3/min)**	**EWR (mm/min)**	**MRR (mm^3/min)**	**EWR (mm/min)**
1	0.0012	0.00742	0.00442	0.00222
2	0.00683	0.00915	0.00704	0.0068
3	0.00712	0.07994	0.00785	0.00658
4	0.00167	0.01179	0.00469	0.00477

5	0.00509	0.03852	0.01009	0.00949
6	0.00622	0.04409	0.00849	0.00497
7	0.00518	0.07971	0.00539	0.00614
8	0.00741	0.07762	0.00892	0.00629
9	0.00733	0.0668	0.00948	0.00674

The comparative data of MRR in both cases are plotted in Fig. A.3. It is clear from the plot that vibration improves the MRR at each parameter setting. The MRR increases significantly with the vibration.

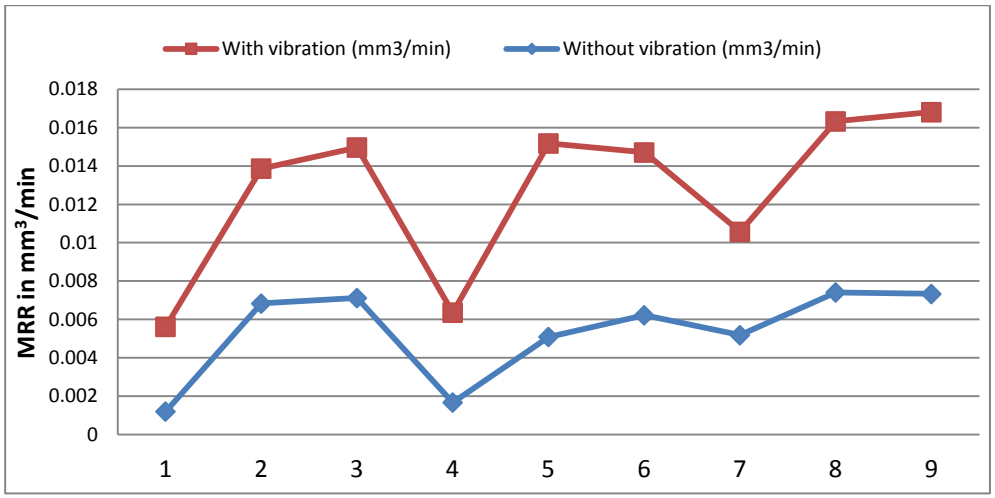

Figure A.3 Plot of MRR in EDM and vibration-assisted EDM

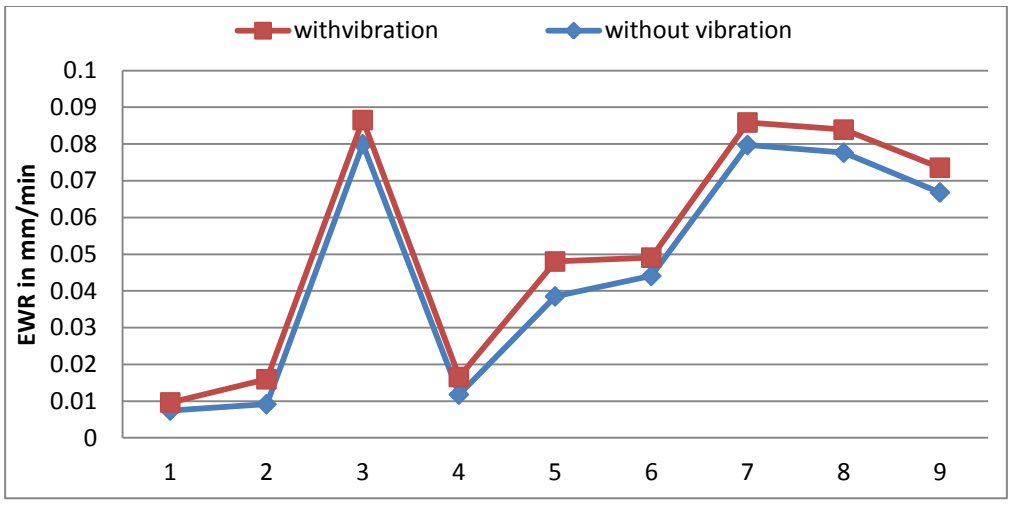

Figure A.4 Plot of EWR in EDM and vibration-assisted EDM

A maximum of 0.01009 mm^3/min MRR is obtained with vibration-assisted EDM but at the same setting 0.00509 mm^3/min MRR is measured with EDM. This shows MRR can be improved by 1.98 times by implementing vibration. The comparative data of EWR are shown in Fig. A.4, it indicates an increase in electrode wear as the vibration is involved.

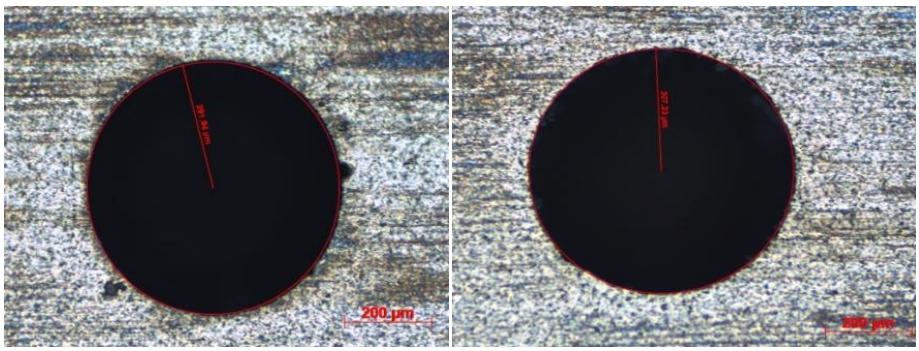

(a) **(b)**

Figure A.5 Microscopic images of holes (a) EDM, (b) Vibration-assisted EDM

The above images (Fig. A5) are taken by an optical microscope at 200× magnification at the optimal parameter where maximum MRR is observed. A change in the diameter of the micro-hole is observed at a higher vibration.

A.3 Conclusions

The hybrid micro EDM process is used to create holes on work-piece. Based on the analysis of the results following conclusions are made.

1. When machining TiN-Al_2O_3 by vibration-assisted micro EDM process, the electrode rotation speed is the most influencing parameter followed by capacitance and vibration. As the value of electrode speed and capacitance increases, the value of MRR increases.
2. A maximum MRR of 0.01009 mm^3/min is obtained with vibration-assisted EDM but at the same setting 0.00509 mm^3/min MRR is measured; thus MRR can be improved 1.98 times by implementing vibration.
3. The electrode wear rate is mainly influenced by electrode speed and vibration. EWR increases with increase in the value of electrode speed and vibration.

4. Vibration-assisted EDM is proven to be the preferable method to machine TiN-Al_2O_3 ceramic-composite as material removal rate is significantly improved than EDM.

Based on the experimental observations, it can be said that hybrid micro EDM with vibration assistant is an effective process for machining of ceramic-composites.

APPENDIX "B" **STUDY ON EFFECTS OF DISCHARGE ENERGY ON GEOMETRIC CHARACTERISTICS OF HIGH ASPECT RATIO MICRO-HOLES ON TiN-Al_2O_3 CERAMICS**

The present work deals with the fabrication of high aspect ratio (AR =25) micro-holes on a newly developed advanced ceramic by µ-EDM. The investigation focuses on the influence of input parameters and discharges energy on Material Removal Rate (MRR), Electrode Wear Rate (EWR). An experimental analysis focusing on the effects of discharge energy on geometrical characteristics is also presented.

B.1 Planning of Experiments

In the present work, the behavior of the EDM is studied with different discharge energy. The effect of the process parameter such as spindle speed (S), capacitance (C), voltage (V) on MRR, EWR, electrode wear ratio (EW), radial overcut (ROC) and taper angle (α) is also observed.

Table B.1 Range of input parameters

Process Parameter	Range	Constant Process	Parameter
Spindle speed (S)	900, 1200, 1500 RPM	Tool Electrode	Tungsten (ø 200 µm)
Capacitance (C)	0.01, 0.1, 0.4 µF	Feed	5%
Voltage (V)	90, 110, 130 Volt	Machine Feed	1.5 mm/min

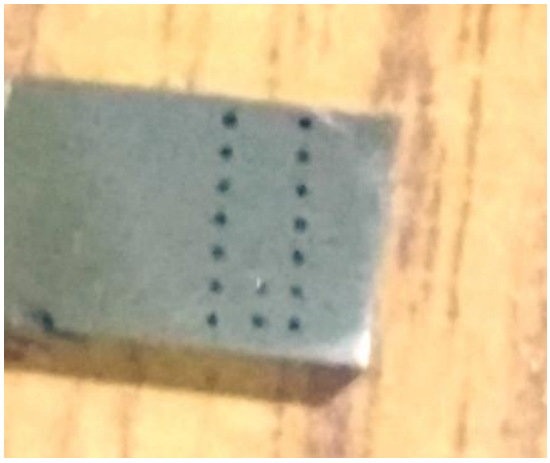

Figure B.1 Work-piece with micro holes

These process parameter and range have been selected on the basis of existing literature, pilot experiments, and machine capability. The process parameter range and constant process parameters are shown in Table B.1.

B.2 Experimental Setup and Procedure

In this present work, the tool electrode is of tungsten (Φ=200 μm) is connected to negative polarity and the ceramic workpiece is connected to positive polarity. The experimental results are given in Table B.3. Statistical analysis consists of the calculation of signal to noise (S/N) ratio values for each response factor.

Table B.2 Experiments design matrix with a set of process parameters and corresponding response parameters

	S	**C**	**V**	**Discharge Energy**	**MRR**	**EW**	**EW Ratio**	**Radial overcut**	**Taper angle**
run	**rpm**	Micro fared	volt	Micro joule	mm^3/min	mm^3/min		micron	radian
1	**900**	0.01	90	40.5	0.002737	0.00030	9.12	70.8	0.2566
2	**900**	0.1	110	605	0.005162	0.00123	4.19	76.35	0.0945
3	**900**	0.4	130	3380	0.006914	0.00075	9.21	80.35	0.2062
4	**1200**	0.01	110	60.5	0.004107	0.00173	2.37	77.95	0.2515
5	**1200**	0.1	130	845	0.004837	0.00252	1.91	75.65	0.3053
6	**1200**	0.4	90	1620	0.006425	0.00387	1.66	79.05	0.3214
7	**1500**	0.01	130	84.5	0.004234	0.00160	2.64	90.1	0.3351
8	**1500**	0.1	90	405	0.003642	0.00211	1.72	61.6	0.2996
9	**1500**	0.4	110	2420	0.004803	0.00294	1.63	70.8	0.1718

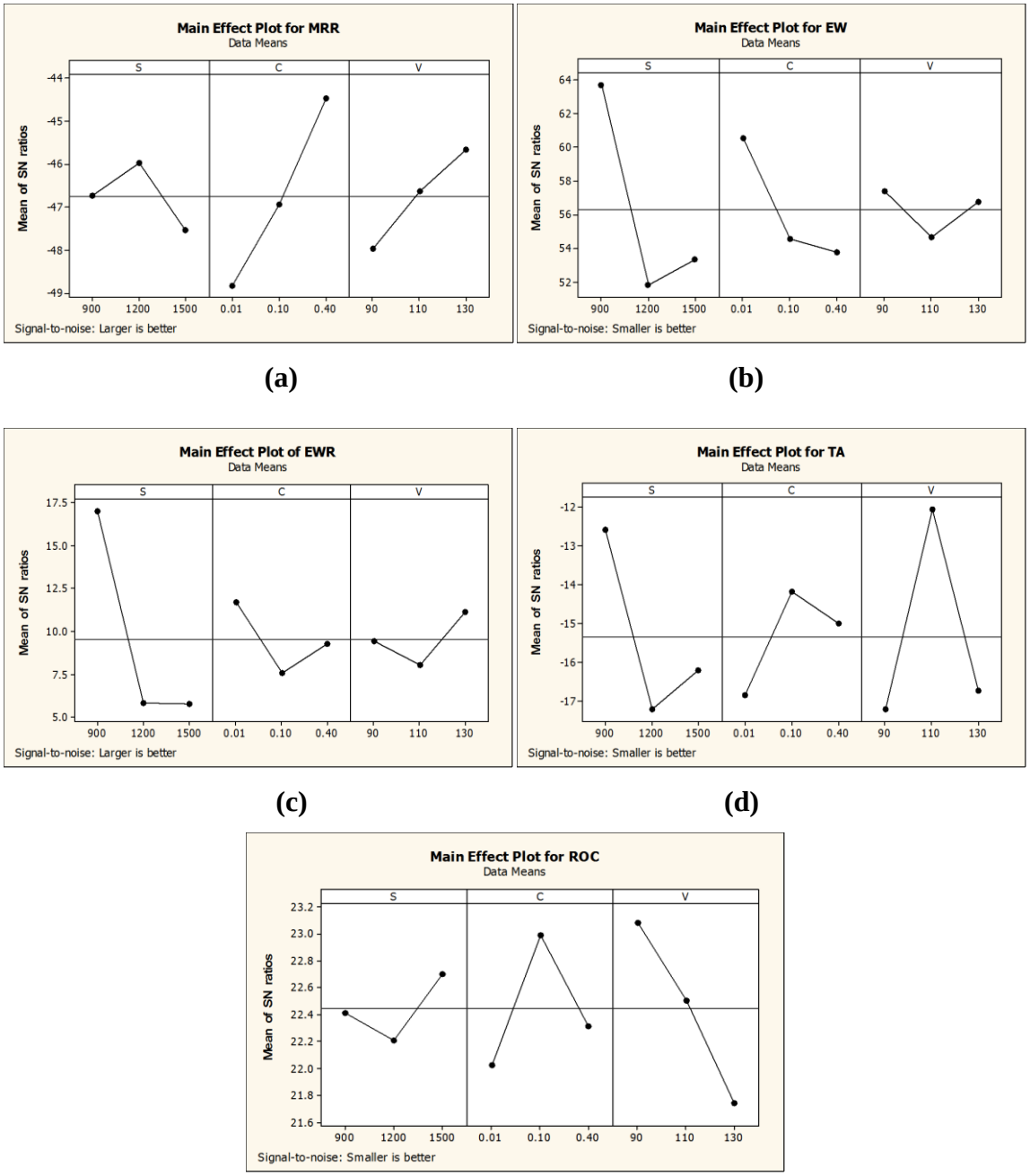

Figure B.2 Main effect plots for (a) MRR, (b) Electrode wear, (c) Electrode wear ratio, (d) taper angle and (e) radial overcut

B.2.1.Effect of Control Parameter on MRR

The S/N ratio for MRR follows larger is better and S/N graph has an increasing trend with capacitance and voltage as shown in Fig. B.2 (a). Spindle speed has a less significant

effect on MRR. Here capacitance has rank one followed by voltage and spindle speed. MRR was found to improve with an increase in the voltage and capacitance as they simultaneously increase the discharge energy thus causing the greater speed of bombarding electron from electrode to the workpiece, resulting in higher MRR.

B.2.2 Effect of Control Parameter on EW and EW Ratio

Calculation of S/N ratio for electrode wear (EW) follows the "Smaller is Better" model. From Fig. B.2(b) and Fig. B.2(c), it is observed that the S/N graph for EW has a steep decreasing trend. Spindle speed holds rank one, thus being the most influencing parameter in case of electrode wear followed by capacitance and voltage. The S/N ratio graph for electrode wear ratio (EW Ratio) is following "larger is better" model electrode wear ratio (MRR/EWR). Electrode wear ratio is high at a low spindle rotation speed. For EW Ratio, speed holds rank one followed by capacitance and voltage.

B.2.3 Effect of Control Parameter on taper angle and radial overcut

For the taper angle, the calculation of S/N ratio follows "smaller the better" model. From Fig. B.2 (d) and Fig. B.2 (e), it is observed that the S/N graph for taper angle has a decreasing trend with speed and increasing trend with voltage. Voltage comes out to be a most influencing parameter with rank one, speed hold rank two and capacitance does not have a significant effect on taper angle and holds rank three. The calculation of S/N ratio for radial overcut follows "smaller the better" model and voltage comes out to be the most influencing parameter followed by capacitance and speed. High voltage and high capacitance results in high discharge energy which further results in large radial overcut.

B.3 Results and discussion

After determining the influencing parameter on responses under these conditions, the effect of discharge energy is also studied on response parameters. The discharge energy is calculated by the formula $E=0.5CV^2$. Experiments are performed at different discharge energy and at various electrode rotation speeds as Shown in Table B.4. It is observed from Fig. B.3(a) that at a lower speed (i.e. 900 rpm), MRR trends to increase with the increase in discharge energy and EW first increases with discharge energy and after reaching a certain value it starts decreasing.

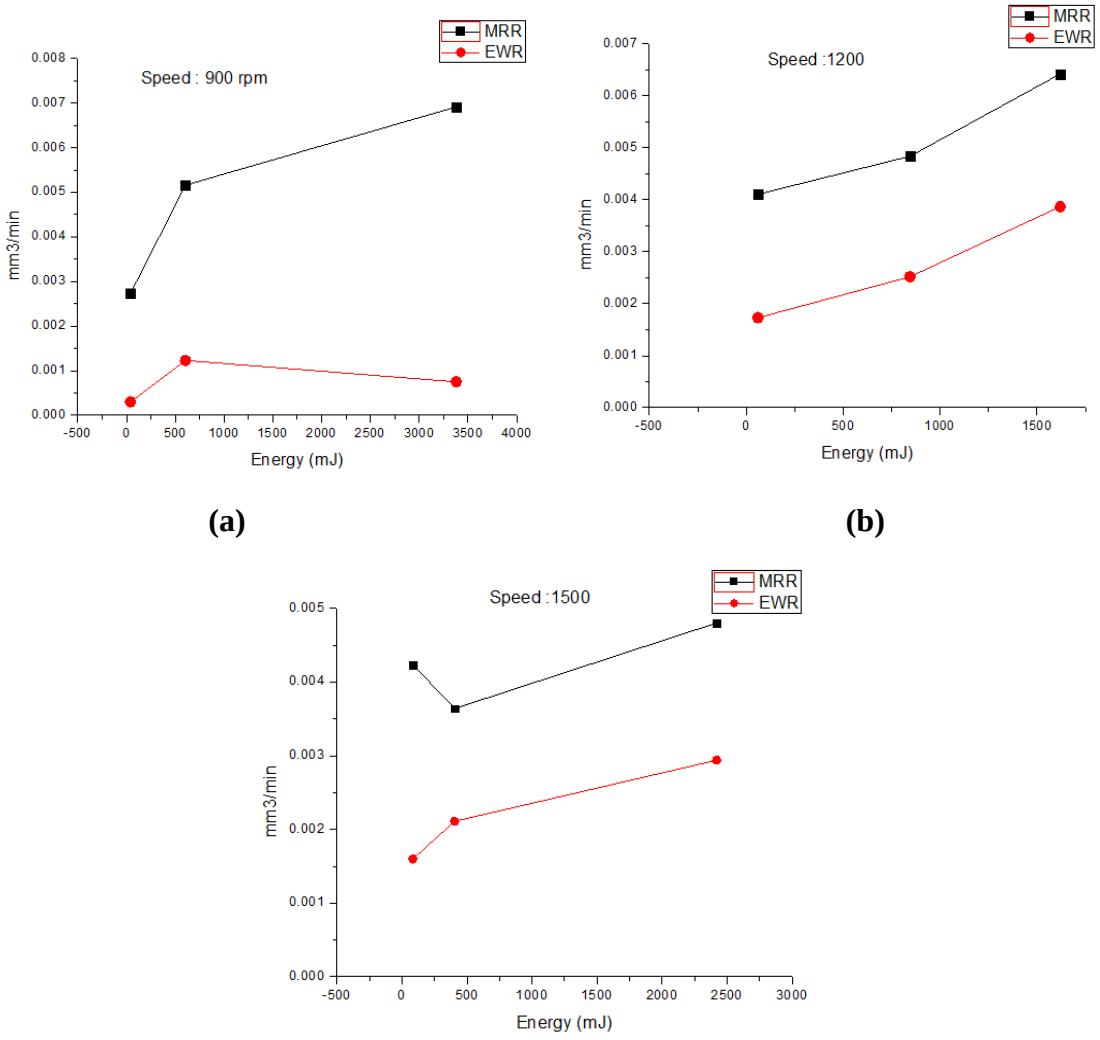

Figure B.3 Effect of discharge energy on MRR at a various spindle speed

At medium speed (i.e. 1200 rpm), MRR and EWR both increases with the discharge energy value {Fig. B.3 (b)}. At higher speed (i.e. 1500), both MRR and EWR increases with discharge energy but only after 500 µJ discharge energy {Fig. B.3(c)}.

To study the effect of discharge energy on geometric characteristics, micro-holes of 200 µm diameter were generated at 1200 rpm speed as shown in Table 4. Tungsten electrode with 200 µm has been used for these experiments.

Table B.3 Response parameters at various discharge energy value

Sn.	ENERGY (micro joule)	MRR (mm3/min)	EW (mm3/min)	EW Ratio	ROC (micron)	TA (radian)
1	320	0.003845	0.000116	33.11	64.05	0.4497
2	405	0.004837	8.82E-05	54.87	59.6	0.4377
3	500	0.005058	0.000143	35.43	64.55	0.3649
4	605	0.005233	0.000329	15.89	67.25	0.7476
5	720	0.004978	0.000217	22.96	67.6	0.3317
6	845	0.004615	0.000212	21.77	66.4	0.4354

B.3.1 Effect of discharge energy on material removal rate (MRR) and electrode wear (EW)

From these experiments, it is observed that MRR is increasing with an increase in the value of discharge energy; maximum MRR observed is 0.005233 mm^3/min at discharge energy of 605 µJ.

The observed MRR variation with discharge energy is shown in Fig. B.4(a). It can be seen that in this working condition (s=1200 rpm) MRR reached its maximum value and after that, it start decreasing with the discharge energy. MRR is good in range 500-600µJ range and after 600 µJ, MRR follows steep downfall.

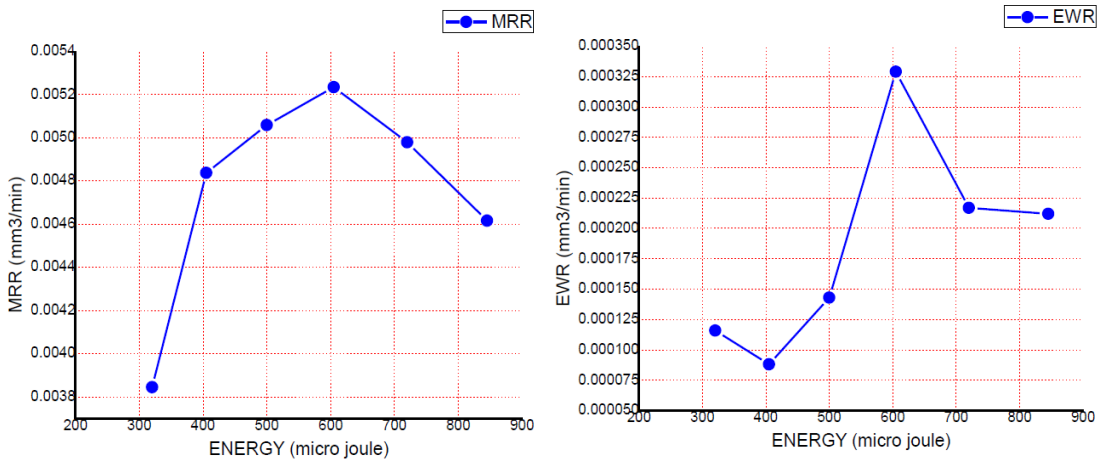

(a) **(b)**

Figure B.4 Effect of discharge energy on (a) MRR and (b) electrode wear

EW is lowest at less discharge energy but at lower energy level MRR is also lowest as shown in Fig. B.4 (b). So we can conclude that 500 µJ discharge energy is suitable for working as MRR and EW both are optimum at this point.

B.3.2 Effect of discharge energy on ROC and TA

The effect of discharge energy on radial overcut (ROC) and taper angle (TA) can be seen in Fig. B. 5(a) and Fig. B 5(b). It can be observed that ROC is less in the range 300-500 µJ discharge energy and lowest at 400 µJ. The taper angle is less at the value of 500 and 700 µJ.

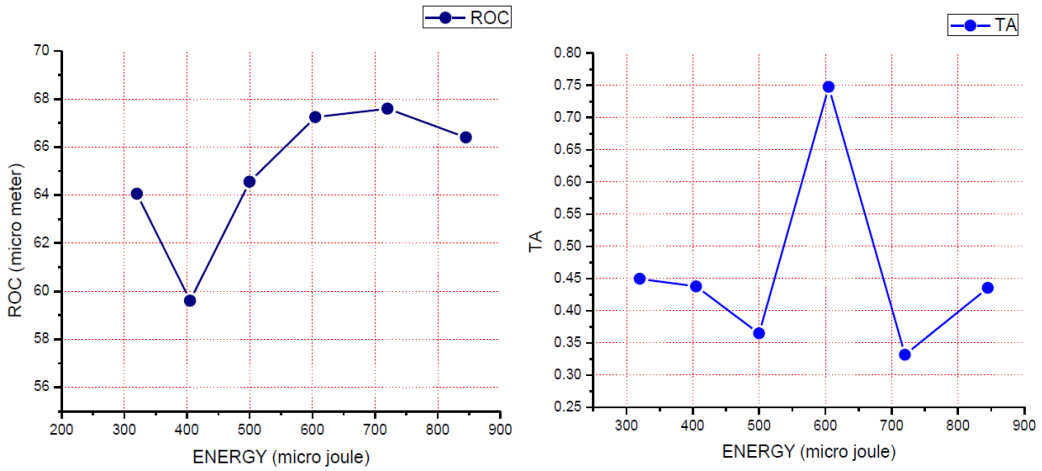

(a) **(b)**

Figure B.5 Effect of discharge energy on (a) ROC and (b) Taper angle

The value of geometric characteristics i.e. ROC and TA should be as lower as possible. It is concluded that the energy range of 400 - 500 µJ is best suited for machining of the TiN-Al_2O_3 ceramic composite as in this range MRR is moderate, EW rate is lowest, ROC and taper angle is lowest.

B.4 SEM Images of Drilled Hole

The topography of the machined surface is studied by SEM image; through holes from the top and bottom side at increasing order of discharge energy as shown in Fig. B.6 and Fig. B.7. As already discussed that for geometrical characteristics 400 µJ to 500 µJ is the best working range.

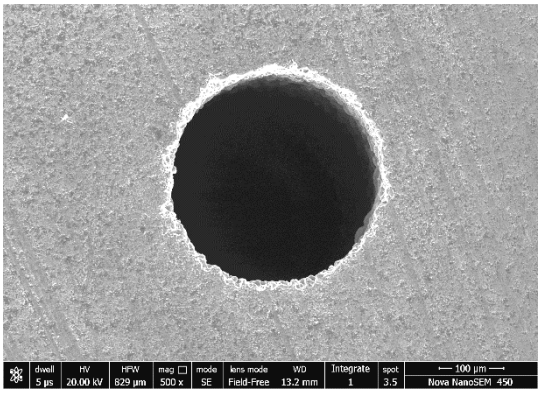

(a) 320 µJ

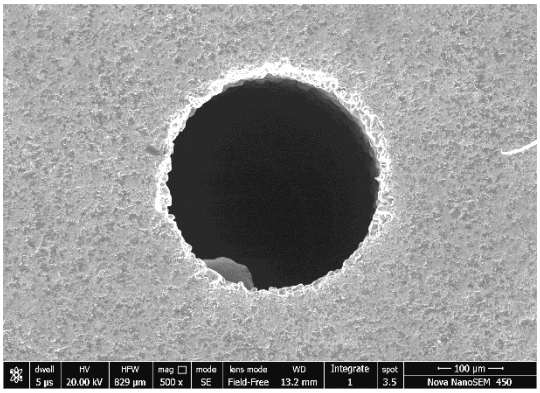

(b) 405 µJ

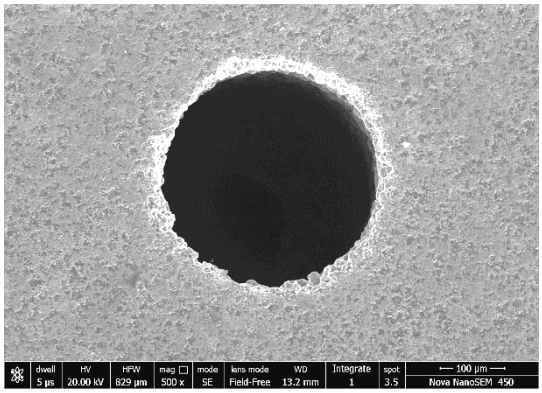

(c) 500 µJ

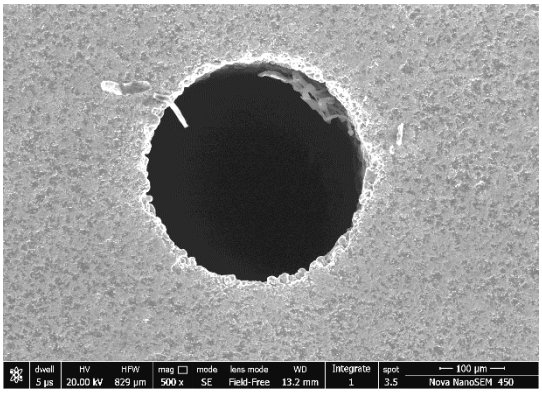

(d) 600 µJ

Figure B.6 SEM images of the drilled hole from the top

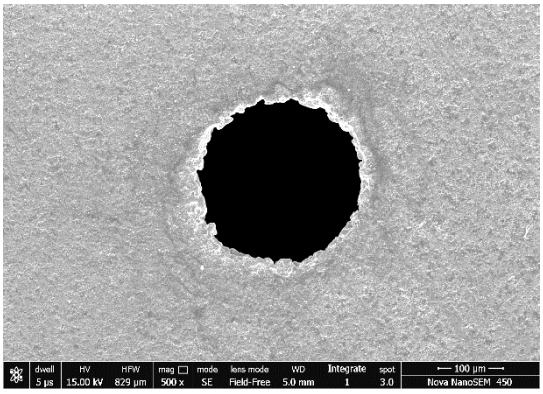

(a) 320 µJ

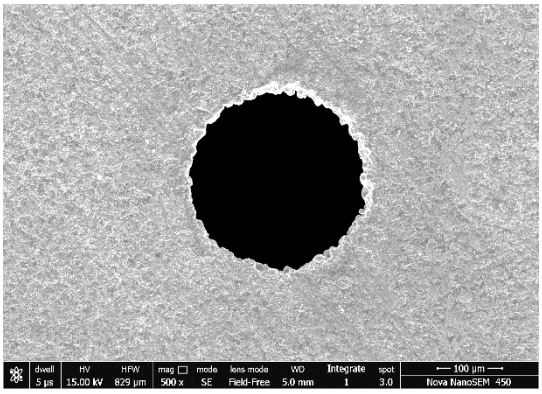

(b) 405 µJ

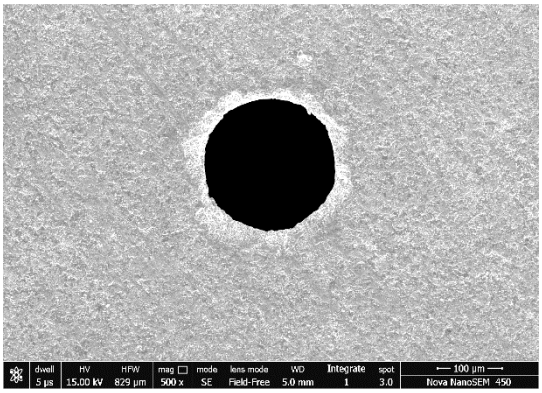

(c) 500 µJ

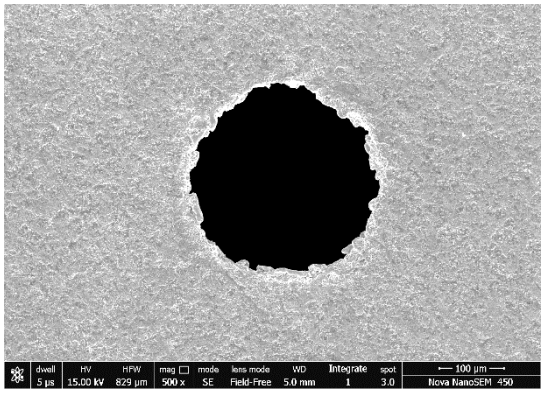

(d) 600 µJ

Figure B.7 SEM images of the drilled hole from the bottom

It is observed from Fig. B.7, that there is no bulging formation at the exit of the hole which is generally observed in macro machining of ceramic-composites. The best circularity of the hole can be observed at 500 µJ discharge energy.

It is also observed that in comparison of macro EDM hole there is a negligible recast layer formation on the periphery of the hole. The top and bottom images of drilled holes (Fig. B.8) are showing bulge formation that is visible at the entry/ top of the holes but from Fig. B.7 it can be observed that there is comparatively no bulge formation in the micro-EDM process. The re-solidification layer observed in macro EDM is due to high discharge energy.

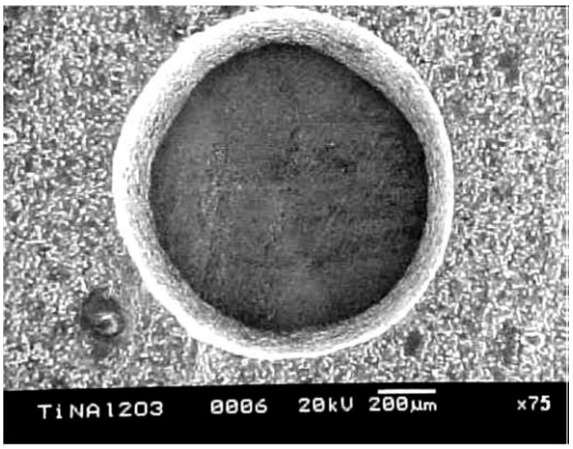

(a)

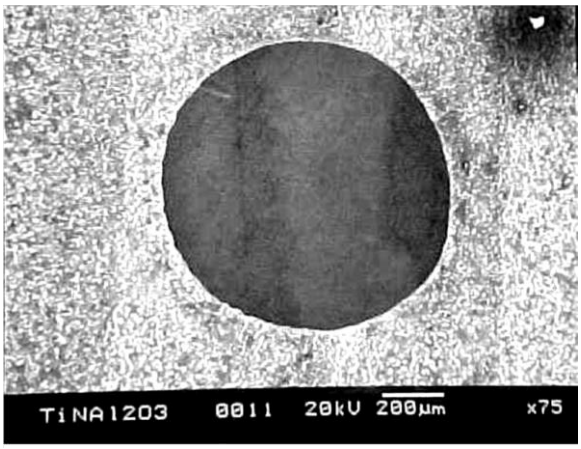

(b)

Figure B.8 SEM images of the macro hole on TiN-Al_2O_3 (a) top and (b) bottom [12]

B.5 Conclusions

High aspect ratio micro holes are needed for several applications like micro-electro-mechanical system (MEMS), heat exchangers, and chemical microreactors, etc., which have been fabricated by the micro-EDM process. Effect of discharge energy on geometric characteristics like taper angle, radial overcut is also studied. Based on this study, the following conclusions can be made:

1. In this present research, machinability study of ceramic composite TiN-Al_2O_3 has been carried out and effect of input parameters (voltage, capacitance, and speed) is observed on each response parameter (i.e. MRR, EW, EW Ratio, Taper Angle, and Radial Overcut).
2. From the analysis, it is observed that the material removal rate is mainly affected by capacitance and voltage i.e. discharge energy and there is a steep downfall in MRR if discharge energy is beyond 600 µJ.
3. EWR also increases with an increase in the value of discharge energy as high discharge leads to high electrode wear. For the optimum value of MRR and EWR discharge energy is 500 µJ.
4. Voltage comes out to be the most influencing parameter with rank one, speed holds rank two and capacitance does not have a significant effect on taper angle and holds rank three. For radial overcut also, voltage is found to be the most influencing parameter with rank one followed by capacitance and speed. High voltage and high capacitance results in high discharge energy which result in large radial overcut.
5. It is also observed that micromachining of the TiN-Al_2O_3 ceramic composite is done more accurately, in terms of geometrical characteristics, compared of macro machining by EDM process as there is no recast layer observed in the case of micro-EDM.
6. The machining performance and effect of discharge energy on geometric characteristics of micro-holes generated on TiN-Al_2O_3 ceramic-composite by the micro-EDM process is analyzed. µ-EDM has inherent ease in the machining of this promising conductive ceramic-composite that is otherwise difficult to machine.

APPENDIX "C" **MICRO TOOL FABRICATION AND MICRO-ED MILLING OF TITANIUM ALUMINA CERAMIC-COMPOSITE**

This study represents the novel approach of on-machine fabrication of high aspect ratio micro-electrodes (Φ=500 μm) and machining characteristics of TiN-Al_2O_3 ceramic-composite with fabricated brass micro-electrodes. Microelectrodes of diameter 500 μm are successfully fabricated using micro turning process on advance ceramic: TiN-Al_2O_3. All the experiments are performed on Hybrid μ-EDM DT-110i machine. The tool electrode is brass of 60 mm in length as shown in Fig. C.1. The micro tool fabrication is done on micro turning machine setup. The details of the tool material and workpiece are given in Table C.1.

Figure C.1 Initial brass tool electrode (Φ= 3)

Table C.1 Details of tool and workpiece

Details of the tool and workpiece	
Electrode material	Brass
Length (mm)	60
Diameter (micron)	500
Machining process	Micro ED- milling and micro turning
Workpiece	TiN-Al_2O_3 ceramic-composite

C.1 Experimentations

The micro tools are fabricated on Hybrid µ-EDM with micro turning setup. The micro tuning setup has carbide single-point cutting tool. The initial diameter of the brass tool was 3.0 mm that was reduced to 500 microns by micro turning process. The carbide insert is used as a single point cutting tool for micro turning process. The micro turning setup is shown in Fig. C.2.

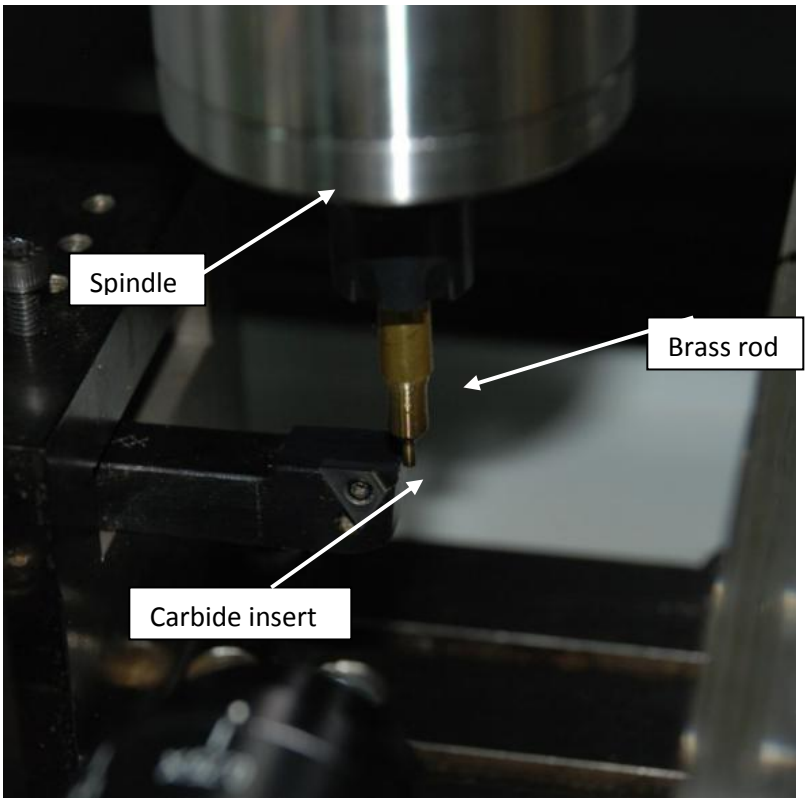

Figure C.2 Micro turning setup

After micro turning process, the microtool is prepared as shown in Fig. C.3. The spindle is rotated at the speed of 1200 rpm. The brass tool is turned in five steps. The depth of cut during tool turning are 300, 300, 250, 250 and 150-micron sequentially and feed rate is taken as 0.2 mm/min. The micro tool (Φ=500 micron) prepared is shown in Fig. C.4.

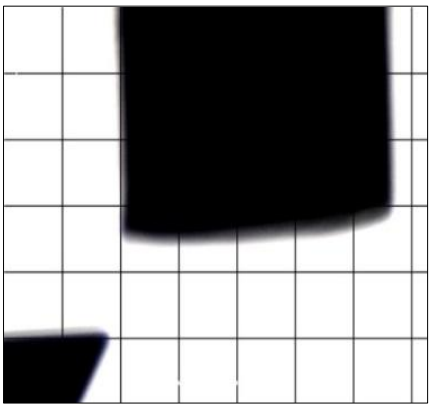

(a) Φ=3000 µm

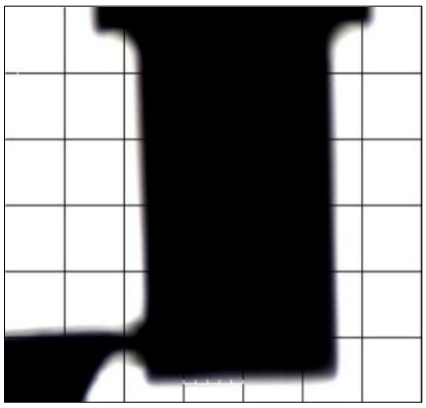

(b) Φ=2400 µm

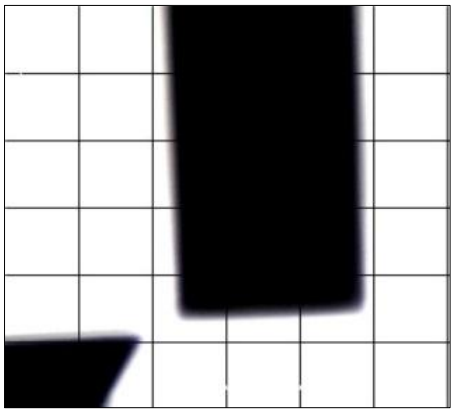

(c) Φ=1800 µm

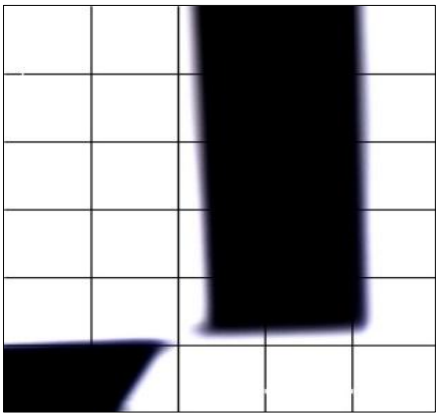

(d) Φ=1300 µm

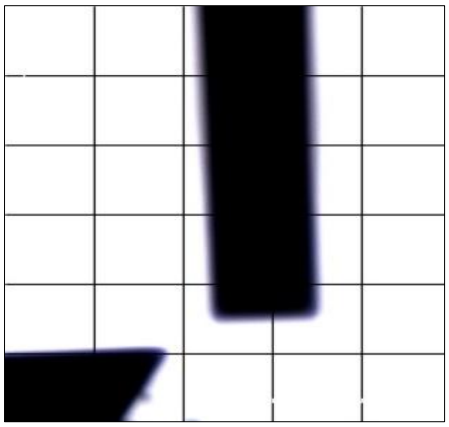

(e) Φ=800 µ

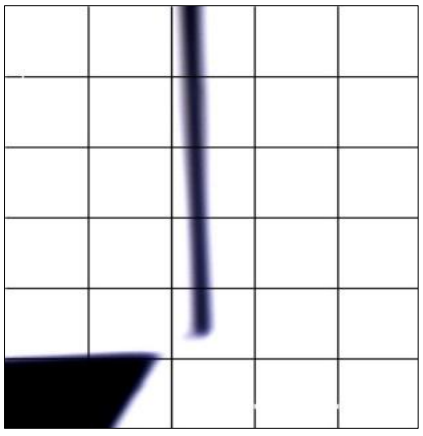

(f) Φ=500 µm

Figure C.3 Fabrication of microelectrode in steps (a, b, c, d, e, and f) by a micro turning process

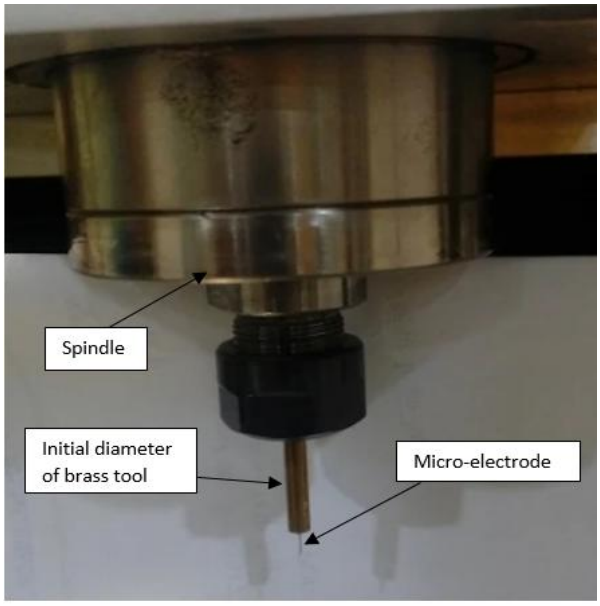

Figure C.4 Fabricated micro-electrode (Φ=500 micron)

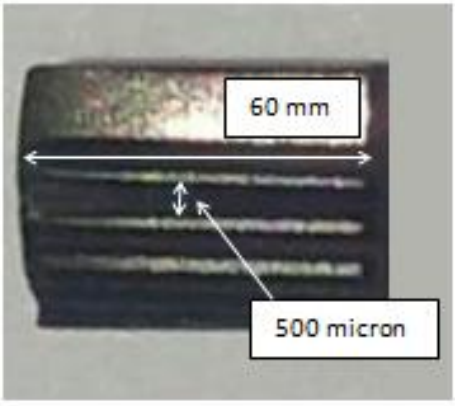

Figure C.5 Micro-channels fabricated by micro-ED milling

The microchannels are fabricated on TiN-Al_2O_3 sample as shown in Fig. C.5; the input parameters and responses are shown in Table C.2. The material removal rate (MRR) is measured by total volume lost per unit machining time. Electrode wear rate (EWR) is also measured by total volume loss per unit time for each experiment. Tool wear ratio is measured as the ratio of MRR to EWR. The discharge energy for each experiment is measured by equation C.1.

$$Discharge\ energy\ (E) = \frac{1}{2}\ CV^2 \qquad \mu J \ldots\ldots\ldots\ldots\ldots\ldots \text{(C.1)}$$

Where C= capacitance in micro-Farad, V= voltage in volt

Table C.2 EDM parameters and response parameter for micro channels

Sn.	Energy (μJ)	Spindle speed (rpm)	MRR (mm^3/min)	TWR (mm^3/min)	TW Ratio
1	500	1000	0.0001390	0.0052124	0.026667178
2	605	1000	0.0003250	0.005440062	0.059741967
3	720	1000	0.0002570	0.005540664	0.046384335
4	845	1000	0.0001396	0.0041679	0.033494084

C.2 Results and Discussion

TiN-Al_2O_3 ceramic-composite has machined and microchannels are fabricated. The dimensions of micro-channels are 4 mm in length and cross-sectional area is 500×500 microns.

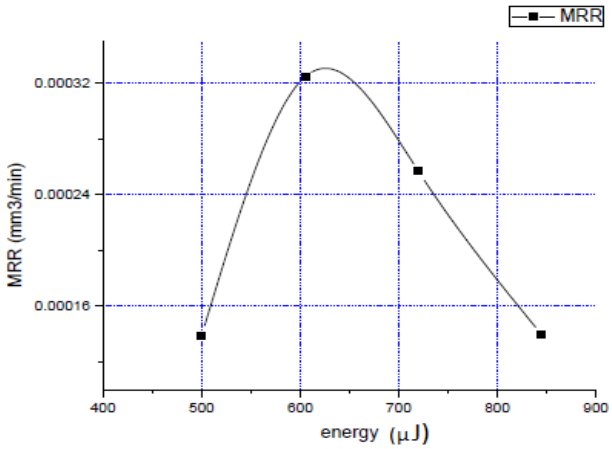

Figure C.6 Plot of MRR with discharge energy

Response parameters are shown in Table C.2. The results show that the material removal rate is less as compared to the electrode wear rate. ED milling of TiN-Al_2O_3 is indicating excessive tool wear out while machining. The EWR plot with discharge energy shows that from 500 μJ to 700 μJ electrode wear rate increases and after that EWR is suddenly falling as shown in Fig. C.7. More tool wear is due to the very high melting temperature of TiN-Al_2O_3 as compared to brass. The results also show that MRR is the highest at 600

μJ and after that MRR decreases as shown in Fig. C.6. This is because at high discharge energy the brass tool could not sustain high temperature. The EWR also shows a similar trend i.e. increases up to approximately 600 μJ and a sudden decrease is noticed beyond that.

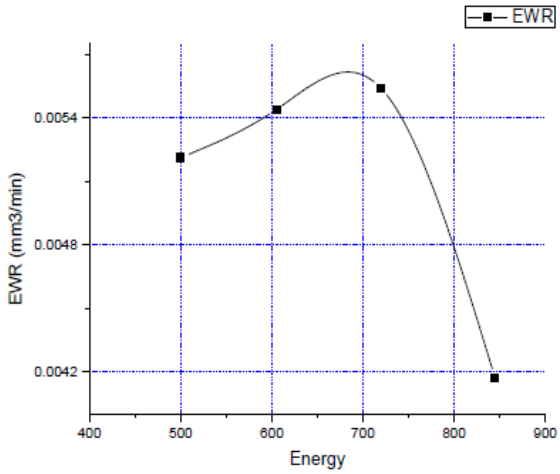

Figure C.7 Plot of EWR with discharge energy

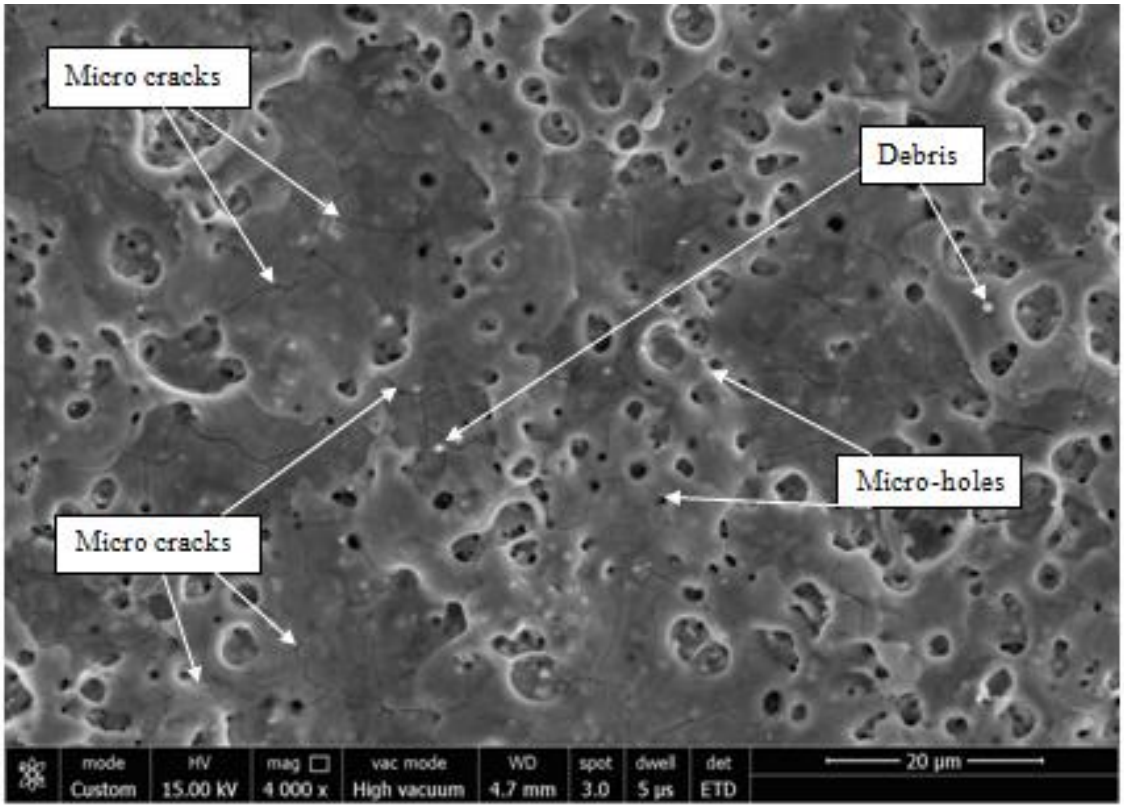

Figure C.8 SEM image of the machined surface

The scanning electron microscope (SEM) images of machined surfaces (Fig. C.8) shows microspores and droplets type of debris which indicates that melting and vaporization are the mechanisms of material removal. The presence of a metal particle on the machined surface also confirms the material migration mechanism in which the tool material is migrated to the workpiece. The machined surfaces are also filled with micro-cracks that show the contraction mechanism of molten metal.

C.4 Conclusions

In this study micro tools are fabricated by "on-machine fabrication technique" and microchannels are machined using these fabricated tools by the μ-ED Milling process. The machined surface of TiN-Al_2O_3 ceramic-composite is studied to understand the material removal mechanism. The machined surfaces show irregular debris, microcracks, and droplets. This study also shows that machining of TiN-Al_2O_3 ceramics using brass electrode at higher energy leads to lower MRR and hence machining at low energy is advised. For better MRR, a material with a higher melting point should be used as tool electrode as brass cannot sustain high temperature.

RESEARCH OUTCOMES

International Journals:-

1. R. Baghel, H. S. Mali and S. K. Biswas (2018) Parametric optimization and surface analysis of diamond grinding-assisted EDM of TiN-Al_2O_3 ceramic, vol. 100 (5-8), ISSN: 0268-3768, IF= 2.601, pp. 1183–1192. **(SCI)**
2. Rupali Baghel, Dr. Harlal Singh Mali, (2018), An experimental study on fabrication of micro channels in titanium nitride alumina composite using electro-discharge milling, International Journal of Modern Manufacturing Technologies(IJMMT), ISSN 2067-3604, Vol. 10(2),pp.24-29, **(Scopus)**
3. Harlal Singh Mali, Rupali Baghel and Deepak Unune (2017), Experimental Investigation on Hybrid Micro-Electro-Discharge Machining of Inconal 718 and Ceramics Materials, International Journal of Conceptions on Mechanical and Civil Engineering Vol. 5, Issue. 1, February' 2017; ISSN: 2357 -2760 **(NON-SCI/Scopus)**

International Conferences:-

4. Rupali Baghel, Dr Harlal Singh Mali (2018), "A study on effects of discharge energy on geometric characteristics of high aspect ratio micro-holes on TiN-Al_2O_3 ceramics", 6th International Conference on Materials Processing and Characterization (ICMPC 2018), held at GRIET, Hyderabad, March 16-18, 2018, in Materials Today: Proceedings, ISSN: 2214-7853, Vol. 5, **(Scopus)**
5. R. Baghel, H.S. Mali and S.K. Biswas (2016), Study of Vibration Assisted Micro Electro-Discharge Milling of Titanium Nitride-Aluminium Oxide Composite, Proceedings of 6th International & 27th All India Manufacturing Technology, Design, and Research Conference(**AIMTDR-2016**)
6. R. Baghel, H.S. Mali and S.K. Biswas (2016) Parameter Optimization of Diamond Grinding Assisted EDM of TiN-Al_2O_3 Ceramics using Taguchi Method, Proceedings of 6th International & 27th All India Manufacturing Technology, Design, and Research Conference**(AIMTDR-2016)**
7. R. Baghel, H.S. Mali and S.K. Biswas (2016), Hybrid Micro-Machinability Study and Surface Analysis of TiN-Al_2O_3 Ceramic Composite, International conference on "Ceramics, Glass and Refractories – Emerging Innovations" – Dec.13-15 **2016 at CSIR**
8. Rupali Baghel, Dr. Harlal Singh Mali and Vivek Baghela (2018), Micro Tool Fabrication and Micro-ED Milling of Titanium Alumina Ceramic-Composite, All India Manufacturing Technology, Design, and Research Conference (AIMTDR) **(accepted)(Scopus)**